The Henryk Niewodniczański
INSTITUTE OF NUCLEAR PHYSICS
Polish Academy of Sciences
ul. Radzikowskiego 152, 31-342 Kraków, Poland

www.ifj.edu.pl/publ/reports/2011/

Kraków, March 2011

Report No. 2049/AP

Effect of atomic-scale microstructure on hardness, fracture and oxidation of metal-nitride coatings

Magdalena M. Parlińska-Wojtan

Habilitation Thesis

Effect of atomic-scale microstructure on hardness, fracture and oxidation of metal-nitride coatings

Magdalena M. Parlinska-Wojtan

EMPA
Materials Science & Technology

March 2011

All truths are easy to understand once they are discovered;

the point is to discover them.

Galileo Galilei

To my Family…

With my deepest gratefulness and love for their constant help & support,

In particular for my beloved Mother for taking care of my two Sunshines.

Table of Content

Abstract

The main goal of this habilitation thesis is to identify and classify the types of interfaces and their role in hardening mechanisms in differently structured transition metal nitride coatings, by direct transmission electron microscopy (TEM) observations. The investigated coatings have been divided according to their structure into three groups: columnar coatings, multilayers and nanocomposites. The microstructural aspects of all three groups have been extensively studied by TEM in as-deposited and heat-treated state or after indentation in order to better visualize the mechanisms governing the coating behavior during plastic deformation. Also the combination of different chemical compositions and their influence on the coating's microstructure has been analyzed.

TEM studies down to the atomic scale, of a compositionally graded TiAlSiN coating allowed putting some light onto the mechanism of formation of the nanocomposite structure. The images taken in the Ti-rich part of the coating showed crystalline columns with neat interfaces, followed by a progressive appearance first of a crystalline and then of an amorphous boundary phase as the Al+Si concentration was increasing. At the top part of the coating the well-known nanocomposite structure consisting of crystalline grains surrounded by an amorphous matrix was observed. In addition it could be shown that the nanocomposite structure, exhibiting high hardness, can only be formed with two phases having sharp interfaces such as TiN/SiN. It was not possible to make a hardness enhanced nanocomposite out of AlN and SiN. This was due to local epitaxy at AlN/SiN interfaces, investigated on a models system of AlN/SiN multilayers. Indeed, it was found that 0.7 nm of SiN, corresponding to about two monolayers, grew crystalline on AlN favoring epitaxy.

The nanocomposite structure is not the only way to achieve a hardness enhancement in these coatings: also columnar coatings can be hard, provided a sufficient density of dislocation barriers, not in form of column boundaries, is present. Two solutions to increase the density of dislocation barriers are presented: one consists in the introduction of compositionally graded multilayers, which distort the lattice but do not obstruct the columnar growth. The second solution is a phase modulated structure *i.e.* inside the columns zones of different phases are formed as it is the case for cubic and hexagonal NbN, which nevertheless has a columnar structure.

In multilayered coatings three types of interfaces, influencing their properties were observed: completely epitaxial, such as in $AlN_{10\ nm}/SiN_{<0.7\ nm}$ layers or NbN/CrN at the NbN/CrN interfaces in the growth direction, semi-coherent, with local epitaxy and non-

coherent such as in TiN/SiN coatings. All of them were barriers for dislocation movement making thus these coatings harder that their reference columnar layouts.

To better visualize and identify the hardening mechanisms based on dislocation blocking in metal nitride coatings, plastic deformation was deliberately induced by nanoindentation. Columnar and multilayered coatings have been extensively investigated by *post-mortem* TEM observations of indents cross-sections. In general, all coatings containing TiN, independently on their structure or layer thickness, deformed by shear sliding at grain boundaries. This mechanism was observed on two different scales: either entire pieces of multilayers or individual grains were vertically displaced over distances of several nanometers. It was particularly well visible for the NbN/TiN and the TiN/amorphous-SiN combinations.

By microstructural observations it could be shown that the substrate governs the deformation in columnar TiN coatings. In the case of columnar TiN deposited on a soft Si substrate during indentation the columns underwent shear sliding at grain boundaries and were pushed into the substrate forming steps at the interface. If columnar TiN is grown on polycrystalline, hard WC-Co substrate, cracks at columnar boundaries are generated. Moreover, these columns, which grow on the soft Co matrix, are also pushed into it, similarly to the TiN/Si combination. Conversely, those columns, which grow on the hard WC grains are bent and internally fractured.

The type of coating structure and thus the interfaces play an important role in oxidation resistance. It could be proved, by microstructural TEM investigations, that coatings with columnar grains, such as TiAlSiN and ZrAlN, are not oxidation resistant independently on their chemical composition. Indeed, the columnar boundaries serve as oxygen diffusion channels. Conversely, a coating with a nanocomposite structure, such as Al-rich TiAlSiN, has an abrupt interface with the oxide grown on its top and no penetration of oxygen into the structure is observed.

KEYWORDS

Hard metal-nitride coatings; hardening mechanisms; interfaces, transmission electron microscopy (TEM); deformation mechanisms; fracture damage; grain boundary sliding; hardness enhancement; nanocomposites; multilayers; oxidation resistance.

Introduction

1 FOREWORD

The first scientist who coated a substrate with a film was Michael Faraday far back in 1830. Yet, only since 30 years the deposition of hard thin films with a few microns in thickness is a common technology to improve the performance of tools, dies and moulds for many different applications [Holl 1986]. Various deposition methods have been developed in the last years. However, the important issue for the future is not which deposition technology is used, but which properties of the coated substrate can be achieved and at which production cost. At this point microstructural design is needed.

1.1 MOTIVATION OF THIS STUDY

Since many decades researchers have worked on designing materials with well-controllable properties. One concept is to apply thin films to coat the bulk material. This thin layer deposited onto the base material allows independently optimizing the properties of the substrate and the coating to achieve desired properties of the whole compound, Figure 1. The substrate guarantees characteristics like shape, weight or toughness. On the contrary the coating is responsible for enhanced hardness, strength, internal stress, fracture toughness, thermal stability and conductivity, better friction properties, decoration and biocompatibility.

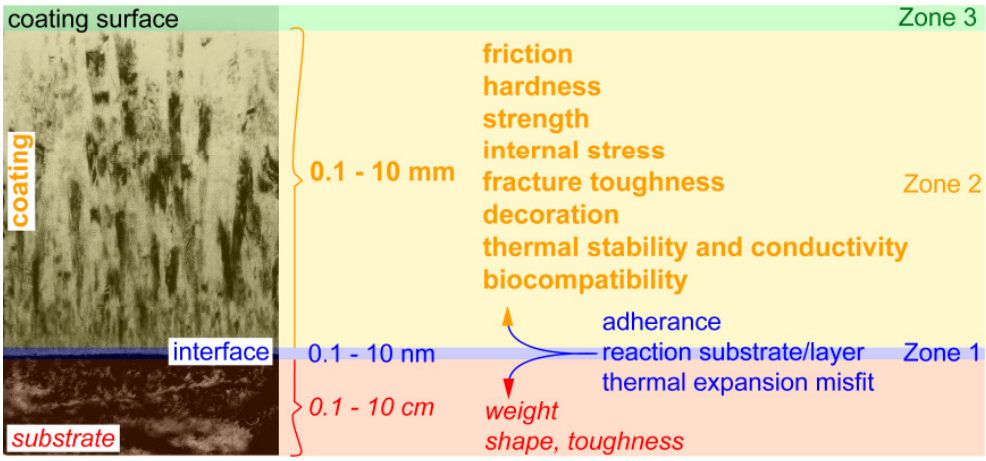

Figure 1 *Characteristics of a cross-section through the substrate, interface and coating on the example of a WC-Co substrate coated by a ZrN layer. The photograph was taken by transmission electron microscopy. Some desired coating properties are listed on the right side of the arrows.*

Three zones, each having different property requirements can be thus distinguished in the coating/substrate system. The *first* one is the *substrate interface* where the adherence, reaction of the substrate with the coating layer, and strains by thermal expansion misfit are critical points. Consequently it is a crucial requirement to optimize the interface. The

composition and microstructure of the *coating*, which is the *second* zone, determine its properties. The *third* zone is the *coating surface* where the interaction of the coating material with a workpiece or with the environment has to be taken into account. The thickness of the coating, depending on the application, can vary between a few tens of nanometers up to several microns. The main factors governing the parameters of the coating are the constitution of the coating-substrate system and the deposition parameters, as shown in Figure 2. Both of these determine the microstructure of the coating.

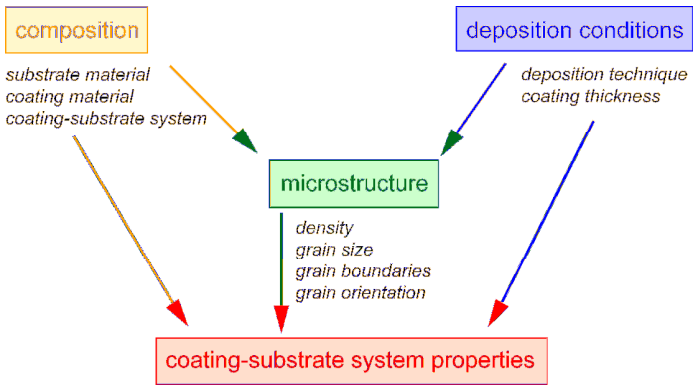

Figure 2 *Main factors influencing the properties of the coating-substrate system (redrawn after Holleck [Holl 1986]).*

The selection of materials composing the coating-substrate system is a crucial issue determining the properties of the resulting system. Indeed, many problems arise, since some desired properties cannot be achieved simultaneously. For example it is impossible to combine in one coating high hardness with high toughness or a good adherence of the coating on the substrate with no surface interactions. Increasing hardness and strength are concurrent with decreasing toughness and adherence.

There are as many approaches to classify hard coatings as authors attempting to establish such classifications. The one presented below is based on Holleck [Holl 1986] and takes into account the character of the dominating type of chemical bonding in the coating material comprising thus the widest selection of hard coatings. According to this classification there are three groups of coatings, shown in Table 1:

a). Coatings with dominant metallic bonding type

These materials, where the chemical bonding are mainly of metallic type, comprise borides, carbides and nitrides of transition metals. They are estimated to be the most

suitable and versatile layer substances. Their linear thermal expansion coefficient is situated between the ones of the covalent and ionic coatings.

b). Coatings with prevailing covalent bonding type

This group, with the majority of covalent type bonding, encloses carbides and nitrides of B, Al, Si and borides of the two latter elements as well as diamond. These materials, except diamond, are mainly used as ternary additives for metallic hard coatings to improve their properties. Moreover they have the lowest linear thermal expansion coefficient.

c). Coatings with mainly ionic bonding type

To these materials belong oxides of Al, Zr, Ti and Be, having primarily an ionic type of chemical bonding. Their elastic modulus is the lowest and their linear thermal expansion coefficient is the highest among these three groups. On the other hand, they are most suitable as surface coatings as they have a high stability and low interaction tendency.

Table 1 *Classification of hard coatings according to the character of the dominating chemical bonding present in the constituting material (after H. Holleck [Holl 1986]).*

MAINLY METALLIC	MAINLY COVALENT	MAINLY IONIC (CERAMIC)
borides, carbides, nitrides of transition metals	borides, carbides, nitrides of Al, Si & B	oxides of Al, Zr, Ti, Be
TiB_2 TiC TiN WC CrN	SiC SiN AlN BN	Al_2O_3 ZrO_2 BeO

Another commonly used classification of hard coatings is according to the element forming the ceramic with the transition metallic elements:

- nitrides (*Me-**N***)
- borides (*Me-**B***)
- carbides (*Me-**C***)

Figure 3, after Löffler [Löf 1994], attempts to classify different coatings deposited on cemented carbide substrates on the basis of microhardness, adhesion properties determined by scratch tests and temperature resistance measured on coatings deposited on metal substrates. This comparison shows, that the best adhesion properties exhibit TiN and CrN-based coatings, which are thus suitable as interfacial layers at the substrate. AlN-based coatings have the best oxidation resistance and can be used as top coatings for elements working in high temperature environments.

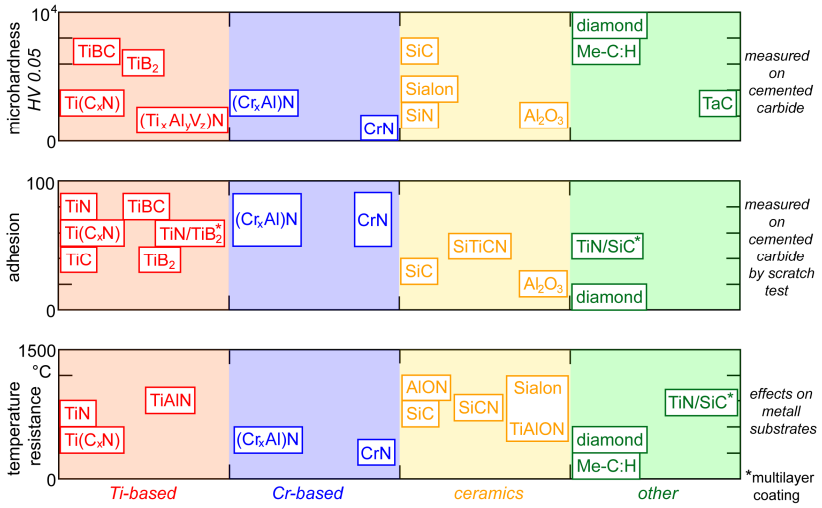

Figure 3 *Properties of various coating systems; some of which are only qualitative (redrawn after F. Löffler [Löf 1994]).*

There are numerous applications for these coatings, below only a few are listed:

- Industrial application in high speed machining tools (cutting, drilling, punching, forming)
- computer and telecommunication domain: processors and memory modules
- automobile industry : fuel-injection systems, camshafts, gears
- protective coatings for architecture glass : color, reflexes and heat management
- aluminum die-casting moulds
- decorative coatings : gold or silver colored

Of course, the hardness, oxidation and wear properties of *Me-N* coatings can still be improved, as they do not depend only on their chemical composition, but also on the deposition technique and parameters influencing their microstructure. Pure transition metal nitride coatings have a columnar structure, with columns about 200 nm wide and reaching the thickness of the coating. One of the first deposited and most popular coatings is *TiN*. By adding different elements to obtain ternary and quaternary compositions, properties of the *Me-N* coating can be controlled. In particular, coatings based on a combination of Ti, Cr, Al and Si nitrides and carbides (e.g. Ti-N, Cr-N, Ti-C-N, Ti-Al-N, Ti-Cr-N, Ti-Al-C-N, Cr-Al-Si-N and Ti-Al-Si-N) are currently available on the market to be used as protective hard coatings for machining tools [Csel 2007], [Vepr 2008]. One of the most promising coating is the nanocomposite structure made of nanocrystalline Ti-Al-N embedded in an amorphous silicon nitride matrix [Holu 1999], [Nied 1999], [Vepr 2004], [Par 2004b],

[Mart 2005]. With such a structure, the hardness of TiN is doubled (from 24 GPa for TiN to 40-45 GPa for TiAlSiN), as well as its maximum application temperature (from 600°C for TiN to > 1000°C for TiAlSiN) [Csel 2005]. The tool life time can hence be considerably improved.

In the nineties the properties of *Me-N* coatings were modulated by changing their structural layout, which resulted in so-called nanocomposite and multilayered structures. Thus scientists seek for controlled design of interfaces to explain and control the properties of the *Me-N* superhard coatings.

1.2 STRUCTURE OF THE PRESENT WORK

The investigations described in this work are mainly focused on *transition metal nitride* (*Me-N*) coatings, their microstructure, fracture damage and deformation modes as well as thermal stability, which have a direct influence on hardness and allow establishing microstructural engineering rules for designing, in a controlled way, a material with desired properties.

The first chapter is an introduction to the domain of hard coatings and presents the motivation of this study. Subsequently, a short review is given on the design and classification of hard nanostructured coatings. In chapter two, special attention is devoted to the material selection criteria and to the hardening mechanisms occurring in the coatings. A particular interest is focused on steering the properties of coatings by adding different elements, the choice of the substrate-coatings system as well as the influence of stress.

In the following paragraphs of this manuscript the main theoretical considerations concerning the type and structure of interfaces, which are applied to influence in a controlled manner the properties of protective *Me-N* coatings, will be presented. Next, the generally known hardening and strengthening mechanisms will be presented. Subsequently, the deformation mechanisms and fracture damage occurring in hard coatings will be discussed.

The hard coatings addressed in this habilitation thesis are based on nitrides of the following elements: *Ti*, *Al*, *Cr*, *Nb*, *Zr, Si* and their combinations. For sake of clarity, these coatings are divided according to their structure into *bulk-columnar coatings, multilayers* and *nanocomposites.* At the end of the second chapter, first the columnar coatings will be described, and then the definition and concept of nanocomposites will be introduced. The

last part of this chapter will be dedicated to multilayers, which are a very promising alternative for nanocomposites.

Chapter three is devoted to the deposition procedure of coatings i.e. the basics of magnetron sputtering and its variant – reactive magnetron sputtering used to grow metal-nitride coatings. Subsequently models of film growth and morphology are discussed.

In chapter four the analytical techniques applied to investigate various properties of the coatings are shortly introduced i.e. nanoindentation used to measure the hardness and induce plastic deformation and TEM used to study the microstructural features of the coatings. Also unique sample preparation methods of TEM samples are presented.

Chapter five, being the key chapter of this manuscript, discusses in detail the findings from the original research performed and the hypotheses established by the author. It is divided into three parts: dealing with applied examples of hardness enhancement in metal-nitride coatings, their fracture damage and deformation mechanisms as well as the substrate influence on the latter ones, and oxidation resistance of these coatings. For each subject several examples are presented and discussed in detail and a summary is given.

All the findings are based on detailed microstructural studies of cross-section through the coating performed by TEM. In the first part of this chapter applied examples of hardness enhancement in coatings with different structures and layouts, involving the introduction supplementary interfaces, are presented. The second part contains information about different deformation mechanisms, which strongly depend on the chemical composition of the coatings and mainly on the substrate hardness, but not necessary on their structural layout. Finally, the influence of the microstructure and of the chemical composition on the oxidation resistance, are discussed.

In the conclusion of this work a broader view on the way to build hard nanostructured coatings is given, based on the knowledge gained from the impact of microstructural features on the macroscopic coating properties. At the end detailed conclusions from the obtained results are presented.

2 MICROSTRUCTURAL DESIGN OF INTERFACES – BASIC IDEAS

The strength of interatomic forces and thus the hardness of materials is a complicated property with more than one variable. Regardless of this, there have been many attempts to relate hardness to bond strength such as cohesive energy [Pen 1962], heat of formation [Gil 1970], surface energy [Murr 1975] and vibrational entropy. However, only rough predictions can be made using such approaches.

2.1 MATERIAL SELECTION FOR HARD ME-N COATINGS

The most suitable candidate elements for hard ceramic coatings are the so-called *nitride forming elements* namely: the group of *IVb – VIb* elements (Ti/Zr/Hf; V/Nb/Ta or Cr/Mo/W) and the *IIIa / IVa* elements: Al and Si. They are generally used to produce refractory ceramic nitride, boride, carbide and oxide coatings with enhanced properties. All of these 11 elements, except Al have melting temperatures around 1400°C or higher like tungsten (3400°C), and are therefore inherently quite refractory. Moreover, the 10 elemental materials exhibit natural thermal stability up to 700°C or above.

Table 2 *Candidate, low-miscibility nitride forming elements, which might be considered for alloying to produce metallic nanocomposite films (after A. Leyland et. al. [Ley 2004]).*

Element	Crystallographic structure	Elastic modulus *E4[GPa]*	Atomic radius *[nm]*	Melting temp. T_m °C
Ti	*hcp*	115	0.14	1675
Zr	*hcp*	68	0.16	1852
Hf	*hcp*	78	0.155	2150
V	*bcc*	128	0.135	1895
Nb	*bcc*	105	0.145	2470
Ta	*bcc*	186	0.145	2996
Cr	*bcc*	280	0.14	1890
Mo	*bcc*	330	0.145	2610
W	*bcc*	410	0.135	3415
Al	*bcc*	70	0.125	660
Si	*fcc (diamond cubic)*	47	0.112	1410

The choice of additives, in form of a second or even third element, into the *Me-N* system requires the respect of some rules. One was proposed by William Hume-Rothery [Hum 1998], the founder of modern metallurgy, and is called the *"14% rule"*. It considers that atoms of two elements, whose atomic radii differ by more than 14%, will be restricted in

their mutual solubility if one element is substituted for the other in the crystallographic structure. Additionally considerable lattice strain occurs, which results in a substantial increase in yield strength and hardness. Consequently, substitutional atoms with very large diameters *i.e.* 0.18 nm and with very small diameters below 0.12 nm would not be highly miscible with an average size metal atom of about 0.15 nm. Even theoretically very similar atoms such as for example the *IVb* metals like Ti (~ 0.14 nm) and Zr (~ 0.16 nm) can be different in size. Thus they cause a lattice strain, when they are in a solid solution.

Additionally many of these elements, as shown in Table 2, exhibit very different crystallographic structures, partially due to their contrasting valence electron configurations. As a consequence, despite of having atoms of similar size, some of these elements, show electronic incompatibilities related to their valence electrons configurations, which often restrict their mutual solubility. When attempts are made to mix several elements with different atom sizes and preferred crystallographic structures, it is often the case, that the formation of a regular, crystalline lattice is disturbed by the existence of many incompatible atom sizes and electron configurations, to the point, that long range order is thermodynamically difficult to establish. Such a phenomenon was predicted over 50 years ago by Turnbull [Turn 1949], who first described the concept of reduced glass transition temperature, which would result in slowing considerably down homogeneous nucleation from an undercooled melt. In addition that these systems do not contain grain boundaries, they exhibit high yield strengths and low moduli, which makes them suitable for mechanical and tribological applications. A particular issue with bulk metallic glasses is their tendency towards brittle behavior, especially in tension. In reality, this observation appears to relate more to shear band localization, which leads to unstable yield behavior and early fracture. A lack of grain boundaries, and thus also of work hardening mechanisms, is believed to be the main cause of such behavior [John 1999]. Thus efforts are put into the introduction of some crystalline phases resulting in the formation of nanocomposite materials, described in more detail in §2.5.2.

2.1.1 PROPERTIES OF HARD ME-N COATINGS

The principal criterion for the choice of all elements constituting a hard coating is related to its application and the required properties, as the addition of one extra element can influence the oxidation resistance, the grain size, the hardness or the wear resistance of the obtained coating. The properties of coatings, which were analyzed in the frame of this

study, are described in more detail i.e. TiN, CrN, AlN, NbN and ZrN. The last two ones i.e. VN and HfN are only shortly presented, as they were not investigated during this study.

A). **TiN**

Titanium nitrides are the most known and investigated hard films among the nitrides. They are a very hard ceramic material, often used as a coating on titanium alloys, steel, carbide, and aluminum components to improve the substrate surface properties. Applied as a thin coating, TiN is used to harden and protect cutting and sliding surfaces as it reaches hardness of 24.5 GPa and as a non-toxic exterior for medical implants. For decorative purposes TiN is often used to coat jewellery, watches and automotive trim because of its metallic gold color.

TiN has excellent infrared reflectivity properties, reflecting in a spectrum similar to elemental gold. Depending on the substrate material and surface finish, TiN will have a coefficient of friction ranging from 0.4 to 0.9 versus itself in non-lubricated conditions. Stoichiometric titanium nitride crystallizes in a stable cubic *fcc*-TiN phase however TiN_x compounds with x ranging from 0.6 to 1.2 are thermodynamically stable. TiN will oxidize at 600 °C at normal atmosphere, and has a melting point of 2930 °C. As shown in Figure 4TiN is miscible with other nitrides. References [Holl 1986], [Löf 1994] contain more data on TiN.

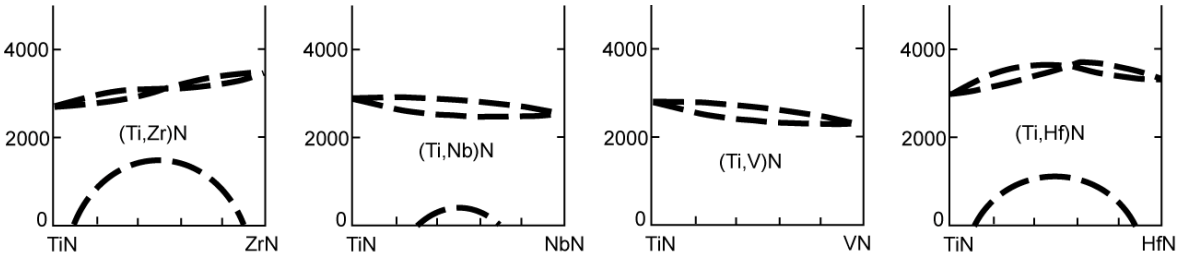

Figure 4 *Miscibility behavior of TiN with other nitrides (redrawn after Holleck [Holl 1986]).*

B). **CrN**

The strength of chromium-based nitride coatings lies in good adhesion properties on most of the commonly used substrates. It is very hard, and is extremely resistant to corrosion. It is an interstitial compound, with nitrogen atoms occupying the octahedral holes in the chromium lattice. Chromium nitride exists in two stable phases: *fcc*-CrN and *hcp*-Cr_2N, and due to the lower reactivity of Cr with nitrogen two phase coatings containing both phases are frequently deposited. CrN can only be used in applications where the

temperature does not reach 1000°C, as above it decomposes into Cr_2N and free nitrogen. In [Löf 1994], [Cas 2007] and [Cas 2008] more information about CrN coatings can be found.

C). **ALN**

Among group III nitrides AlN has the widest band gap (6.2 eV) giving it potential application for deep ultraviolet optoelectronics. AlN films are mostly used in field emission devices, UV light emitters, anti-oxidation coatings or optical films with tailored refractive indices. Aluminum nitride is a mainly covalently bonded material and has a hexagonal crystal structure called wurtzite. It can easily be deposited by sputtering techniques. AlN coatings are also suitable for oxidation resistant and optically transparent coatings with satisfying hardness values. The material is stable at very high temperatures in inert atmospheres. In air, surface oxidation occurs above 700°C, which protects the material up to 1370°C. In [Löf 1994] and [Pél 2009] valuable information on AlN is presented.

D). **NBN**

NbN coatings are very interesting for technological applications due to their superconducting properties with regard to high critical temperature such as 16K [Shii 2010]. At low temperatures, niobium nitride becomes a superconductor, and is used in detectors for infrared light. Niobium nitride is also employed in absorbing anti-reflective coatings. The NbN system crystallizes in several phases: *i.e. hexagonal* β-Nb_2N and δ'-NbN, and *fcc* δ-NbN [Benk 2004]. Thus the NbN films present excellent hardness properties related to the intrinsic hardness of each constituent phase and to the morphology of the films. More information about NbN coatings can be found in [Sand 2006] and [Benk 2004].

E). **ZRN**

Zirconium nitride, being the least studied system among nitrides, is a hard ceramic, similar to titanium nitride, and a cement-like refractory material. When deposited using the sputtering process, it is commonly used for coating medical devices, industrial parts, automotive and aerospace components and other parts subjected to high wear, corrosive environments and high temperatures. It is also used in refractories, cermets and laboratory crucibles. Zirconium nitride has an *fcc* structure and is a superconductor below 10K. More details on ZrN coatings are available in [Lamn 2005], [Lamn 2006] and [Mus 1999].

F). **VN**

Vanadium nitride is formed during nitriding of steel and increases wear resistance. Another phase, V_2N, also referred to as vanadium nitride, can be formed along with VN during nitriding. VN has an *fcc*, rock salt structure. There is also a low temperature form which contains V_4 clusters. It is a strong-coupled superconductor. Nanocrystalline vanadium nitride has been claimed to have potential for use in supercapacitors. Coatings based on vanadium nitride are most wanted for their catalytic properties. More information on VN can be found in [Ma 2001], [Glas 2007], [Sun 2008].

G). **HfN**

Hafnium nitrides are used because their hardness is much higher at elevated temperatures compared to the one of TiN. They are usually deposited on tools operating at very high speeds and thus reaching high temperatures. Reference [Ley 2004] provides more data on HfN.

2.1.2 INFLUENCE OF ADDITION OF DIFFERENT ELEMENTS ON COATING PROPERTIES

The addition of different elements will affect the properties of the resulting ternary or quaternary nitride coatings. It is worth mentioning, that not only the properties, but also the crystallography of the nitride phase formed by the added element are important. The miscibility of the added element has to be considered, together with the possibility of incorporation of the added element into the lattice of the existing nitride. Moreover, when choosing the additive, the crystallographic compatibility of nitride phases formed by the original and the added element have to be considered. Below the most popular additives and their influence on the coating performances are enumerated:

A). **ALUMINUM**

Aluminum addition into TiN leads to higher strength at elevated temperatures, an enhanced oxidation resistance and better thermal barrier [Holl 2008], [Kut 2005a], [Kut 2005b] and [Mos 2007]. Consequently, tools coated with TiAlN are ideally qualified for abrasive cuts with high cutting temperatures. Unfortunately, TiAlN exhibits lower heat conductivity and a higher friction coefficient, what leads in interrupted cutting to high stresses upon the cutting edge resulting in more frequent break-outs and edge chipping of the tool. Al is the only element, which forms a hexagonal nitride phase. However, when added in small amounts it is incorporated into the *fcc* lattice of the existing nitride. If the volume of Al

exceeds the solubility within the base nitride phase it segregates in form of a second phase, which thus is hexagonal, as it is the most energetically favorable AlN phase. In this way a strong two-phase composite material is formed, which exhibits enhanced hardness properties.

B). **CHROMIUM**

Chromium is often used as an oxidation resistance enhancing additive, similarly to Al. The most popular combination is TiCrN, either in form of a solid solution or as a multilayered system [Sol 2008], [Will 2008].

C). **HAFNIUM**

Due to its very high melting point Hafnium is added into TiN or TiCN coatings in order to improve their thermal stability. Also improvement of wear behavior in coatings containing Hf has been reported [Kut 2005b].

D). **TANTALUM**

Tantalum can be added into TiN coatings to improve their optical properties. In this way, if their thickness is below 30 nm, they can be applied as optically selective coatings. The tantalum replaces the Ti in the TiN lattice giving rise to electrical conductivity increase and enhanced IR reflectance as well as a better visible transmittance [Bour 2007].

E). **NIOBIUM**

The addition of niobium influences in a positive way the oxidation resistance and the strength of the Me-N coatings. Therefore it often used as a ternary additive into TiN [Kut 2005b].

F). **SILICON**

A very interesting element is silicon as it is responsible for grain refinement of almost all transition metal nitride coatings. One exception is AlN, which will be discussed in detail in §5.2.2 and [Pél 2007]. Up to 3 at.% of Si are first incorporated substitutionally for the Me element in the Me-N lattice. Additions of higher amounts of Si result in a formation of a second amorphous SiN_x phase, which is located at grains boundaries of the crystalline grains of the Me-N phase, resulting in amazing hardness enhancements of these materials [Benk 2004], [Vepr 1995], [Vepr 1999], [Pat2001], [Pat 2003] and [Mus 1998].

G). **YTTRIUM**

Yttrium has a similar influence on Me-N coatings as silicon. Yttrium incorporation has a considerable impact on the oxidation performance of the coatings, in particular in combination with Al, most probably due to its property of grain reduction of the structure [Mos 2007].

H). **CARBON**

The TiCN coating is harder than pure TiN, because the addition of carbon refines the grain size. It has a lower coefficient of friction than pure TiN and is more resistant to corrosion. However, it is not a direct replacement for TiN in all applications and it is only recommended for cutting, punching and wear applications where moderate temperatures will be generated [Mit 1999].

Summarizing, it seems obvious, that by exploiting the materials science know-how, coatings with highly specialized properties can be deposited. The miscibility gap, which is a metastable state of two neighboring phases, occurs naturally during the deposition of the coatings and results in retaining of positive properties such as extreme hardness even at high operating temperatures.

2.2 SELECTION OF THE COATING / SUBSTRATE SYSTEM

The criteria for selecting a particular coating material depend on the used substrate and on the application. The parameters, which must be considered when selecting the coating/substrate materials, are: mutual adhesion, the respective Young's moduli, effects of both intrinsic and extrinsic stresses on the internal strength and the hardness of the coating.

2.2.1 MATERIAL MATCHING

The choice of elements constituting the coating will depend directly on the aimed application. One of the important parameter is the adjustment of the thermal expansion coefficients of the coating and the substrate materials, mainly if high temperatures are reached during the fabrication process or in the course of their use.

Another important point, which has to be taken into account discussing hard materials, is the anisotropy in properties of the grown coating. The hardness of TiB_2 or TiC for instance can differ by 30% depending on the crystallographic orientation of the coating [Holl 1986].

The deposition process however, often allows adjusting specified orientations, thus providing control of the desired properties.

The adhesion of the coating to the substrate is a crucial issue for the functionality of the coated workpiece. To ensure a good mutual adhesion, one solution is to deposit a so-called adhesion layer between the substrate and the coating, TiN or CrN is most used for this purpose. Another possibility consists in deposition of films with functionally graded composition throughout the coating thickness, in this way the transition between the adhesion layer and the functional coating can be made less abrupt. This allows matching elastically the coatings/substrate interface. Moreover, the nitrogen, carbon, boron or oxygen content in the coating can be adjusted with the deposition time to generate an increasing high-modulus ceramic phase content near the surface of the film.

It is important to take into account the differences in the sizes of atoms of the metal element to form a nitride, as well as the differences in the electronic structures of the atoms to be mixed. In some cases the resulting solid solution can be amorphous if this state is more favorable energetically. Ternary or quaternary additives can improve certain properties of a basic coating, such as adhesion, oxidation resistance or hardness. However, when considering elements to be added into a coating: miscibility and crystallographic compatibility of the obtained nitride phases have to be taken into account. The excess of an added element can drastically change the properties of the obtained coating. An excellent example is Si: when up to 6 at.% are added into TiN, a superhard nanocomposite consisting of TiN crystallites surrounded by an amorphous SiN_x matrix. If Si is added in excess, the volume fraction of the matrix becomes too important, and thus governs the hardness behavior of this system, which is softer than pure TiN. On the contrary the addition of a too high amount of Al into TiN is beneficial for the hardness. Some of the Al forms a hard TiAlN solid solution and its excess forms an *hcp*-AlN second phase, consequently the whole structure becomes a phase modulated composite. Although this coating will still remain columnar it will be harder than pure TiN.

2.2.2 TYPES OF STRESSES

In applications where the coated object is subjected to high load, the imposed strain results in a stress discontinuity at the coating/substrate interface if the elastic modulus of the coating and the substrate are very different [Kut 2005b]. Thermal stresses, which are due to a mismatch in thermal expansion coefficients between the coating and the substrate, can be tensile or compressive, but the tensile ones are generally more damaging [Kut 2005b],

[Bour 2007], [Mos 2007], [Rov 2008], [Sen 2004], [Kub 1988], [Zhao 1984], [Call 1985], [Kuhl 1989], [Barn 1988], [Mayr 2006a] and [Alm 1984]. Tensile stresses are generated during cooling from the deposition temperature in coatings having the thermal expansion coefficient larger than the one of the substrate. Needless to say, that both types of stresses should be made as small as possible by choosing optimum coating/substrate combinations. At last, intrinsic stresses generated during the deposition of the films are also detrimental to adhesion. Of course, intrinsic stresses can be either tensile or compressive and depend on the deposition conditions [Bla 1973], [Hof 1966] and [Klo 1968], but in Me-N films, they are principally compressive.

The coating adhesion must be sufficiently high so that the stresses discussed above do not cause delamination at the coating/substrate interface. In deposition procedures such as magnetron sputtering, the residual stress resulting from sputtering deposition comprising mainly growth-induced stress is generally opposite in sign and roughly equal in quantity to the thermal stress induced by the difference in the coefficient of thermal expansion between the film and the Si-wafer substrate. As a result the magnetron sputtered films can be deposited almost stress-free. Additionally, to ensure a good adhesion of the coating to the substrate, an interfacial zone is either formed by the deposition of an adhesion layer [Helm 1985] or by using ion bombardment to promote collisional mixing at the interface [Pan 1982]. Another way to ensure good adhesion is to use substrates being structurally similar to the coating material. Indeed, structural and chemical matching between coating and substrate results in low interface energy and thus promotes high adhesion [Ash 1976].

2.2.3 PROHIBITION OF CRACK GENERATION AND PROPAGATION

Additionally to adhesion, there are other parameters, which have to be considered. The mechanical strength and ductility of the coating itself should be as high as possible. Cracks generated in the coating may cause crack initiation in the substrate and thus a complete failure of the entire system [Kut 2005b]. This problem occurs often in high-speed steel tools coated by a hard film. A relation between the coating thickness and the fracture strength of the steel substrate can be established: as long as the coating thickness is less than the size of the stress raisers within the substrate structure, which is usually around 1-5 μm for high speed steels, the amount of crack initiation from the coating is small. Nevertheless, the crack initiation can be avoided by the use of coating materials with high toughness.

2.3 HARD MATERIALS & HARDENING MECHANISMS IN ME-N COATINGS

Me-N coatings are generally divided according to their hardness into hard (20 GPa < H < 40 GPa) and superhard (H ≥ 40 GPa) coatings. In addition to a large amount of hard materials such as nitrides, oxides and borides, there are only two intrinsically superhard materials: diamond (H_V = 70 - 90 GPa) and cubic boron nitride *c*-BN (H_V = 48 GPa). These high hardness values are due to the bonding type in the materials. The best example is diamond, which has purely covalent bonds, while cubic boron nitride (*fcc*-BN), the second hardest material known, is predominantly covalently bonded, however with a small ionic contribution. The theoretical achievable hardness of a material is defined as 10% of its shear modulus G. Unfortunately the practically realizable strength and hardness of materials is orders of magnitude smaller than the theoretical one. Yet, superhardness can be achieved in a variety of nanostructured materials by an appropriate engineering of their microstructure [Zhan 2008], [Vepr 1999] and [Vepr 2008]. However it is very important to know that there are *two origins of hardness* in superhard materials: their *nanostructure*, which can be controlled by the right choice of the constituting materials and by the deposition parameters, and *internal stresses*, which are due to the deposition process. It is worth mentioning, that the superhardness originating from the microstructure is stable upon annealing, while the high hardness resulting from the high compressive stresses drops, when these stresses are released, see §2.3.4.

There are two main layouts of structures commonly used for hardness enhancement engineering in coatings: layered and granular. The first one consists of alternated layers of transition metal nitrides, which are either both crystalline, Figure 5(a), or one is crystalline and the other one amorphous, Figure 5(b). For the granular heterostructure there are two possibilities. The first one consists of different phases in neighboring nanocrystalline (*nc*-) grains, Figure 5(c), like in *nc*-TiN/BN [Zha 2008], [Vepr 2008]. The second one is composed of crystalline *Me-N* nanograins embedded within an amorphous (*a*-) matrix of a covalent nitride, Figure 5(d): *i.e.* *nc*-TiN/*a*-SiN_x [Vepr 1999], [Mus 2000], [Bull 2001] and [Män 2001] or *nc*-$(Ti_{1-x}Al_x)N$/*a*-SiN_x [Par 2004a], [Münz 2001]. These nanostructured coatings remain stable upon annealing up to temperatures of 1100°C and do not lose their hardness. To influence in a controlled way the nanostructure and thus enhance the hardness values, all strengthening mechanisms described in the above paragraphs may be applied.

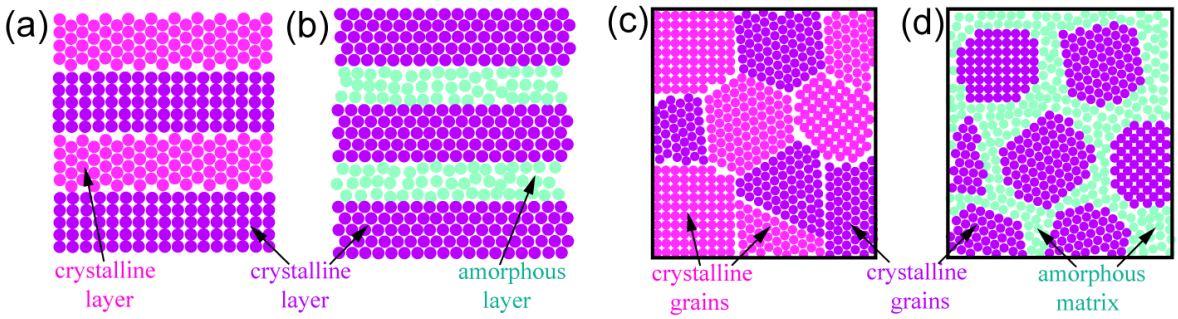

Figure 5 *Layouts of structures commonly used for hardness enhancement engineering in coatings:* **(a)** *Alternated crystalline layers;* **(b)** *Alternated crystalline and amorphous layers;* **(c)** *Nanogranular with adjacent crystalline grains;* **(d)** *Nanogranular with crystalline grains embedded in an amorphous matrix.*

For the design and the control of the microstructure of hard coatings, it is important to know the different mechanisms that can lead to the hardening of a crystalline material, mainly acting by hindering or retarding the deformation generated by dislocation movement. These mechanisms are reviewed for example in [Arzt 1998], [Mayr 2006a], [Rave 2007] and [Zhan 2007f]. In the case of crystalline thin films they can be divided into: 1. grain boundary hardening, 2. solid solution hardening, 3. age hardening and 4. hardening by energetic ion bombardment.

2.3.1 GRAIN BOUNDARY STRENGTHENING: HALL-PETCH EFFECT

The Hall-Petch effect describes a method of strengthening of materials by decreasing their average grain size. In metals, alloys and crystalline films, a decrease of the grain size below 1 µm hinders the multiplication and the movement of dislocation pile-ups at grain boundaries, so that the hardness of the material is increased according to the Hall-Petch relation [Hall 1951], [Petc 1953]:

$$H = H_0 + kd^{-1/2}$$

Where: H is the hardness, H_0 is the intrinsic hardness, k the Hall-Petch constant and d the grain size. This phenomenon is particularly well visible for grain sizes in the range between 50 – 100 nm. For $d \leq 10 - 20$ nm the dislocation activity is entirely blocked due to the absence of dislocation sources [Arzt 1998] and another deformation mechanism comes into play. The material shows than a so-called “reverse Hall-Petch” behavior, which is a decrease of hardness with decreasing grain size.

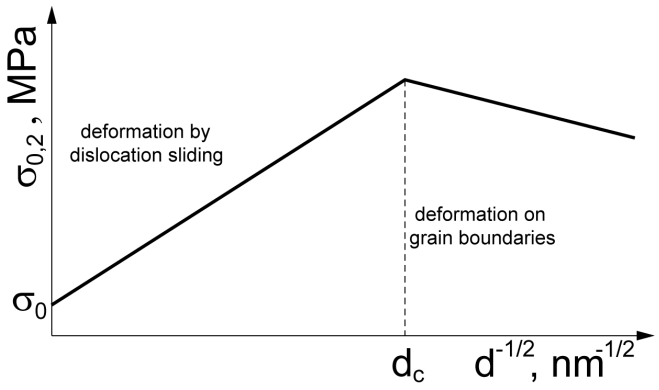

Figure 6 *Schematic representation of the Hall-Petch relation for nanocrystalline materials: above a certain critical value d_0 the deformation mechanism changes from dislocation sliding to grain boundary sliding and the hardness of the materials drops – inverse Hall-Petch effect, redrawn after Kurzydłowski et. al. [Kurz 2010].*

The origin of this effect is still under discussion and investigation [Tjon 2004]. In nanocrystalline metals, this effect is mainly attributed to grain boundary sliding. [Schi 1998], [Swy 2002]. In nanocrystalline ceramics, however grain boundary sliding, grain rotation events and formation of intergranular dislocations termed as intergranular stick-slip can interplay, with the possibility of a cooperative mechanical response from grains coupled by an amorphous intergranular grain boundary phase [Szlu 2005]. Strengthening the grain boundaries is performed by the formation of an intergranular phase made of immiscible materials. This phase also called matrix or tissue phase must form strong and defect-free interfaces with the nanocrystalline phase to be able to block grain boundary sliding. It must be also thin enough so that crack propagation is efficiently inhibited by numerous deflections at the surface of the crystalline grains. The above described arguments constitute the basic design principles of hard Me-N coatings.

Grain boundary in form of planar interfaces can also play an important role in layered structures, although the hardening mechanisms that occur are different, than the ones in nanocrystalline materials. When the bilayer thickness Λ of a periodic layered structure is in the range of about 5 nm, a significant hardness increase is observed. Dislocation blocking at the layer interface and Hall-Petch strengthening were identified as dominant effects explaining the hardening [Chu 1995], [Yas 1999]. The dislocation blocking is caused by the difference in shear moduli of the individual layers, as the dislocations prefer to remain within the layer exhibiting the lower modulus [Koe 1970]. A minimum shear stress is required to force the dislocation motion across the interface. The hardness increase is obtained in structures where the individual layers are too thin as to allow dislocation motion within them. The Hall-Petch relation assumes that dislocations cannot move across

grain boundaries. Consequently, it is only applicable for multilayer systems composed of materials having different crystallographic structures and thus different dislocation slip systems that is non-isostructural layers. The hardening effect occurs only up to an individual layers thickness in the order of 10-20 nm [Arzt 1998], [Yas 1999].

2.3.2 SOLID SOLUTION HARDENING

Solid solution hardening originates from lattice distortions generated by the insertion of atoms of the alloying element, so-called solute atoms either in interstitial or substitutional lattice positions. The resulting strain and stress fields impede the dislocation motion, increasing the yield strength of the material. By increasing the solute concentration and thus the strain caused by the solute, the shear stress needed to move the dislocations increases, however there is a limit to this effect called the solubility limit of the solute. For concentrations of the solute above the solubility limit, the excess of the solute atoms tend to precipitate either in form of particles of the solute or form a new phase of the solute with nitrogen. The solubility limit can be increased, if the films are grown in a non-equilibrium process, such as kinetically limited PVD deposition at low substrate temperature [Holl 1988]. Thus a supersaturated metastable solid solution can be deposited [Mayr 2006a], [Zha 2007]. The most well-known example in the field of hard coatings is the deposition of a metastable *fcc*-$Ti_{1-x}Al_xN$ solid solution with an Al content up to $x \approx 0.7$, whereas the solid solubility of Al in TiN is normally limited to a few atomic percent [Hult 2000], [Mayr 2006b], [Mayr 2007b]. Further examples are the following systems: Ti-C-N, Cr-Al-N or Cr-Zr-N, described by Zhang [Zha 2007].

2.3.3 AGE HARDENING

Age hardening, also called “precipitation” or “dispersion strengthening” [Arzt 1998], is a widely used process for strengthening of bulk materials. It is achieved by precipitation of a second phase from a supersaturated metastable phase. This mechanism can be accelerated and controlled by a post-deposition annealing treatment. The alloy composition and a careful control of the precipitated particles enable to maximize the strengthening effect. It results from the balance between “cutting” and “by-passing” stress, which has to be overcome for dislocation motion. The cutting stress that operates for solute atoms and coherent precipitates is proportional to $\sqrt{R}$, where R is the radius of the particle. The by-passing stress (Orowan mechanism) of particles impenetrable for dislocations varies 1/R for a constant volume fraction of particles [Arzt 1998]. Age hardening was observed for

example in TiAlN alloys, which undergo a thermodynamically driven and diffusion rate-controlled phase segregation, into nanometre-sized coherent cubic domains of *fcc*-TiN and *fcc*-AlN [Mayr 2003], [Mayr 2007a]. If additional thermal activation is provided to the TiAlN system, a phase transformation into thermodynamically stable *fcc*-TiN and wurztite AlN can occur, resulting in hardness decrease [Mayr 2003]. In the last years, thermally induced self-hardening was reported in Ti-B-N [Mayr 2006b] and in Zr-Al-N [Sanj 2006].

2.3.4 HARDENING BY ENERGETIC ION BOMBARDMENT

Ion bombardment during the film growth can be used to densify and modify the morphology of the films [Matt 1989]. It usually results in a better adhesion of the film to the substrate and is often correlated to an increasing compressive biaxial residual stress in the deposited film. This effect is commonly observed in films deposited by magnetron sputtering at low temperatures < 300°C [Vepr 2005]. It typically reaches 4–6 GPa but can even exceed values of 10 GPa. During energetic ion bombardment, gas atoms are implanted and defects are created by collision cascades, resulting in creation of interstitials or vacancies below the film surface. These point defects can interact and lead to the formation of one- (dislocations), two- (grain boundaries, twins) or three- (voids, cracks, particles) dimensional defects. These defects in turn cause lattice distortion, which was denoted as *atomic pinning* [D'Heu 1970]. The hyperthermal particles, which impinge on the film surface during deposition, can be incorporated underneath the surface by knock-on processes. Through a series of primary and recoil collisions these particles can displace bulk lattice atoms thus creating point or cluster defects [Win 1992]. Since the thin film is attached to the substrate, any microstructural change inside the layer will induce a stress in the film. This stress corresponds to a compressive bi-axial stress component for the case of defects creating a lattice expansion. It is supposed, that texture change, like for example in TiN from (001) to (111) with increasing film thickness, is related to strain energy minimization [Pel 1991], [Zhao 1997], [Oh 1993] and [Lim 2003]. Thus the grains having lower strain energy grow at the expense of those more highly strained. However, there are numerous studies [Gre 1995], [Ban 2002], [Li 2002], [Pat 2004] and [Mah 2005], which report the major role of kinetic-driven mechanisms related to anisotropy in adatom mobility and surface diffusion [Gall 2003]. It is not known if it is indeed the compressive stress, which is responsible for the hardness enhancement or the defects generating the residual stress, which act as an effective barrier for dislocation motion.

However, hardening by energetic ion bombardment yields coatings with low thermal stability [Vepr 2005], [Mayr 2006a]. Annealing leads to recovery of the deposition-induced lattice defects by migration and recombination [Hul 2000], [Mayr 2006a]. The annihilation of defects leads to relaxation of the biaxial compressive stress and consequently a decrease of hardness.

There are a lot more parameters which influence the film hardness and performance. Gradients and inhomogeneities over the film thickness are typically present in industrial coatings and result from the deposition chamber design. Due to the low deposition temperature the thermodynamic equilibrium is not reached in these coatings. Therefore only metastable phases and artificial structures such as multilayers or nanocomposites can be synthesized. Subsequently, these coatings can be subjected to controlled annealing resulting in stress relaxation, interdiffusion, recrystallization or phase transformation. These phenomena are technologically relevant since the resulting structure has a large impact on the film properties. Therefore post-annealing after the deposition procedure can allow precisely controlling the properties of the coatings.

In this manuscript only examples of hardness enhancement based on manipulation of the nanostructure of coatings will be presented.

2.4 DEFORMATION & FRACTURE DAMAGE IN HARD COATINGS

The combination of depth sensing nanoindentation and TEM imaging of cross-sections through the deformed regions applied in the present study has made possible to shed new light on the mechanisms underlying the deformation during indentation of TiN and other MeN-based coatings on soft Si and hard WC-Co substrates. The traditional approach to the mechanical characterization of coatings includes a measurement of hardness in which low loads and penetration depths, typically 10% of the coating thickness, are used to extract the film hardness. Unfortunately, electron microscopy is rarely applied to show, that in the deformed samples plasticity is indeed present on the scale predicted by hardness models. Also the fracture damage has been rarely examined in detail by direct imaging in TEM. For example bending induced cracks at the edge of the indentation and below the center, originating from the free surface and the interface, respectively, have been investigated along with the nested cracks that form parallel to the indenter edges [Kni 1989]. Some authors pointed out, that columnar films, in particular TiN growing on Si tend to slip

parallel to their columnar boundaries leading to substrate cracking [Wep 1996], [Xie 2006], [Bho 2004], [Jay 2006] and [Ma 2005]. Noticeably lacking are any detailed experimental studies on the film thickness, contact shape and size, indentation load and substrate hardness. Therefore in the frame of this study the influence of substrate hardness on the deformation mechanisms and fracture damage of columnar TiN coatings was investigated.

According to literature, in thin films the following deformation mechanisms, which are directly connected with their microstructure, are likely to occur. In columnar coatings composed of large, longitudinal columns sliding between these grains is the main deformation mode accompanied by the formation of intergranular cracks. No transverse displacement of column boundaries takes place, thereby ruling out any major role of dislocation slip [Jay 2006]. Thus the system response is a combination of an elastic film that undergoes shear cracking at a critical stress and an underlying elastic-plastic substrate as shown schematically in Figure 7(a) after [Jay 2006].

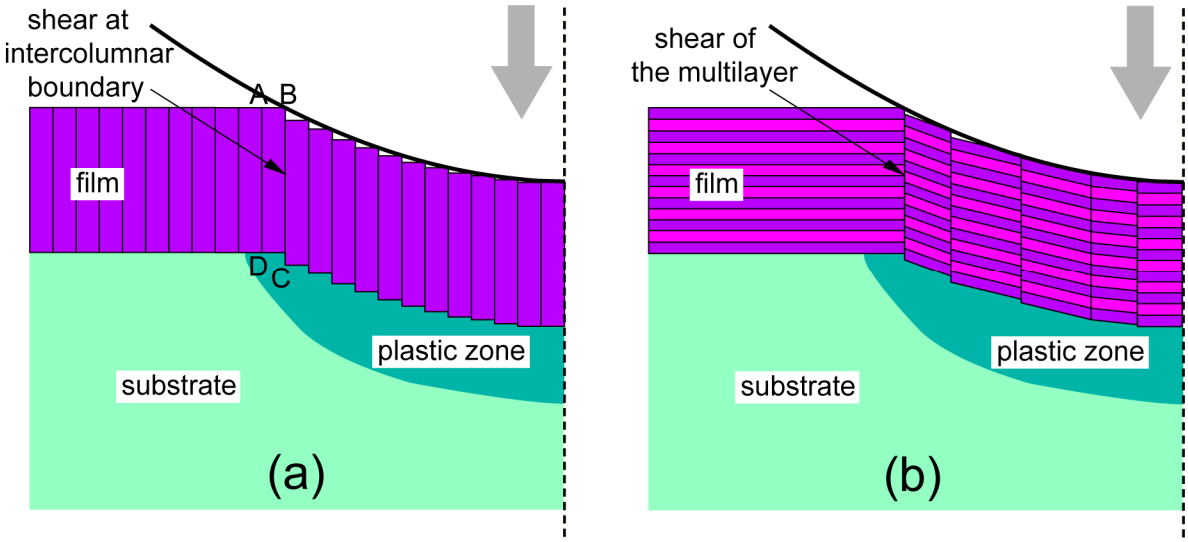

Figure 7 *Schematic representation of the partitioning of load between:* **(a)** *TiN annulus ABCD and the expanding cavity in the steel substrate, redrawn after [Jay 2006];* **(b)** *Multilayered film and a soft Si substrate, drawn based on TEM observations of the author.*

In multilayered coatings the deformation mechanism taking place can be column sliding and/or fracture depending on the thickness of the individual layers, their microstructure and properties (ductile or stiff layers), Figure 7(a) and [Par 2010], [Rze 2009a] and [Rze 2009b]. The so-called nanocomposite coatings composed of small grains separated by an amorphous matrix are subjected to grain boundary sliding accompanied by irregular cracks appearing between the grains [Cai 2005].

The intergranular shear sliding enables monolithic and multilayered coatings to absorb considerable contact strain on ductile substrates [Xie 2006], [Bho 2004], [Car 2003] and [Ma 2005]. The resistance of the grains to shear sliding *i.e.* intergranular shear stress is the parameter, which defines the coating high-load hardness and its structural integrity [Xie 2006], [Bho 2004].

While the intercolumnar shear sliding in columnar coatings is a desirable mechanism to a certain extent as it prevents failure, an increase in the resistance of these coatings to intercolumnar sliding will enhance their load-bearing ability. In a recent study on a columnar TiN coating it was demonstrated, that by increasing the residual compressive stress in TiN coatings, the resistance to intercolumnar shear sliding was accordingly increased. Nevertheless, increasing the residual stress may generate negative effects in TiN coatings *i.e.* delamination at the coating-substrate interface.

A solution for this problem may be a layered structure containing either stiff (*nc*-TiSiN) or ductile (metallic Ti) layers providing a microstructural configuration, which results in a higher resistance to deformation, than monolithic TiN coatings, as it can absorb a relatively high level of plastic strain under contact load.

In contrast to the above mechanism of accommodation, which is microstructure based, a completely different mode of fracture, that appears to be driven by the stress field, was observed by the author in bulk single crystalline TiN/MgO coatings and by Jayaram in thick DLC films on stainless steel substrates [Jar 2006]. Bulk, single crystalline, coatings, which do not have these easy boundaries for slipping, are more prone to fracture when the substrate begins to deform. This type of behavior is characterized mainly by shear cracking on inclined planes, corresponding in the case of the single crystal to the easy crystallographic directions i.e. <002>, <111> and <220>, Figure 8. While other modes of cracking, such as the bending cracks and surface nested cracks co-exist with the inclined cracks, the latter are significantly longer and are able to combine with the others and lead to spalling. Thus the little quasi-plasticity, that the film exhibited by inter-columnar sliding, is absent here and the system coating-substrate undergoes severe fracture. Jayaram [Jar 2006] showed in his work, that on a suitably hard substrate, such as tool steel, the inclined cracks never appear, even when the indenter displacement is several times the film thickness.

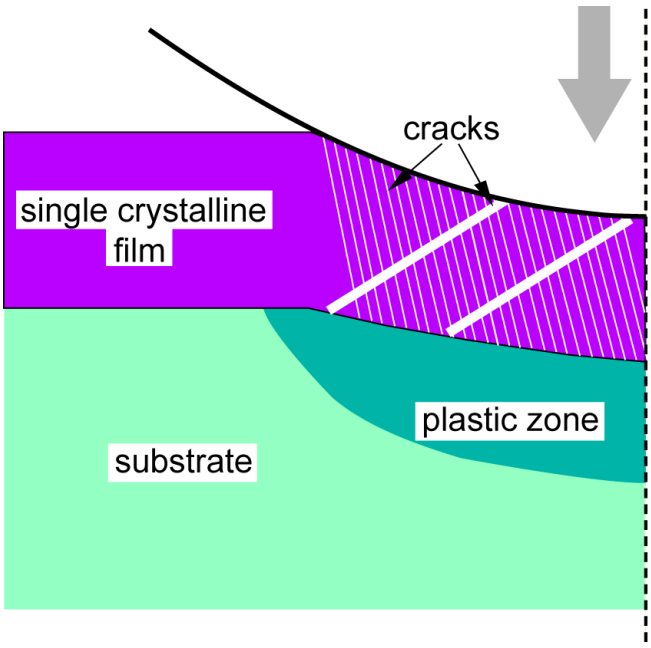

Figure 8 *Schematic representation of the partitioning of load between a single crystalline film and a soft substrate, drawn based on TEM observations of the author.*

The justification for the change in fracture behavior with film thickness and substrate plasticity comes from the fact, that if the substrate is too soft or too far away due to the too thick film, than the average stress along the TiN columns does not reach the critical value before significant plasticity sets in. During this period, a large strain mis-match develops between a predominantly elastic film and a plastically deforming substrate. This analysis was confirmed by carrying out a purely elastic analysis of Hertzian contact in a bi-material system using the method of Hankel transformation [Li 1997].

The perspective on thin films design that now emerges is the one in which the usefulness of columnar coatings stems for their ability to accommodate point loading through a mechanism that permits deformation without fracture but at a reasonably high stress, so that the substrate is indeed protected by the coating. Equiaxed, amorphous or single-crystalline coatings, which do not have columnar boundaries for slipping, tend more to fracture when the substrate is deformed.

According to Jayaram [Jar 2006], it appears that for soft substrates, on which nitrides such as TiN are deposited for decoration or corrosion protection, should not be given a too thick coating, which is in contrast to the intuitive tendency to protect a weak material by increasing the thickness of the protective layer. Hard substrates, such as tool steels and cemented carbides, which can withstand thick coatings, without exhibiting inclined or other forms of fracture, can exploit the added protection of thicker films in applications

where high contact stresses may lead to gradual coating removal over a period of time. The prediction of such a maximum useful thickness that is dictated by the substrate yield in strength and the inter-columnar shear strength, is another constraint to use for such coatings in addition to the one dictated by the limits imposed by spontaneous spalling due to the residual stress in the film.

2.5 TYPES OF COATING STRUCTURES WITH ARTIFICIALLY INDUCED INTERFACES

The coatings can be divided into three categories according to their microstructure: monolythic columnar coatings, nanocomposites and multilayers. These layouts should enhance the hardness properties.

2.5.1 MONOLITHIC COLUMNAR COATINGS

When deposited, all binary transition metal nitrides, with the exception of SiN, grow as large columns, Figure 9(a). Their length can reach up to the entire coating thickness and their width is up to 200 nm. In binary metal nitride coatings the columns are separated by straight grain boundaries, Figure 9(a). Depending on the deposition conditions in particular the temperature, the columns can be single-crystalline throughout their entire length or be composed of several zones of different orientation, crystallographic phases or chemical composition, Figure 9(b). These zones are separated by low angle grain boundaries, which are composed of dislocations. Such structures are harder due to the decreased mobility of dislocations inside the columns.

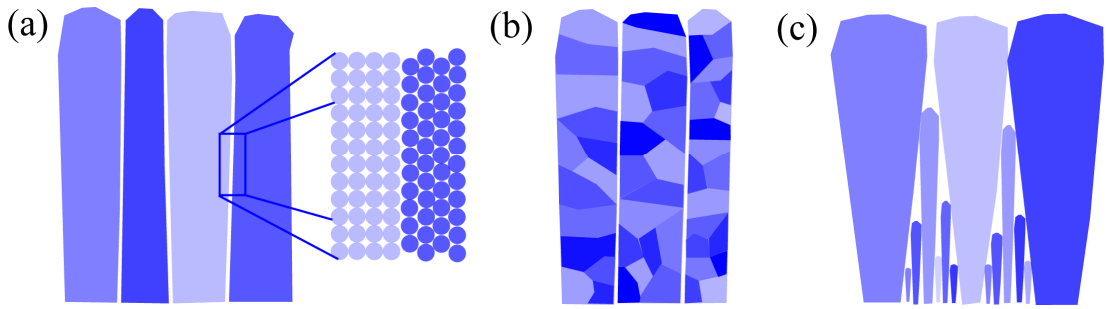

Figure 9 *Schematic representation of different types of columnar structures:* **(a)** *Typical columnar structure, where each column has a single crystalline character and the magnification showing the atomic arrangement at the interface of two adjacent grains;* **(b)** *Columnar structure with grains composed of zones of different orientations, see text for details;* **(c)** *Cauliflower-like columnar coating: the small grains at the bottom result from the shadowing effects.*

The shape of the columns can change depending on the nitride system and the deposition conditions. For most of the *Me-N* coatings, the columns are nearly straight, but in some cases this difference in width between the bottom and top is much more pronounced, Figure 9(c). This leads to a so-called *cauliflower structure* consisting of large trapezoidal grains located next to each other and the free spaces in between are filled with very fine grains or remain as voids. The effect at the origin of this kind of structure is called the *shadowing effect*. It is an effect preventing a uniform coverage of surface features during sputter deposition: the atoms and ions from the target reaching the substrate under certain angle will not uniformly coat the substrate surface [Dir 1977]. The surface roughness of the substrate also significantly influences the coating: a higher substrate surface roughness results in a less complete coverage of the substrate with the coating material because of shadowing effects during PVD film growth.

The shadowing effect occurs mainly in ZrN coatings, Figure 10(a). Coatings exhibiting trapezoidal grains due to the shadowing effect have often an underdense structure, contain many voids and exhibit thus lower hardness values. The magnified dark field image of one of the columns, Figure 10(b), clearly shows, that the column possesses an internal structure, as schematically shown in Figure 9(b), and is far from being single crystalline. This is also confirmed by the HRTEM image, Figure 10(c) containing Moiré fringes. Indeed, Moiré fringes originate from the overlapping of two lattice systems, which are either rotated in respect to each other by a very small angle or which have slightly different lattice constants without being rotated.

In some coatings, in which a lot of stresses arise during the deposition procedure, twinning as a result of accommodation of stresses occurs. This is very nicely illustrated in the NbN coating, Figure 10(d), where the twinning is a stress release mechanism. The twinning lamellas are also clearly visible in the HRTEM image shown in Figure 10(e). More information on the structure of this coating is presented in [Sand 2006].

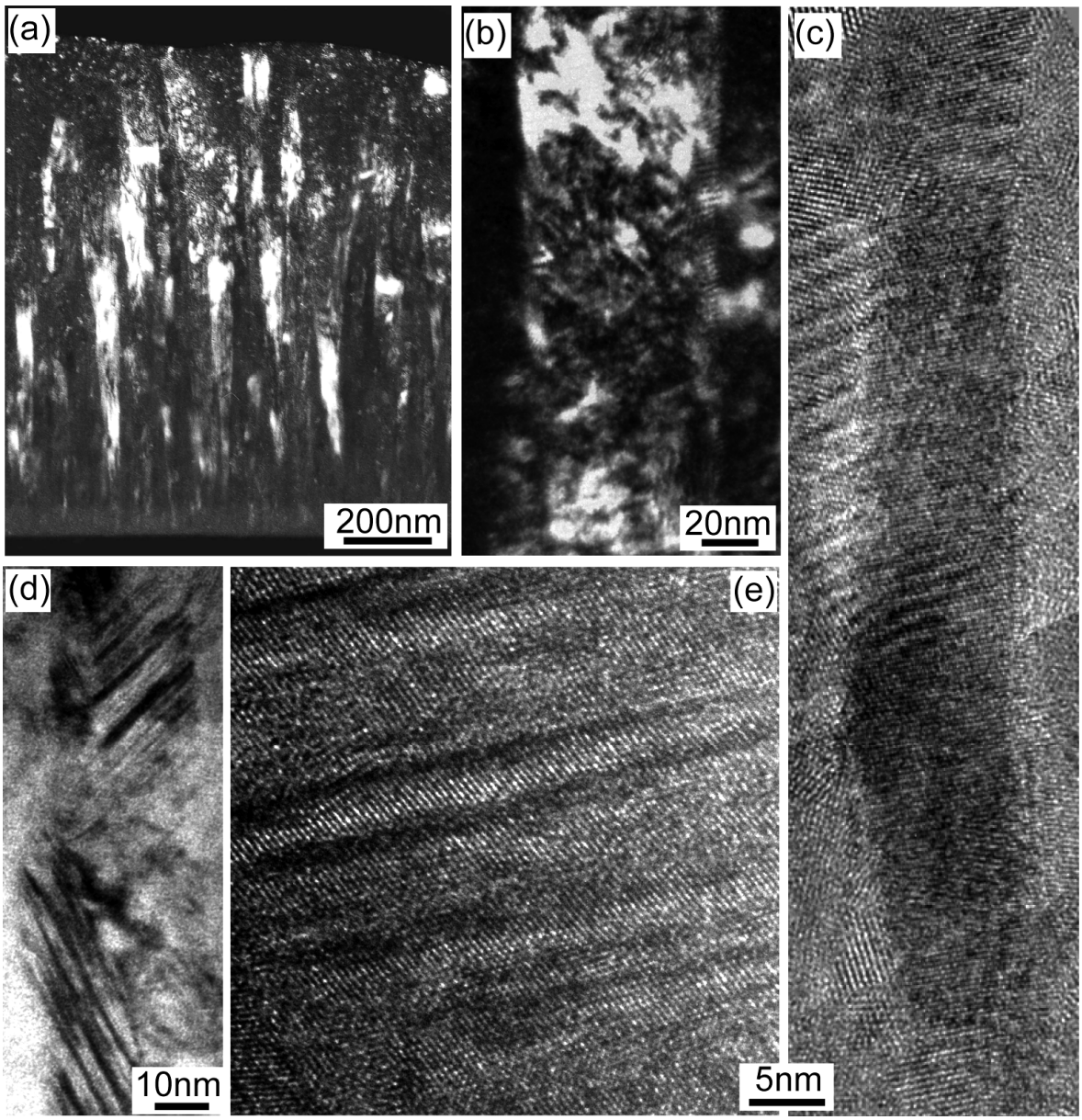

Figure 10 (a) *TEM dark field image of the ZrN coating cross-section;* **(b)** *Magnified dark field view of one column clearly showing, that the column has not a single-crystalline structure;* **(c)** *HRTEM image of one of the ZrN column. The Moiré fringes prove the presence of differently oriented atomic planes;* **(d)** *Bright field of one NbN column containing two different twinning systems;* **(e)** *HRTEM image of the twinning inside the NbN column.*

Moreover, at least for some *Me-N* systems, there is a dependence of the film orientation on the film thickness: the first few deposited monolayers have a certain orientation, which is stable and remains if the film is left at this thickness, but it changes to a different although stable orientation, if the deposition is continued to obtain a thicker coating [Gre 1995].

It is also possible to differentiate these zones chemically by adding a second metallic element into the *Me-N* coating hence it is either dissolved in the lattice and the columns

remain single-crystalline or the element forms a second phase, which is also located inside the columnar grains leading to the formation of differently oriented zones which are in addition chemically dissimilar.

A particular behavior is observed in the case of silicon addition. Most of the metal nitrides have a very low solubility of Si, consequently an amorphous SiN_x phase is formed, which precipitates at grain boundaries, thus blocking the growth of columnar grains. Therefore, the more Si is added into the *Me-N* coating the smaller its grain size as schematically shown in Figure 11, after Patscheider *et. al.* [Pat 2001].

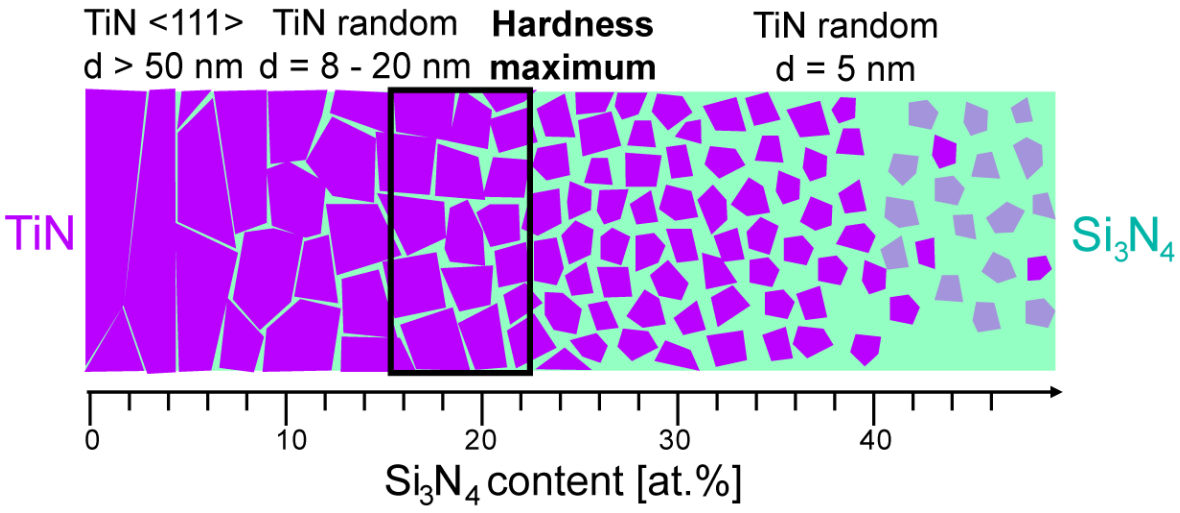

Figure 11 *Schematic representation of the TiN grain size reduction with the increasing concentration of the amorphous Si_3N_4 phased. The zone highlighted by the black square corresponds to the hardness maximum. After Patscheider et. al. [Pat 2001].*

When reaching 6% Si the volume of the SiN_x phase, it is important enough to form a monolayer of SiN around each *Me-N* grain leading to the formation of a so-called *matrix*. Thus the obtained structure is called a *nanocomposite* described in detail in the following paragraph.

2.5.2 NANOCOMPOSITES

In the case of thin film the designation of "nanocomposite" is very specific, and does not necessarily correspond to the definition of nanocomposite used in other groups of materials. The main aim to create this kind of structure in the coating is to achieve a hardening effect. According to Patscheider [Pat 2001] high hardness in nanocomposite coatings is obtained when they consist of crystalline nanograins of having the size between 5-10 nm separated statistically by 2-3 atomic layers of an amorphous phase, Figure 12. The hardness is directly linked to the nanostructure of the nanocomposite. For this kind of

structure the volume fraction of the amorphous phase is well defined. The grains, which can be a nitride or carbide of a transition metal, should be *equiaxed*, *i.e.* have a nearly spherical shape. The matrix is always amorphous and in most of the cases it is SiN or SiC.

Another condition to produce superhard coatings from such multi-phase systems is that both phases have to be immiscible. An excellent example of what happens, when the immiscibility rule is not respected are AlSiN coatings presented in detail in §5.2.2 and [Péli 2007]. An additional requirement is that the cohesive energy at the interface between the phases must be high [Vepr 2006].

The formation of a nanostructure in superhard nanocomposites is based on a spontaneous unmixing of inherently immiscible binary metal alloys at the limit of metastability: the so-called *spinodal decomposition*, which occurs in a spontaneous way during the deposition procedure [Vepr 1995].

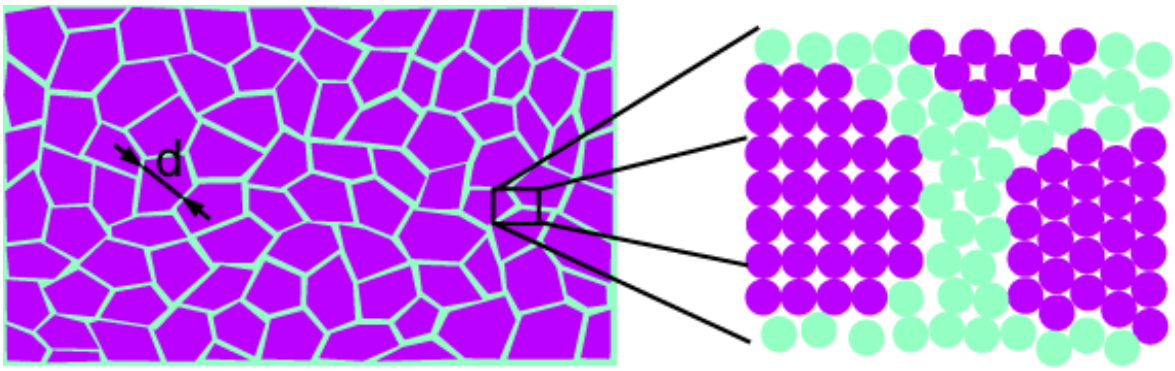

Figure 12 *Schematic representations of a nanocomposite and its magnification showing the atomic arrangement at the interface of three adjacent grains separated by an amorphous tissue layer.*

Deposition techniques, which allow evaporating different materials simultaneously from targets by sputtering either in a reactive or non-reactive atmosphere, are very useful tools for preparation of nanocomposites with varying amounts of nanocrystalline and amorphous phases. Thus by the simultaneous growth of immiscible phases, nanocrystalline compound materials can be obtained by vapor deposition. For this, the films must grow in the miscibility gap of quasi-binary compound systems. There, continuous nucleation and growth by segregation of insoluble elements and formation of thin segregated layers of the second phase on top of the growing nuclei take place. This process prevents coalescence and repeated nucleation, thus limiting grain size to about 10 nm in the film. The amount and type of phases and additional elements can be used to control the orientation and the crystalline grain size of the films [Vepr 1996].

Thus, an appropriate selection of binary or ternary refractory hard materials allows one to prepare superhard nanocomposites whose nanostructure and the resultant hardness remain stable up to high temperatures of 1100°C. In these nanocomposites, the nanocrystals of the transition metal nitride are embedded within about 1 monolayer thin amorphous tissue phase, which provides the materials with a high hardness, resistance against crack formation and propagation and as well as good thermal stability. Examples of such systems are *nc-MeN/a-*Si_3N_4 (*Me = Ti, W, V,* ($Ti_{1-x}Al_x$), and other hard transition metal nitrides [Vepr 1995], [Vepr 1999]). Another possibility to form a nanocomposite structure is a combination of two nanocrystalline phases such as (*nc-TiN/nc-*TiB_2 [Mit 1999] or *nc-TiN /BN*) resulting in the formation of a so-called *phase modulated nanocomposite*.

2.5.3 NANOMULTILAYERS

If two different materials are deposited on top of each other in form of layers, having a thickness in the nanometer range, the resulting coating is called *multilayer* or *superlattice*, Figure 13. Considering the properties of the individual hard materials, it is possible to construct coatings in which the layer next to the substrate provides good adherence, one or more intermediate layers, which are responsible for hardness and strength and the outer most layer, which reduces the friction, adhesion and reactivity.

Multilayered structures are often deposited as model structures for nanocomposites. In this way the problem of studying three-dimensional nanocomposites can be reduced to two dimensions, or even to one, if the interest is focused on the interface.

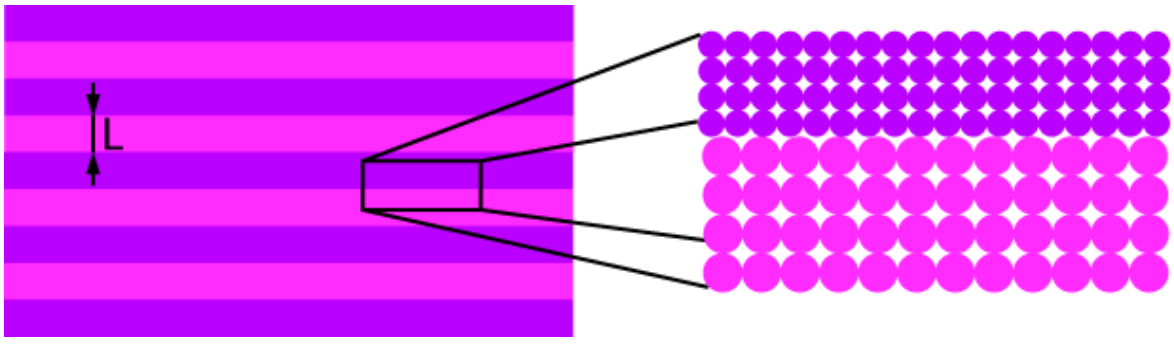

Figure 13 *Schematic representations of a multilayer stack and its magnification showing the atomic arrangement at the interface.*

The hardening mechanisms, described in detail in Chapter 2 §2.3 for nanocomposites, are also valid for multilayers. The composition and thickness of the individual layers have a large impact on the properties of the resulting system. To design in a controlled manner very hard multilayers consisting of nanometer scale layers of different nitrides the origin of high hardness values has to be elucidated. The bi-layer period Λ seems to be one of the crucial parameters since the high hardness values are achieved mainly in the range $\Lambda \approx 5\text{-}10$ *nm*.

In multilayered coatings the most important element is the interface, which can enhance or deteriorate certain properties of the resulting system. Depending on the interface type the multilayers can be divided into two categories: *isostructural* and *non-isostructural*. Both are based on the phase difference concept applied for nanocomposites, described in § 5.1.2 with the difference that in nanocomposites dislocations can not be generated inside grains with a size below 10 nm, whereas in multilayers, with a layer thickness superior to 10 nm, they can.

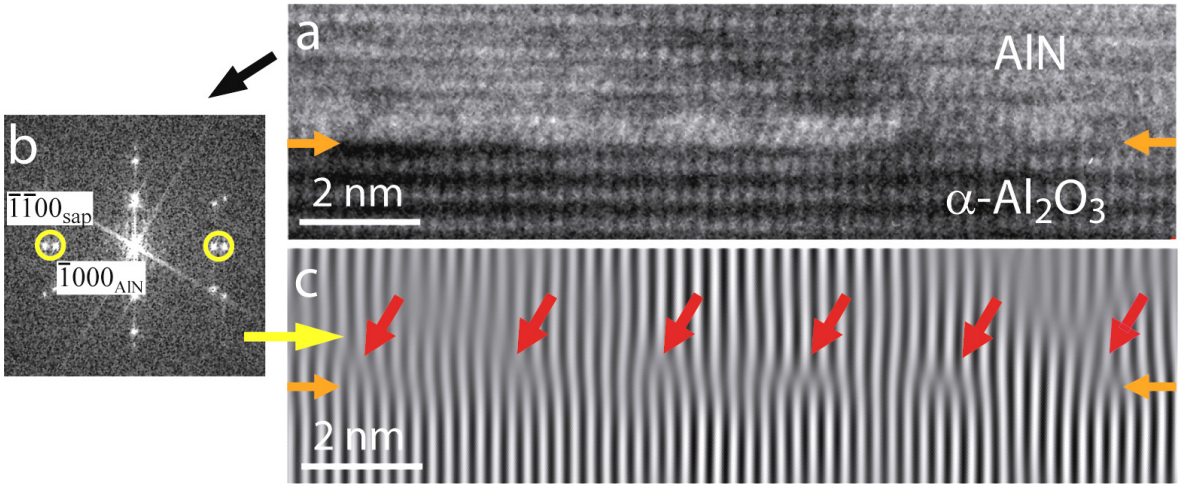

Figure 14 (a) *Epitaxial interface between Al_2O_3 and AlN marked by orange arrows;* **(b)** *Corresponding FFT pattern with two sets of spots originating from the two lattices;* **(c)** *Inversed FFT from the two spots marked in yellow, showing regular misfit dislocations at the semi-coherent interface occurring every 8 or 9 atomic planes.*

Isostructural layers are defined as those, in which the individual layers have the same structure. To form an epitaxial interface between two adjacent layers, such as shown in Figure 14(a) between Al_2O_3 and AlN, the crystals should have the same orientation but slightly different lattice parameters. Thus both crystalline lattices have to be deformed until both lattices can be fitted. The resulting interface contains misfit dislocations arranged

periodically and is thus referred to as a semi-coherent interface. When a strained layer grows with a semi-coherent interface, the elastic strain energy increases proportionally to the volume, but can be released by introduction of crystal dislocations into the interface. They are called *misfit dislocations,* shown by red arrows in Figure 14(c), and allow the lattice parameter to return to the stress-free equilibrium value. These misfit dislocations generate strain fields inside the multilayers, which however has a negligible influence on the hardness enhancement.

Coherent interfaces are most commonly observed for metallic hard materials, which are able to form coherent or partially coherent interfaces with metals or other metallic hard materials. Thus low energy interfaces with optimum adherence can be obtained. They usually have the same dislocation slip systems consequently it is possible for dislocations to move across layer interfaces. The most popular among *Me-N* isostructural layers are combinations of TiN, CrN and NbN. The mechanical properties, hardness and deformation mechanisms of multilayers consisting of combinations of those materials are presented in [Rze 2009a] and discussed in detail in §6.

Yet, to enhance hardness of the multilayer it is necessary to provide a barrier for the dislocation motion at the interfaces. One possibility is to design two adjacent layers exhibiting different shear moduli. Thus they have different dislocation line energies. Subsequently the dislocations prefer to remain within the layer having the lower shear modulus. To move the dislocation into the layer with the higher shear modulus an additional stress is required, compared to the stress necessary to move the dislocation inside a homogeneous layer with a lower shear modulus.

Another possibility is to deposit non-isostructural multilayers where the neighboring layers act as dislocation barriers. These layers exhibit different structures and consequently different dislocations slip systems. A further barrier for dislocation motion is thus provided.

In some cases the so-called *epitaxial stabilization effect* is observed. It occurs, when two materials having different crystal structures, which should not be able to form a coherent or semi-coherent interface, are deposited in a multilayered structure. At certain conditions one layer can crystallize in a metastable structure, which does form a epitaxial interface with the other layer. The metastable structure is almost always observed in layers with individual layer thicknesses below 2 nm. This is due to the extremely high amount of interfacial energy in this type of structures. The best known example is the TiN/AlN

multilayer [Mad 1997]. AlN crystallizes usually in a hexagonal wurztite-type structure, while the TiN is cubic. Nevertheless, in the multilayer system with individual layer thickness below 2 nm the AlN is forced to crystallize in a cubic *NaCl*-type structure, thus forming a coherent interface with TiN. Additionally to dislocation blocking mechanisms, which appear in the thus formed isostructural layers, the bulk modulus, and presumably the hardness of the metastable AlN layer, is much higher for the *NaCl* structure than for the *hexagonal wurztite*-type one [Mad 1997]. Therefore by stabilizing a new crystal structure, the mechanical properties of the coating can be controlled, yet the hardness prediction for the obtained multilayer system is difficult, due to the fact, that the mechanical properties of these metastable structures are generally unknown.

The second way to obtain non-isostructural multilayers presumes that one material forms a hard crystalline Me-N phase the other an amorphous phase. The most popular example is a multilayer consisting of *fcc*-TiN alternated with *a*-SiN described in detail in [Par 2001] and §5.3.2.

In multilayers the hardness can also be improved by the so-called *supermodulus* effect being defined as a large enhancement of the elastic constants. Thus since the hardness depends on the elastic properties of the material, the increasing of the elastic constants explains the hardness enhancement [Mir 1990]. However, due to the fact, that it is very difficult to measure accurately the elastic properties of thin films, this effect is very challenging to be studied.

Experimental details

3 DEPOSITION PROCEDURE OF COATINGS:

The coatings investigated in [Par 2004a], [Par 2004b], [Par 2010], [Rze 2009a], [Rze 2009b] and [Péli 2007] were deposited by *reactive magnetron sputter deposition*, which is one of the variants of the physical vapor deposition (*PVD*). The PVD process is a general term used to describe a variety of methods to deposit thin films by the condensation of a vaporized form of material onto various bulk materials. This method involves purely physical processes such as high temperature vacuum evaporation or plasma sputter bombardment, contrary to chemical vapor deposition, which involves a chemical reaction at the coated surface. The term physical vapor deposition was first introduced in 1966 by C.F. Powell, J.H. Oxley and J.M. Blocher *Jr.* in the book *"Vapor deposition"* [Pow 1966].

3.1 SPUTTERING PROCESS

Sputtering is a physical vapor deposition (PVD) process that involves the kinetic ejection of atoms from a solid source known as target. This is the result of a sequence of energetic collisions with accelerated ions from a gas phase. The incident particles are implanted in the material and the sputter yield drops since little energy is released near the target surface. The sputter yield is defined as the ratio between the number of emitted particles and the number of incident particles.

In sputter deposition, the ion bombardment of the target surface is usually realized in a plasma environment. In the plasma system, a plasma of neutral (Ar) and/or reactive gas (N_2, O_2, CH_4, He) is created between an anode and a cathode. The anode is usually the grounded chamber wall. The target material is biased negatively and constitutes the cathode. Positive ions in the plasma near the cathode region are accelerated at high energy onto the cathode surface and cause the sputtering of the target surface. In this configuration, the plasma is sustained by the emission of secondary electrons from the cathode surface caused by ion bombardment. These electrons are quickly accelerated in the gas phase and cause additional ionization of gas atoms.

3.2 MAGNETRON SPUTTER DEPOSITION: PRINCIPLE

When a magnetic field is added near the cathode region, a magnetic confinement of the plasma can be created. This means, that small magnets are arranged in an ellipse-like or a circular ring at the back of the target so that the drift path of electrons forms a closed loop. In the case of a planar target with a circular arrangement of magnets, the magnetic field is

radial to the surface and the closed-loop path is a broad circular band at the target surface. In this region, the target erosion proceeds faster and the erosion track, called “the racetrack”, is progressively formed during sputtering.

3.2.1 REACTIVE MAGNETRON SPUTTERING

Metallic multicomponent films can be deposited from compound targets with the desired stoichiometry. Oxide, nitride, carbide and sulfide compounds can however also be deposited by sputtering from metallic targets in the presence of a reactive gas (oxygen, nitrogen, acetylene, etc.) usually mixed with an inert working gas (Ar). Since high purity metal targets are easier to manufacture than compound targets, they are used more often in combination with high purity gases commercially available. Depending on the amount of reactive species introduced in the deposition chamber, a solid solution of metal doped with the reactive element can be deposited as well as a compound or a multiphase alloy. A wide range of composition is accessible. The deposition conditions strongly depend on the reactive gas flow. Low flows of the reactive gas lead to entire removal from the gas phase of the reactive species by adsorption at the substrate and the cathode surface. As a result the chamber pressure remains constant, as if no reactive gas was added, resulting in a metal-rich film. By increasing the gas flow, the concentration of the reactive species in the deposited film increases and they start to react with the target surface: the sputter target becomes “poisoned”. Consequently the sputter yield of the compound target surface is reduced, as compared to the sputter yield of the pure metallic surface.

Additionally, a bias can be applied to the substrate to increase the ion bombardment of the growing surface so as to densify the structure. However, the increasing energy of impinging ions as the bias is increased results in lattice damages, compressive stresses and inert gas incorporation.

Reactive magnetron sputtering is an attractive industrial deposition technology due to high sputter rates. Two or more magnetron sources (cathode with target + magnets at its back) are operated in a controlled atmosphere of one non-reactive gas such as Ar and one or more reactive gases. Numerous coatings can be produced by magnetron sputtering. In Löffler *et al.* [Löf 1994], the popular coating systems deposited by combining various target materials with different reactive gas components can be found. Each of these coatings can be deposited in wide composition range and hence with varying properties.

To deposit multilayered coatings the magnetron sources are operated permanently and the respective shutters are opened in alternance to obtain the desired multilayer sequence.

To deposit nanocomposites with $a\text{-}Si_3N_4$ tissue phase, silicon may be introduced into the coatings by concurrent operation of a titanium magnetron source operating with a silicon cathode. This approach has been successful both by simultaneous deposition of the two fluxes and by alternating arc and magnetron deposition [Münz 2001], [Pel 1991] and [Mus 1998]. Moreover it is possible to use specially alloyed Me-Si targets with different Si contents.

3.3 FILM GROWTH AND MORPHOLOGY

The major advantage of magnetron sputter deposition compared to evaporation or CVD processes is the high deposition rate and the low substrate temperature T_s, which is often lower than 0.2-0.3 of the melting point T_m (in Kelvin). The films are grown far from thermodynamic equilibrium and kinetic effects play a major role, so that metastable phases can be synthesized [Holl 1988]. The film microstructure: grain size, crystallographic orientation, defects, surface and bulk morphology, depends on the used deposition conditions. The most important physical parameters for the control of the microstructural evolution of thin films are surface and bulk diffusion rates. The primary parameter that controls diffusion rates and subsequently the film microstructure is the so-called homologous temperature T_s/T_m. Structure Zone Models (SZM), constructed by the compilation of experimental results, have been developed to systematically categorize the structural evolution of thin films during PVD deposition, as a function of the homologous temperature or other deposition parameters. These other parameters can be: the deposition pressure [Thor 1974], the substrate bias [Mess 1984] and the ion-to-atom ratio at the substrate [Kell 1998] are the chosen parameters. The most famous SZM is shown in Figure 15 and was developed by Thornton [Thor 1974] [Thor 1977].

This structure zone model consists of three zones and a transition zone between zone 1 and zone 2. At low homologous temperatures corresponding to zone 1, the adatom mobility is low and the films develop an underdense structure with a fine fiber texture. In this regime atomic shadowing is the dominant process. The columns, composed of equiaxed grains, are separated by pores, or voids. The surface roughness is usually quite important. With increasing homologous temperatures, the surface diffusion process becomes more important corresponding to zone T in the scheme in Figure 15. The columnar structure is

preserved but the formation of voids is suppressed thus the films are dense. Grain coarsening occurs during coalescence of small islands and thus the crystallites grow with preferential orientation. As the film grows, small randomly oriented crystallites at the substrate develop into larger crystallites with a pronounced texture (preferred crystallographic orientation), resulting in characteristic cauliflower-shape grains, Figure 9(c). This growth mode is called *competitive grain growth* and the resulting structure is inhomogeneous along the film thickness. The dominant crystallographic orientation is determined by anisotropic surface diffusivities and adatom potential energies. Kinetically disadvantaged columns quickly disappear during the growth. This is intensified by simultaneous atomic shadowing effects. The grain boundary migration (bulk diffusion) remains limited in this region.

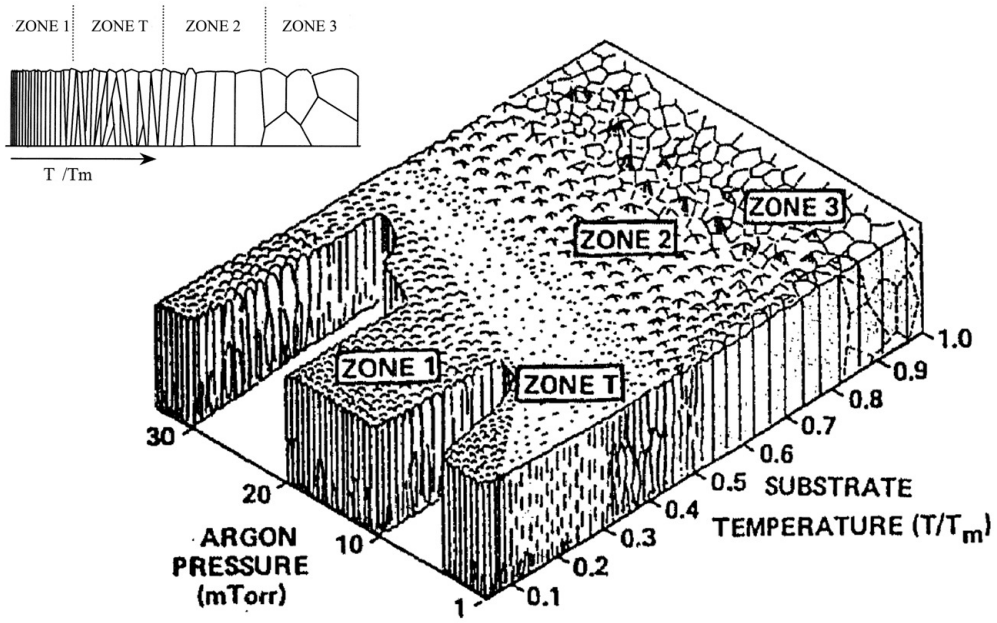

Figure 15 *Structure zone model developed by Thornton [Thor 1977]: schematic representation of the influence of argon pressure and substrate temperature on the morphology of the growing film. T is the absolute temperature and T_m is the melting temperature of the coating material. A profile of the structure model is given in insert to emphasize the main structural characteristics [Barn 1998].*

By further increasing T_s/T_m zone 2 is reached. There bulk diffusion becomes considerable and grain migration can also occur to minimize interface and surface energies. The surface roughness decreases and the grains are larger due to orientation selection at the initial growth stages. The film structure is homogeneous in thickness: the columns extend from

the bottom to the top of the film with vertical grain boundaries. At higher substrate temperatures passing to zone 3, the columnar structure of the films is suppressed and they consist of equiaxed three dimensional grains as a result of bulk diffusion process, recrystallization and grain growth. The structure is fully dense.

Often, impurities act as grain refiners through a solute drag effect on grain boundary motion [Cahn 1962] [Mich 1999]. At very high concentrations, complete impurity layers (tissue phase) can entirely cover the surface of growing crystallites, stopping their growth and forcing repeated nucleation of random oriented crystallites. The grain size can be decreased in the nanometer range and the columnar structure is lost. The obtained structure is dense and the surface roughness remains low. The two-phase structure moreover ensures a higher thermal stability by efficiently blocking grain coarsening due to the presence of an immiscible phase at the grain boundaries. This effect is used in the deposition of hard nanocomposite coatings [Petr 03] [Musi 01c].

4 CHARACTERIZATION TECHNIQUES

4.1 NANOINDENTATION

Indentation techniques are used to determine the hardness of a material. These techniques consist in pressing an indenter of known geometry into a surface under a fixed load. The depth of penetration or the area of the resulting impression can be used as a measure of the resistance against deformation of the studied material. The hardness H of a material is defined as its resistance to plastic deformation and is expressed as the ratio between maximum load P_{max} and contact area A:

$$H = P_{max} A$$

In conventional hardness testing A is measured after the test on the residual imprint in the surface. Hardness is not an intrinsic property of a material but is a sum of many effects contributing to the finally measured hardness. These effects comprise yield strength, grain boundary effects, defect distribution etc.

4.1.1 THEORY OF INSTRUMENTED INDENTATION TESTING

Nanoindentation technique is used to study the mechanical properties of thin films at very small depth in the micrometer range or below. When a diamond indenter is driven into the

specimen surface the applied load is dynamically recorded as a function of displacement. As the indenter is pushed into the material having a very smooth and flat surface, both elastic and plastic deformation, cause the formation of a hardness impression conforming to the shape of the indenter to some contact depth, h_c. As the indenter is withdrawn, only the elastic portion of the displacement is recovered. This is the recovery, which allows the determination of the elastic properties of a material. Hardness and Young's modulus, also called elastic modulus or E modulus, are deduced from load-displacement curves, as well as the projected contact area A_c. To calculate H and E, "Oliver and Pharr" and "Field and Swain" methods are most commonly used. They are all reviewed in [Fisc 2000].

4.1.2 INSTRUMENT AND INDENTER TIP

All indentations investigated in this study were performed on an MTS Nano Indenter XP system equipped with a Berkovich tip specially designed for small depth indentation, as it produces plasticity at very low loads. The Berkovich tip is a three-sided pyramid with an angle of 65.3° between the normal to the sample surface and tip face.

4.2 TRANSMISSION ELECTRON MICROSCOPY TECHNIQUE

The transmission electron microscope (TEM) is one of the most powerful tools in materials science research. It allows studying locally the microstructure of the material providing insight into the structure of the material down to the atomic level, including also crystallographic and chemical information. However the technique itself, although very powerful, is complicated and requires a lot of theoretical background to interpret the obtained micrographs. The sample preparation is very time consuming and the success in observation depends mostly on the sample quality. In paragraph 4.3 the two sample preparation techniques used by the author, are shortly described.

In a conventional transmission electron microscope (*TEM*) [Edi 1974] a few tens of nanometers thin specimen is irradiated with an electron beam of uniform energy and current density. The electron energy is in the range of 100 to 300keV. The electrons are emitted in the electron gun by thermoionic emission from a LaB_6 crystal or by field emission from a pointed tungsten filament, when high gun brightness is required. A two-stage condenser-lens system permits the variation of the specimen area that is illuminated. Bright field contrast is produced either by absorption of the electrons scattered to angles larger than the objective aperture (scattering contrast) or by interference between the scattered wave and the incident wave at the image point (phase contrast). The electron-

intensity distribution behind the specimen is imaged with a three or four lens system onto a fluorescent screen. The best resolution which is achieved now a days is about 0.5 Å with the newest aberration corrected TEM equipped with a high brightness gun [Erni 2009].

4.2.1 IMAGING MODES

- *Bright field imaging*: this mode provides insight on features like grain shape and size, grain boundaries, interfaces, dislocations, stacking faults, twins, different phases but also cracks, voids, bubbles and other imperfections at the micro and nanoscale.
- *Diffraction patterns*: supply knowledge about the crystallinity of the specimen and its constituent phases, lattice parameter, superstructures, epitaxial relations of different phases, etc.
- *Dark field imaging*: the image taken with one of the diffracted beams contains information about the grain orientation in the material and allows to image defects like dislocations or precipitates at larger scale.
- HRTEM: *high resolution* allows seeing the atomic structure of the material, but also defects such as dislocations or stacking faults.
- STEM (scanning TEM): in STEM information about the specimen is collected in a serial acquisition mode. The specimen is illuminated with a convergent electron beam which is focused to a small spot at the height of the specimen. The image is recorded by scanning the electron probe in transmission mode and projected on a bright field (BF), dark field (DF) or high angular annular dark field (HAADF) detector. The BF and DF field images are qualitatively complementary to each other. The HAADF image contains chemical information from the sample (z-contrast) depending on the atomic number of an element: higher number elements will be brighter on the HAADF image.

The electrons interact strongly with atoms by elastic and inelastic scattering. The specimen must therefore be very thin, typically of the order of 5 nm to 200 nm for 200keV, depending on the density and elemental composition of the sample and the resolution desired. Special preparation techniques are needed to obtain electron transparent specimens. Two preparation techniques: *mechanical polishing followed by ion milling* and *focused ion beam thinning* are presented in paragraph 4.3.

4.2.2 ANALYTICAL MODES

A). **ENERGY DISPERSIVE X-RAY SPECTROSCOPY (EDS OR EDX):**

EDX is an analytical technique used for elemental analysis of a sample. It is particularly sensitive to heavier elements. The electron transparent sample is irradiated by the electron beam with energy of typically 100-300 keV. Thus X-rays, characteristic of an element's atomic structure, are emitted from the sample and then detected and analyzed by the energy dispersive spectrometer. They can be identified uniquely from each other. Elements of low atomic number are difficult to detect by EDX, as the EDX detector is often protected by a Beryllium window. The absorption of the soft X-rays by the Be precludes the detection of elements below an atomic number of 11 (Na). By moving the electron beam across the material one dimensional linescans and two dimensional maps of elemental distribution inside the sample can be obtained. However, due to the low X-ray intensity, images usually take several minutes to an hour for acquisition.

B). **ELECTRON ENERGY LOSS SPECTROSCOPY (EELS)**

EELS allows measuring atomic composition, chemical bonding, valence and conduction band electronic properties, surface properties, and element-specific pair distance distribution functions. It is most suitable for the analysis of elements with relatively low atomic numbers. In electron energy loss spectroscopy the sample is exposed to a beam of electrons with a known, narrow range of kinetic energies. Some of the electrons will undergo inelastic scattering, which means that they lose energy and have their paths slightly and randomly deflected. The amount of energy loss can be measured via an electron spectrometer and interpreted in terms of what caused the energy loss. The shape of the peaks in the EELS spectra contain information about the valence state of the element detected in the specimen. This ability to "fingerprint" different forms of the same element is a strong advantage of EELS over EDX. This difference is mainly due to the difference in energy resolution between the two techniques (~1 eV or better for EELS and about a few times 10 eV for EDX). More information about electron microscopy can be found in Edington [Edi 1974] and Williams & Carter [Wil 2004].

4.3 PREPARATION TECHNIQUES OF SPECIMENS FOR TEM

4.3.1 TRIPOD POLISHING

The cross-sections through the coatings for TEM analysis were prepared by the TRIPOD method. This method consists in first gluing two pieces of a sample coating against coating to form a sandwich, Figure 16(a). Subsequently this sample is mechanically polished in wedge-shape down to about 100 - 300 nm, Figure 16(b), which equals to electron transparency for some materials *e.g.* Si, and thus reduces considerably the ion milling time. For polishing the sample is mounted on a sample holder like the one shown in Figure 16(c). The three micrometer screws allow for adjustment of the sample flatness and introduction of an angle during polishing.

This procedure can be used to produce samples for both SEM and TEM analysis and was originally developed by *Klepeis, Benedict and Anderson* [Kle 1987] at *IBM Laboratories, East Fischkill, NY, USA* for preparing plane view and cross-sectional samples. It is dedicated mainly to thin films deposited on a substrate, complex semi-conductor devices and composites containing nanoparticles or nanofibres, ceramics or concrete as well as bulk metal samples.

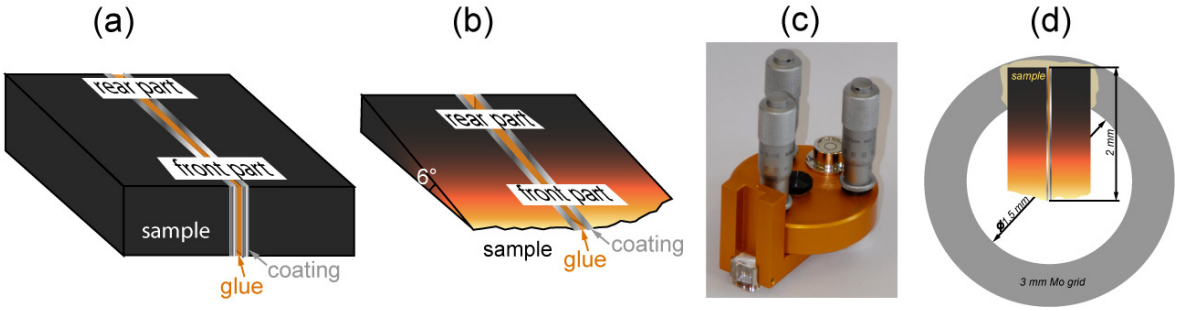

Figure 16 *Schematic representation of:* **(a)** *sample glued together coating against coating to form a sandwich;* **(b)** *Wedge-shapes sandwich after mechanical polishing;* **(c)** *Photograph of the Tripod sample holder for polishing;* **(d)** *Schematic representation of top view of the TEM lamella ready for final thinning by ion milling glued on a molybdenum ring. The colors are really visible in transmitted light in an optical microscope in a Si substrate mechanically polished down to electron transparency.*

The main advantage of the Tripod method is the considerable reduction of the ion milling time because the sample is mechanically polished down to sub-micrometer thickness and consequently a shorter time required for sample preparation (between 1 to 4 hours). Additionally samples with large electron transparent areas, very good surface quality and only a thin amorphized layer (about 5 nm) are obtained. Moreover, this method allows to dry-polish materials for which a polishing liquid such as water, oil, xylol or alcohol can not

be used. The schematic view of a ready TEM sample glued on a molybdenum ring is shown in Figure 16(d).

One of the disadvantages of the Tripod method is that it can not be applied to samples composed of two materials having very different ion milling rates like *e.g.* very hard thin films, which are thicker than 500 nm, deposited on a soft substrate; for example 1 µm TiN on Si substrate. During the milling process, the whole substrate is removed while the film remains at a thickness not transparent for electrons. Another disadvantage of this method is that the sample contains relatively large electron transparent areas and is therefore very fragile and not suitable for transport especially outside the lab, because the thin zones in the middle break off.

4.3.2 INDENT CROSS-SECTIONS PREPARED BY FIB

The classical mechanical polishing followed by ion milling method for TEM lamella preparation, described in the previous paragraph, allows obtaining thin areas at random position of the sample. However, in specific cases the electron transparent zone has to be in a precisely defined area, like for example a cross-section through an indent. To achieve this, only the technique of focused ion beam (FIB) is adequate for sample preparation. Figure 17(a) shows a SEM image of a TiN/SiN film surface, deformed by nanoindentation, which is a widely used technique to measure the hardness of a material. For FIB sample preparation first a protective layer of about 1µm Pt film is deposited with the electron beam and then with Ga+ ion beam on the surface of the indent, Figure 17(b).

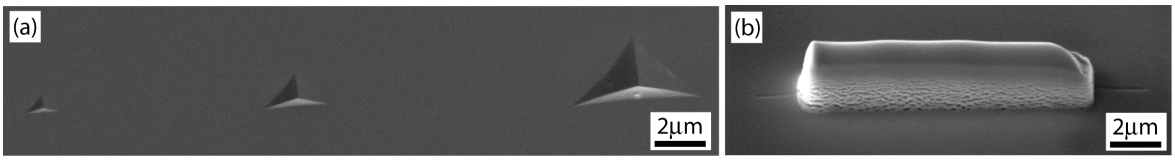

Figure 17 (a) *SEM image of the three indents made at 250 nm, 500 nm and 1000 nm depth.* **(b)** *Indent coated by a protective Pt layer.*

The milling geometry of the specimen is visible in Figure 18(a). Cuts with Ga+ ion beam into the sample to a depth of 5µm are made and the thus shaped lamella is polished down to a thickness of about 40 - 80 nm to become electron transparent. It is a challenge to prepare thin lamella from a multilayered TiN/SiN hard film deposited on a soft Si substrate as the sample exhibits high residual stresses. If these stresses are not released by vertical cuts next to the indent through the whole film thickness, the lamella, even though it is not

yet transparent to electrons, first bends (Figure 18(b)) and then breaks as seen in Figure 18(c).

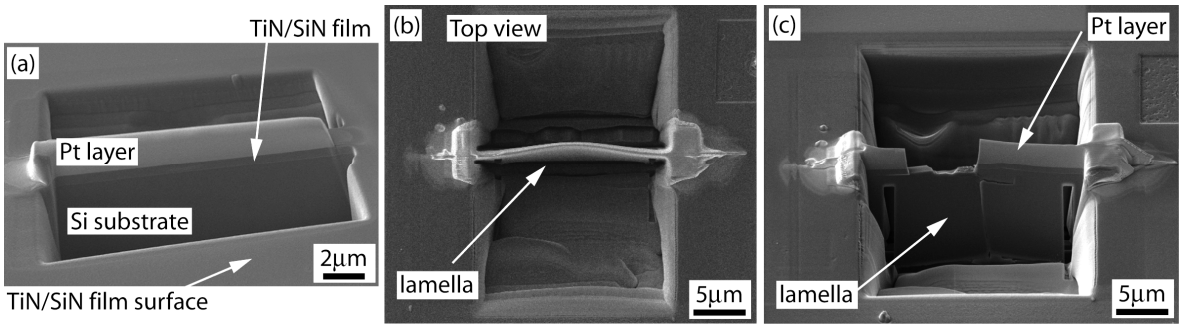

Figure 18 (a) *Milling scheme;* **(b)** *Top view of the lamella deformation due to residual stresses in the TiN/SiN film;* **(c)** *Broken lamella if relaxation cuts are not performed to reduce the stresses in the coating.*

The obtained lamella with final dimensions of 20µm x 5µm x 80 nm, shown in Figure 19(a) has the electron transparent area in its central part, and the indented film is clearly seen. It is now ready to be transferred under an optical microscope onto a 3mm Cu grid coated by a carbon film for TEM observations, Figure 19(b).

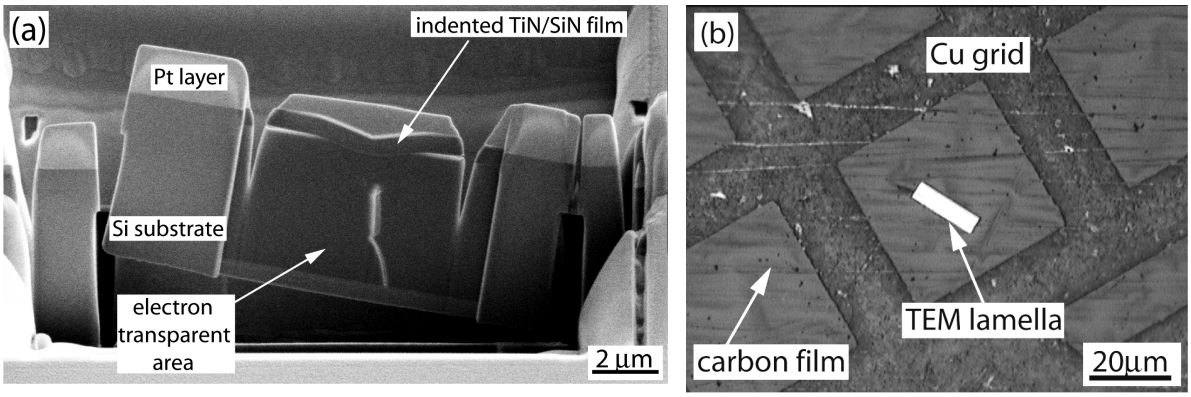

Figure 19 (a) *SEM image of the finished cross-sectional TEM lamella of an indented TiN/SiN film on Si substrate prepared by FIB ready to be transferred onto the Cu grid.* **(b)** *Optical photographs of the lamella deposited on a 3mm Cu grid coated by a carbon film.*

Results

Influence of various interfaces and microstructure on coating properties

The aim of this habilitation thesis is to determine, based on TEM observations, the dependence of the macroscopic properties such as hardness and oxidation resistance of transition metal nitride coatings on their microstructural features. All the hardening mechanisms are based on hindering the dislocation mobility. Therefore the key issue, are interfaces, their structure on the atomic scale, their type and quality. Two interface types at different scales were defined in the frame of this manuscript in hard Me-N coatings:

- *Interfaces* are found in columnar coatings inside the columns between zones of different crystallographic orientations, in nanocomposite coatings between the grains or the grains and the matrix and in multilayer coatings between the respective layers.
- *Intergranular interfaces* further called *grain boundaries* are found in columnar coatings between the respective columns and in multilayered coatings as vertical grain boundaries between respective grains in one layer.

The development of hard coatings for a particular application relies on interface design, which is based on a controlled introduction of a certain density of interfaces at different scales in different types of structures. These interfaces will thus provide a barrier for dislocation motion in the coatings leading to hardness increase. Different microstructural and compositional solutions of hardness enhancement in monolithic coatings will be discussed based on various examples.

Moreover by inducing deformation into the material it is possible to determine the occurring mechanisms and define the parameters, which contribute to the hardening effects. In the frame of this habilitation thesis the fracture damage and deformation mechanisms occurring in various types of coatings after being observed experimentally by TEM, could be identified and classified. The dependence of fracture damage and grain boundary sliding on the substrate hardness and structure could be clearly demonstrated based on experimental observations. Hence, this chapter is intended to summarize the microstructural investigations in the field of hard nanostructured coatings, in order to explain the influence of different parameters on the coating properties.

In the following sections I summarize the results obtained in the framework of my own research, consisting in extensive microstructural studies, including chemical analysis, of

various Me-N hard coating systems. These results were published in papers [Par 2004a], [Par 2004b], [Par 2010], [Rze 2009a], [Rze 2009b] and [Péli 2007].

5 APPLIED EXAMPLES OF HARDNESS ENHANCEMENT IN HARD ME-N COATINGS

In the two following paragraphs results and interpretations concerning the presence of artificially induced interfaces and their atomic scale structure influencing the hardness enhancement of coatings will be presented. The paragraphs give examples of solutions of hardness enhancement applied in columnar, nanocomposite and multilayered coatings.

5.1 SOLUTIONS OF HARDNESS ENHANCEMENT IN MONOLITHIC, COLUMNAR COATINGS

The hardening mechanisms occurring in metal-nitride coatings are commonly related to their microstructure. However, as will be shown in the following, the destruction of the columnar structure is not a condition to obtain a hardness enhancement. Indeed, in industry and in laboratory conditions it is possible to deposit coatings with preserved columnar structure and hardness values exceeding 30 GPa.

In the paragraph below two solutions of hardness enhancement in Me-N coatings, preserving their columnar structure will be presented. The first one is based on the $TiAlSiN_x$ system, which is a commercially available coating deposited and sold on market by Platit AG. Although it has incorporated compositionally modulated multilayers the columnar structure is preserved, [Par 2004a]. The second solution consists in the introduction of two crystallographically different phases such as *fcc*-NbN and *hcp*-NbN [Rze 2009b] forming nanosized grain inside the columns resulting in the formation of a so-called phase modulated nanocomposite, see §5.1.2.

5.1.1 COMPOSITIONALLY MODULATED MULTILAYERS INCORPORATED INTO THE COLUMNAR STRUCTURE

One of the first deposited and most popular coatings is TiN. Although it is characterized by high hardness values and good wear resistance, there are still some other properties, which can be ameliorated. Therefore different elements forming ternary and quaternary compositions are added to tune in a controlled way the properties of the *Me-N* coatings.

The quaternary TiAlSiN system is based on TiN and has thus similar properties. The presence of Al is of benefit for the oxidation resistance, as discussed in details in [Par 2004b] and in §7, and causes also structural changes of the TiN depending on the Al amount added. Another element, which is also widely used in combination with TiN or TiAlN is Si, as it has a high impact on the grain size of the resulting film and thus on the hardness. The influence of the Al in combination with Si on the microstructure of the TiN coating was studied extensively by TEM in [Par 2004a] and 5.2.1.

The TiAlSiN coatings were deposited by Platit AG in a commercial batch coater type RCS from Balzers. Four arc sources have been used to deposit Si alloyed TiAlN single- and multilayers. By using TiAlSi-targets in all of the sources TiAlSiN coatings have been deposited with a 50 nm thick TiN or Ti_2N adhesion layer onto WC-Co substrates mounted on a rotating substrate holder. In other experiments alternating TiAlSi and TiAl targets have been used resulting in the deposition of compositionally graded TiAlN/TiAlSiN multilayers. In all cases, pure nitrogen atmosphere was used to deposit the coatings. The pressure during deposition was in the range of 0.1–3 Pa at a temperature of approximately 500°C. In all cases, the substrate bias was held at 50V during deposition resulting in a deposition rate of approximately 1 µm/h. The thickness of all the samples was approximately 2.5 µm.

Industrially deposited coatings, due to the geometry of the deposition chamber, are almost always multilayered. The multilayering is due to the passage of the substrate in front of different targets, so the deposited layers have slight variations in their chemical composition. In the case of the TiAlSiN coating the targets were TiAl and TiAlSi with different contents of Ti, Al and Si. During deposition the substrates are subjected to double rotation: around a central and around their own axis. Hence the substrate distance from the respective targets is varying. Thus the layers deposited closer to the TiAl target are slightly richer in Ti and the ones deposited near the TiAlSi target are richer in Al and Si. There is no sharp transition between the layers, their interfaces are very smooth and the columnar growth of the coating is not disturbed. In general, these coatings are very hard, reaching 32 GPa, due to their compositional modulation.

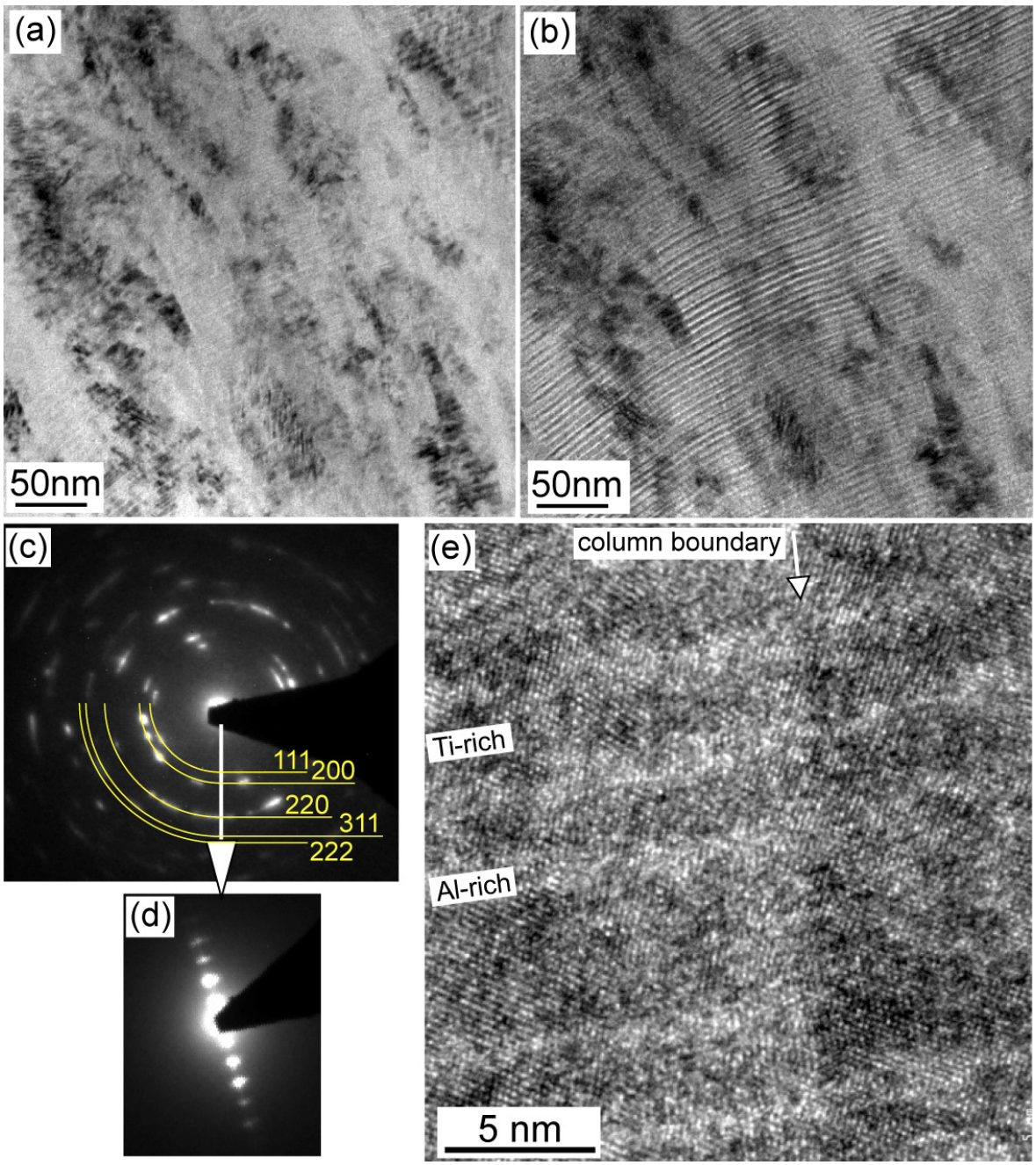

Figure 20 *TEM bright field cross-section through the TiAlSiN coating:* **(a)** *focused;* **(b)** *underfocussed; the multilayering is visible only in the underfocussed conditions;* **(c)** *Selected area diffraction pattern from the entire coating cross-section;* **(d)** *magnified view of the transmitted spot showing satellite spots originating from the superstructure of the multilayering;* **(e)** *HRTEM image of the compositionally graded multilayers: layers with light contrast are richer in Al and have a more distorted atomic-scale structure, the ones with dark contrast contain more Ti and are better crystallized.*

By taking TEM cross-sectional images of the TiAlSiN coating in focused conditions, Figure 20(a) a very interesting observation was made. The multilayering is visible only when the sample is under- or overfocussed, Figure 20(b). This phenomenon is related to the phase contrast transfer function (CTF) [Edi 1974], [Wil 2004] of the TEM, which is

defined as the function of limiting apertures and aberrations in the imaging lenses of a microscope:

$$T(k) = -\sin\left[\frac{\pi}{2} C_s \lambda^3 k^4 + \pi \Delta f \lambda k^2\right]$$

Clearly, it will be a complicated curve which will depend on:

- C_s - the quality of objective lens defined by spherical aberration coefficient
- λ - wave-length defined by accelerating voltage
- Δf - the defocus value
- k - spatial frequency

The CTF for a FEG TEM operating at 300 keV with a super-twin lens in focused conditions and with -200 nm defocus is depicted in Figure 21(a). Indeed, for a sample like the TiAlSiN multilayers having a periodicity of between 5 and 7 nm, no phase contrast is transferred in the focused conditions and therefore the multilayering is not visible. However, for a defocus of -200 nm the contrast transfer is different than zero and thus the multilayers are visible.

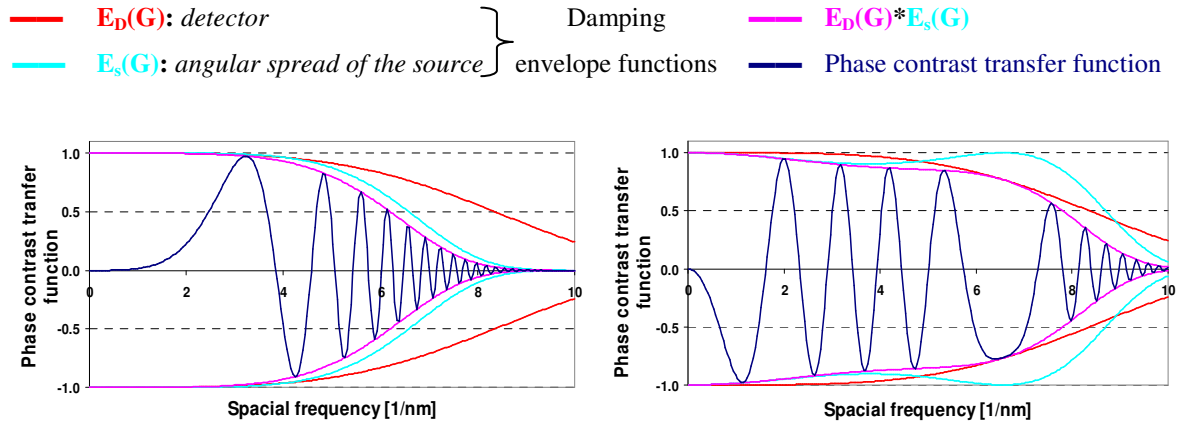

Figure 21 *Phase contrast transfer function for:* **(a)** *sample in focus;* **(b)** *sample with -200 nm defocus.*

In the diffraction pattern of the coating, Figure 20(c), the central, transmitted spot, Figure 20(d), contains well visible satellite spots originating from the multilayering. It could be indexed with *fcc*-TiN therefore it is assumed, that the coating is a solid solution of TiAlSiN, as no rings corresponding the *hcp*-AlN or *fcc*-AlN [Mad 1997] could be observed indicating a phase separation. The TEM image at atomic resolution reveals the absence of abrupt interfaces between the layers. The Al-rich layers, appear with a lighter contrast, due to their lower scattering factor [Mad 1997], and have a slightly more disordered structure due to the presence of a higher amount of Si. This is however not sufficient to disturb the

columnar growth of the coating. The thickness of the Al-rich layers could be estimated to 2 nm based on the HRTEM image.

To experimentally prove the gradient in composition of these multilayers analyses with EDX were performed in the STEM mode, Figure 22(a). The resulting Ti and Al maps are shown in Figure 22(b) and (c), respectively. Although the periodicity of these layers is below 10 nm, even at that scale, the multilayering is clearly visible in the maps. The Ti-rich layers, which have a light contrast on the Ti map, Figure 22(b), are dark on the Al map, Figure 22(c), and vice versa. It has to be underlined, that the differences in composition are of the order of a few percents, and that the Ti-rich layers also contain Al and Si and the Al+Si-rich layers contain Ti.

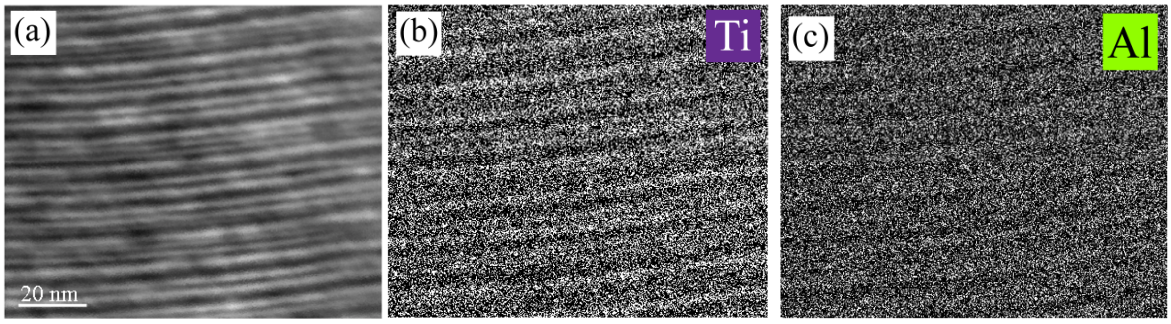

Figure 22 (a) *Bright field STEM image of the TiAlSiN multilayers;* **(b)** *EDX Ti map;* **(c)** *EDX Al map: the layers containing the respective elements are lighter.*

5.1.2 PHASE MODULATED NANOCOMPOSITES WITH A PRESERVERD COLUMNAR STRUCTURE

A phase modulated nanocomposite is composed of nanograins exhibiting two different crystallographic phases having nevertheless the same chemical composition, presented in detail in §2.5.2. These structures reach hardness values above 30GPa due to their nanocomposite structure. An excellent example is the NbN coating, which was deposited in ultra high vacuum by dc (direct current) magnetron sputtering in a Leybold L400Sp system on (100) oriented Si wafers at 70°C. More technical details concerning the deposition procedure are given in [Wrz 2003], [Rze 2009a] and [Rze 2009b], respectively. The hardness of the NbN coating measured with the Triboindenter [Rze 2009b] was about 26.5 GPa and the value calculated from the *in-situ* picoindentation reached almost 38 GPa. These values were more than two times higher than the ones estimated for the monolithic TiN 15 GPa and CrN 16.6 GPa coatings deposited under the same conditions in the same deposition unit. Therefore it was assumed that the high hardness of the NbN coating is related to some particular microstructural features. The TEM analysis of cross-sections

through the NbN coating, Figure 23(a), reveals a not very pronounced columnar structure. The dark field image in Figure 23(b) was taken with a mixture of the [111], *[100]*, *[110]* and [220] reflexions, as they are too close together to choose only one of them. It shows that the coating consists of long columns reaching the entire coating thickness, which was not so evident from the bright field image. The average column width was estimated to ~70 nm. The columns are composed, conversely to a monolythic TiN coating, of many small zones with the same contrast separated by zones of similar size exhibiting opposite contrast. At the interface with the Si wafer substrate a nucleation zone of unresolved nature (amorphous or nanocrystalline) was observed. From the diffraction pattern, Figure 23(c), two phases could be identified: cubic δ-NbN and hexagonal δ'-NbN. No preferential orientation could be observed.

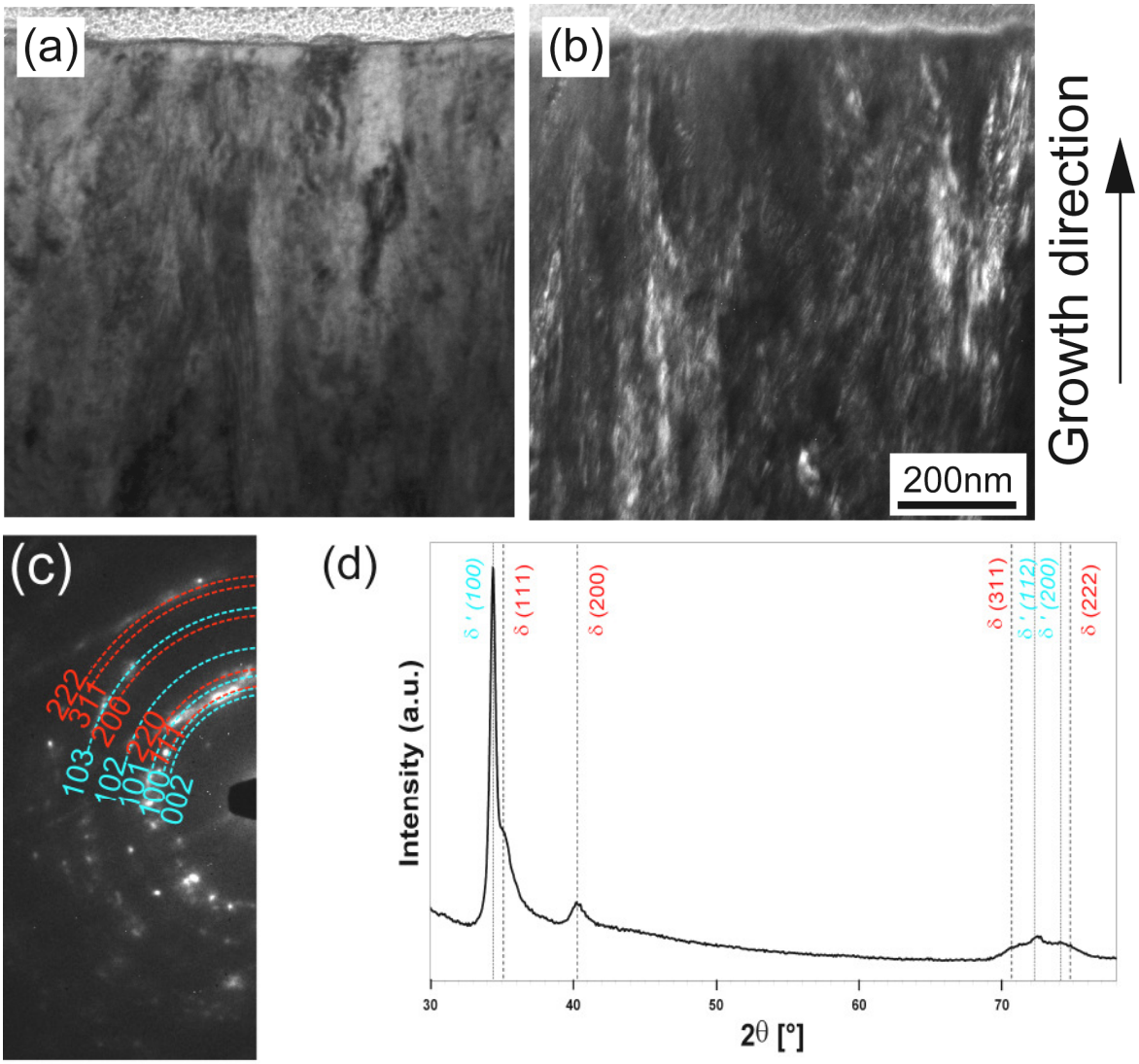

Figure 23 *TEM cross-sections through the monolithic NbN coating:* **(a)** *bright field;* **(b)** *dark field;* **(c)** *SAED pattern and* **(d)** *XRD diffractogram showing the presence of two phases fcc δ-NbN and δ'-NbN.*

The presence of these two phases is also confirmed by the XRD diffractogram, which is shown in Figure 23(c). Peaks belonging to different crystal orientations of the cubic δ-NbN and hexagonal δ'-NbN phases are present. Such a mixture of two phases δ-NbN and δ'-NbN, forms a so-called phase modulated nanocomposite.

The explanation of δ-NbN and δ'-NbN phase mixture formation, has to be regarded from the viewpoint of thermodynamics and kinetics. According to Thompson [Tho 1993] the competition between the surface and strain energy minimization influences the texture in polycrystalline films. Wen [Wen 2008], [Wen 2009] showed, that the cubic δ-NbN (002) has the lowest surface energy and hence at low stresses this phase should appear. Indeed in §6.2.2 it will be shown that the TiN/NbN coating is composed only from *fcc*-TiN and δ-NbN and it has a strong (002) texture originating from both components.

As the dark field image was taken with the [111] spot of the *fcc* δ-NbN and the overlapping [101] spot of the hexagonal δ'-NbN phase, it reveals the presence of many small, differently oriented zones inside the columns. This observation would also indicate that the NbN forms a phase modulated nanocomposite structure with δ and δ' nanograins forming columns. In addition, as these columns have no single-crystalline character, the angle between their boundaries can vary locally along the column length.

Comparing the hexagonal and cubic electronic structures, the δ'-NbN is more covalent than the δ-NbN. The prominent covalent bonding in this hexagonal nitride can be related to its higher intrinsic hardness values compared to these of the cubic phase [Sand 2006b]. Indeed it is the mixture of the *fcc* δ-NbN and hexagonal δ'-NbN phases, which leads to the formation of a phase modulated nanocomposite structure, increasing the hardness of this coating to almost 38 GPa.

5.2 HARDNESS ENHANCEMENT THROUGH FORMATION OF A NANOCOMPOSITE STRUCTURE

Nanocomposites based on TiSiN are known to exhibit extremely high hardness values exceeding 40GPa [Vepr 1999], [Vepr 2008] and [Mus 2000]. However, the formation sequence of a nanocomposite structure is not very clear. Therefore, in the paragraph below an attempt to elucidate the formation sequence of the nanocomposite structure by TEM microstructural analysis is presented. It was performed on a particular TiAlSiN sample having a chemical composition varying from Ti-rich at the WC-Co substrate to Al+Si-rich

at the coating surface. The second example described below is a very interesting and inconvenient tentative to produce a nanocomposite composed of Al and Si, resulting in an AlN/SiN_x nanogranular structure, which was assumed to be similar to TiSiN, exhibiting however only a small hardness enhancement [Péli 2007].

5.2.1 FORMATION SEQUENCE OF A NANOCOMPOSITE ON THE EXAMPLE OF TIALSIN

In industrial coatings a common practice is to deposit functional coatings, which have a gradient in the chemical composition, which changes with the film thickness. The coating discussed in this paragraph is composed of TiAlSiN and was deposited with the same industrial coater as the coatings described in §5.1.1. It is rich in TiN at the WC-Co substrate and the Al-Si content is increasing with the film thickness to reach its maximum at the top. Therefore the microstructure of the film changes gradually throughout the coating thickness, what is clearly visible from Figure 24(a). In the Ti-rich part the film starts to grow in form of columns, which become smaller and smaller, as the Al+Si concentration increases, to reach at the film top a diameter of about 2-5 nm, which is the typical grain size in nanocomposites. This sample is of particular interest for microstructural studies, as it is possible to directly observe the reduction of the grain size with the chemical composition. Moreover this type of sample allows to study on atomic scale by HRTEM the interfaces between grains, which have a different size and structure depending on their chemical composition. Thus the formation sequence of the nanocomposite structure will be proposed.

The chemical composition of the coating was determined by EDX. As the coating was known to be stoichiometric the amount of nitrogen was estimated to 50 at.% as it is a light element and it can not be quantified precisely with EDX. The Ti, Al and Si at.% given in [Par 2004a] are absolute values of the concentration of these elements, which were however not normalized for a 50 at.% content of nitrogen.

The HRTEM image of an interface between two columns in the bottom part of the coating, Figure 24(b), clearly shows that this interface is neat and both columns are well crystallized. The diffraction pattern taken from this region, Figure 24(b'), contains spots originating from the columnar structure of the *fcc*-TiN phase.

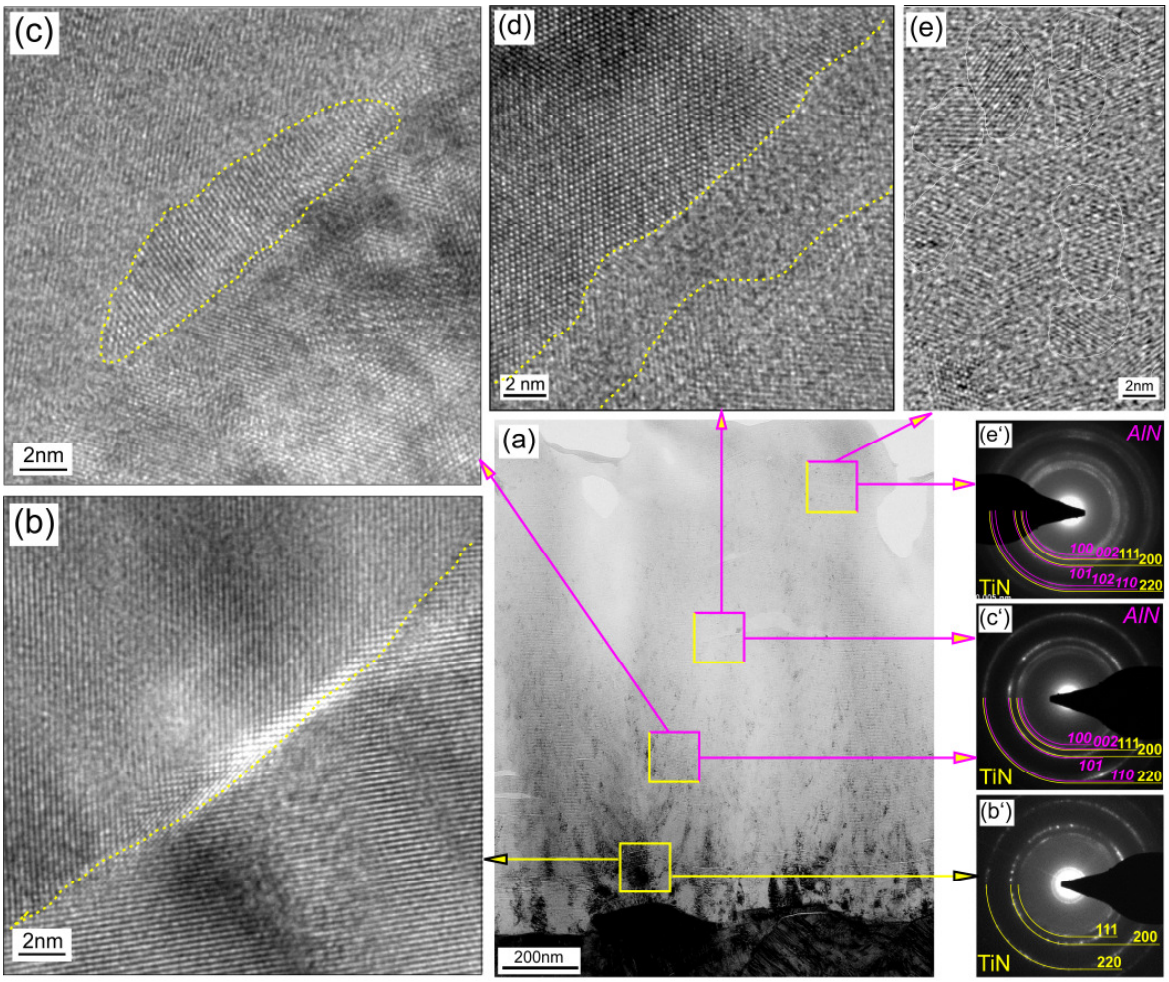

Figure 24 (a) *Bright field TEM image of a cross-section through a compositionally graded TiAlSiN coating. It is rich in Ti at the substrate (bottom of the image) and the Al+Si content increases towards the top of the coating;* **(b)** *HRTEM image of an interface between two TiN columns;* **(b')** *Corresponding SAED pattern composed of the fcc-TiN phase;* **(c)** *HRTEM image of an interface between two columns in the middle part of the film containing a small differently oriented zone;* **(c')** *Corresponding SAED pattern, showing fcc-TiN and traces of hcp-AlN phase;* **(d)** *HRTEM image of another interface with a clearly visible amorphous region between two crystalline columns;* **(e)** *HRTEM image of the top part of the coating showing of small crystalline grains* **(e')** *Corresponding SAED pattern indexed with fcc-TiN and hcp-AlN lattice parameter.*

In the middle part of the coating, the grain size is reduced, Figure 24(a), what is also visible from the diffraction pattern, where less spots are present, Figure 24(c'). The diffraction pattern contains, in addition to the *fcc*-TiN phase, traces of the *hcp*-AlN phase, due to the increasing Al content in the coating. The AlN phase is most probably not pure AlN, but AlSiN as Si can be easily incorporated substitutionally into the AlN, as will be shown in §5.2.2, §5.3.1, [Péli 2007] and [Péli 2009]. However the difference in lattice parameter between pure AlN and AlSiN is so small, that it is impossible to distinguish between these two phases only by electron diffraction. The HRTEM image, Figure 24(c),

taken at the interface between two well crystallized grains shows the presence of a small crystalline zone, with a width of approximately 2 nm. This zone, with a completely different orientation of the atomic planes than the surrounding, might be rich in Al and Si, as some *hcp*-AlN is visible in the diffraction pattern.

Moreover, this assumption is supported by the next HRTEM image, Figure 24(d), taken in a region with even more Al+Si concentration, where the interfacial zone between the two crystalline grains is larger and amorphous, due to the fact that the SiN_x would form the amorphous matrix.

The top part of the coating, where the Al+Si concentration reaches its maximum has a nanocomposite structure visible on the HRTEM image, Figure 24(e). Crystalline grains with differently oriented lattice planes depending on the grain and amorphous zones besides the grains are clearly visible. Some of them have been artificially delimited by white lines for sake of clarity. The diffraction pattern taken from the top part of the coating, Figure 24(e') shows the presence of *fcc*-TiN and *hcp*-AlN composed of full rings confirming small grain size.

This observation on atomic level of the microstructural evolution towards a progressive amorphization of the microstructure with the increasing Al+Si content strongly suggests that the mechanism of the formation of a nanocomposite structure, in the case when the components of the coating are immiscible, would be the following:

- First neat interfaces between well crystallized, large columnar grains are formed.
- With the increasing Al+Si content grain size is reduced and the second phase, in this case the AlSiN phase, would segregate at the grain boundaries first in a crystalline state, as AlN is crystalline and it would contain only traces of SiN_x.
- The above assumption would be supported by the fact, that by further increasing the Al and Si concentration in the coating the interfacial zones become larger and turn amorphous, what would be not surprising, if they contain SiN_x, which is amorphous.
- Finally, when a maximum concentration of Al and Si is reached the sample becomes a nanocomposite. It has to be additionally mentioned, that the crystalline grains are not necessarily pure TiN, at higher Al contents, they can be a solid solution of TiAlN.

This quaternary TiAlSiN system is a very complicated one, as compared to TiSiN, where only TiN crystallites embedded in an amorphous SiN matrix are present. Indeed, the addition of aluminum complicates the system behavior for two reasons. First it can form a

solid solution with TiN, thus the crystallites are composed of TiAlN and the excess of Al, which cannot be incorporated in the TiAlN solid solution segregates as a second phase *i.e.* *hcp*-AlN. The second reason is that Si can be substitutionally incorporated into *hcp*-AlN up to 6at% [Péli 2009], and only after saturating the AlN structure it will form amorphous SiN_x. However, as the films are deposited by reactive magnetron sputtering, various metastable states and structures can be formed, therefore it is very difficult to explicitly determine, the exact composition of the grains and interfacial zones in the analyzed coating.

Of course it is not possible to resolve unambiguously from the HRTEM image, if the amorphous zones between the crystalline grains correspond to an amorphous SiN_x phase or to TiAlSiN crystalline nanograins, which are misoriented towards the electron beam and thus appear amorphous. Therefore it is impossible to estimate the thickness of the amorphous matrix between the crystalline grains. It can vary from only one atomic layer, which would be too thin to be observed by HRTEM, to several atomic layers or even the entire amorphous zones.

Similar HRTEM images of nanostructured thin films were taken by other authors [Vepr 1995], however only in TiSiN composites, which did not contain Al. These authors claimed to have a structure consisting of crystalline TiN nanograins surrounded by amorphous regions, which however could also correspond to misoriented TiN grains.

5.2.2 ADDITION OF SI INTO ALN - COMPARISON WITH THE TISIN SYSTEM

There are numerous functionalities of AlSiN coatings, which are widely used for applications in field emission devices, UV light emitters, anti-oxidation coatings or optical films with tailored refractive indices. In [Péli 2007] it is proposed to explore the suitability of the AlSiN system for new oxidation resistant, hardness-enhanced and optically transparent coatings, with a hardness exceeding that of Al_2O_3. In fact, in others systems such as the extensively studied TiSiN system, the addition of Si into TiN leads to the formation of a hard nanocomposite. The initial idea of forming a superhard nanocomposite structure in the TiSiN system originates from Veprek [Vepr 1995], [Vepr 1999], and constrains that the TiN and Si_3N_4 phases are immiscible. Thus the progressive increasing of the Si amount in the TiSiN system refines the columnar structure leading finally the formation a two phase configuration consisting of TiN nanocrystallites surrounded by an amorphous SiN_x matrix, Figure 26(b).

As AlN is a transparent coating offering numerous possible applications, it would be a challenge to increase its hardness by adding Si to form a superhard nanocomposite. Indeed, according to the existing ternary phase diagram for the AlSiN system [Rogl 1992], AlN and Si_3N_4 are expected to be immiscible. However, some authors found that the co-deposition of AlN and Si_3N_4 at high temperature may lead to an AlSiN solid solution [Tan 2001], [Her 2005] whereas others suggested the formation of a two phase composite [Maz 1997]. From the available data, a co-deposition at low substrate temperature is hence expected to lead either to an AlN/*a*-SiN_x nanocomposite, or to an AlSiN solid solution [Holl 1988]. In the paper [Péli 2007] we report the structural and mechanical properties of AlSiN thin films depending on their Si content. The films were deposited by DC unbalanced magnetron sputtering from confocally arranged Al and Si targets in an Ar/N_2 reactive atmosphere at a total pressure of 0.3 Pa at 200°C. The base pressure of the deposition chamber at room temperature was about 10^{-6} Pa. Si (100) substrates were mounted face-down on a heated substrate holder rotating 12 cm above the 5 cm diameter targets. The composition of the coatings was varied from pure AlN to Al–Si–N with 23 at.% of Si by keeping the power applied to the Al target constant and progressively increasing the power on the Si target. No substrate bias was applied. The argon and nitrogen flows were set at 15 sccm and 7 sccm respectively for all depositions. More details about the deposition procedure and conditions can be found in [Péli 2007] and [Péli 2009].

Cross-sections of coatings of pure AlN and AlSiN containing 4 at.% and 16 at.% of Si respectively have been analyzed by TEM. For each sample a high resolution image, a general view dark field in the (002) direction and a diffraction pattern are presented in Figure 25.

The diffraction patterns as well as the interplanar distances measured from the HRTEM images correspond to *hcp*-AlN structure with a (002) preferential orientation in the growth direction, which are in agreement with XRD results. Concerning the film morphology, all coatings exhibited a columnar growth up to 16 at.% of Si. From the dark field images it seems that the columns propagate throughout the whole film thickness.

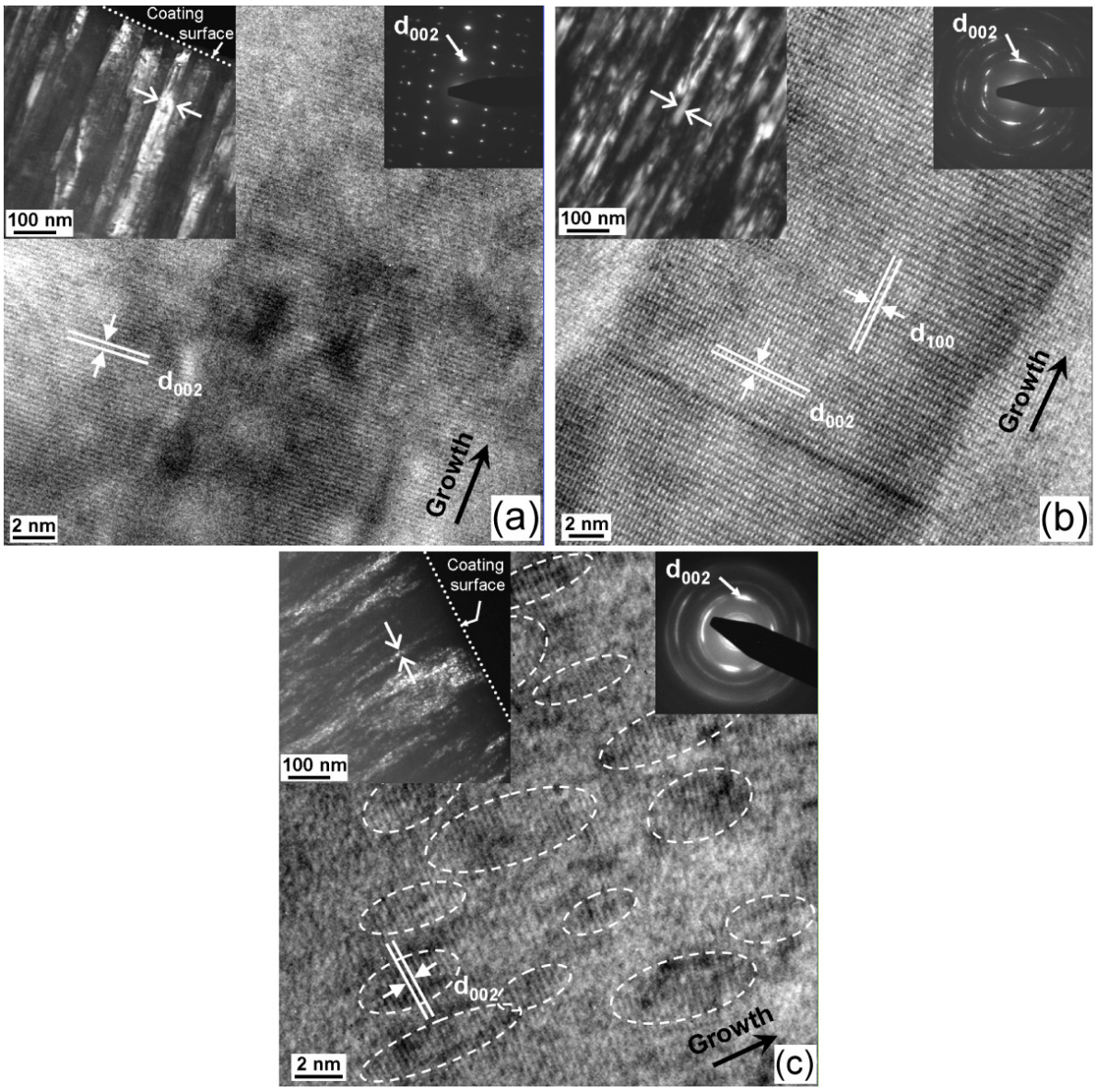

Figure 25 *TEM high resolution micrographs, dark fields taken with the [002] spot and diffraction patterns corresponding to cross-sections through:* **(a)** *pure AlN coating;* **(b)** *AlSiN coating containing 4 at.% Si;* **(c)** *AlSiN coatings with 16 at.% Si with black dashed contours added to ease the distinction of individual crystallites. The growth direction is indicated on each of the images. One individual column is delimited with arrows in each DF image.*

In the case of the pure AlN film, Figure 25(a), the diffraction pattern is composed of a periodic array of spots, which is an indication for good crystalline quality of the film. This is confirmed by the DF image revealing a film consisting of large (30–60 nm) polycrystalline columnar grains, each composed of several zones with similar crystallographic orientations. One of these zones was imaged in high resolution and shows the same orientation over the whole field of view, with (002) planes parallel to the coating

surface. Note that on DF images, the contour of these zones is diffuse. Thus they cannot be clearly identified as single crystallites with a well defined shape and size. This is most probably due to the superposition of several crystallites over the thickness of the TEM specimen reaching a few tens of nanometers. As a consequence we only propose here a rough estimation of the column width from both bright field (not shown here) and dark field images, but no estimation of the mean crystallite size to be compared with the XRD data available in [Péli 2007].

When adding 4 at.% of Si in AlN, Figure 25(b), the column width is reduced, thus smaller zones of similar crystallographic orientation are present inside the columns. The appearance of circular arcs with an increasing width instead of dot-like spots in the diffraction pattern confirms the increasing misorientation and the decreasing size of crystallites in the film.

On the high resolution image, a single crystalline column with well defined edges is visible. The column is about 20 nm wide and a stacking fault parallel to (002) planes – *i.e.* in growth direction – is visible, Figure 25(b). As for the AlSiN film with 16 at.% of Si, Figure 25(c), the circular arcs in the diffraction pattern are even larger, indicating very small crystallites. This is confirmed by the DF image, where the columns consist of small (2–5 nm) zones of similar crystallographic orientation. On the HR image, such zones are evidenced with a (002) texture in the growth direction. The angular spread of orientation of (002) planes is nicely visible.

For the above mentioned coating it was shown that the hardness, measured after the annealing remains unchanged up to a temperature of 900-1100°C where recrystallization begins. The highest recrystallization temperature is achieved for nanocomposites with the optimal Si_3N_4 content corresponding to the percolation threshold and lowest crystallite size of about 10 nm.

Results of the nanohardness performed on samples deposited at 200°C and 500°C are given in Figure 26(a). The data show a faint hardness maximum of about 30 GPa at 10 at.% of Si which decreases for AlSiN films with Si contents ≥ 16 at.%. On the contrary, for a TiN/Si_3N_4 nanocomposite, an evident maximum for the hardness evolution as a function of the amorphous phase content is visible in Figure 26(b) after Patscheider *et. al.* [Pat 2003]. It is clearly shown, that for this coating the hardness depends on the microstructure *i.e.* grain size and the volume fraction of the amorphous tissue phase.

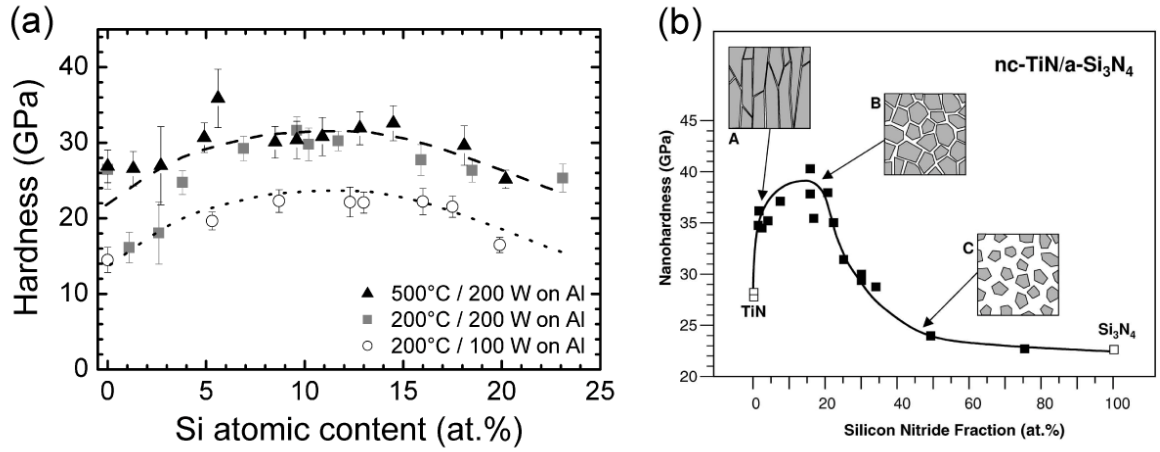

Figure 26 (a) *Evolution of the hardness (black triangles) of AlSiN films deposited at 200°C and 500°C as a function of the Si content determined from nanoindentation measurements. The error bars represent the standard deviation on about 20 individual indents on each sample. Samples with 1 to 4 at.% of Si had a cracked surface, hence the corresponding large uncertainty of the measurements [Péli 2007];* **(b)** *Dependence of hardness on the Si_3N_4 phase content (in at. %) in TiN/a-Si_3N_4 nanocomposite coatings with the respective schematic morphologies of the grains, after Patscheider et. al. [Pat 2003].*

Considering the hardness behavior, it is commonly agreed that the requirements to obtain a significant nanostructure hardening are to create **(1)** a two phase material with **(2)** sufficiently small crystallites, so as to prevent dislocation activity, **(3)** embedded in a thin matrix phase, so that no crack propagation is possible, and **(4)** with a strong and sharp interfaces between the two phases, so as to hinder grain boundary sliding [Vepr 1999]. In the present case, a two phase composite is obtained for Si atomic content exceeding 6 at.%, with a crystallite size reaching the sub-10 nm size, but we measure only a slight hardness enhancement. The points **(1)**, **(2)** and **(3)** are obviously fulfilled, but most probably not the point **(4)**. One of the possible explanations is based on arguments concerning the nature of the involved materials. Both AlN and Si_3N_4 are covalent nitrides with same metalloid coordination numbers and similar mechanical properties, in particular similar E moduli, which is not the case for transition metal nitrides–silicon nitride nanocomposites [Holl 1986]. Moreover, AlN has a hexagonal crystallographic structure; this also differs from widely used transition metallic nitrides (such as TiN, CrN, ZrN etc.) which have a cubic NaCl structure. The above mentioned similarities between AlN and Si_3N_4 probably result in weak diffuse interfaces between the two phases. The study of the exact nature of the grain boundaries, in terms of atomic arrangement between involved phases would provide more information enabling to explain their properties. However, this study would be

difficultly realizable on a three dimensional structure such as a nanocomposite, as it is not possible with the now-a-days available techniques to prepare a TEM lamella of 10 nm, which would thus contain not-overlapping nanograins. Therefore a two-dimensional model system consisting of AlN/SiN multilayer structure with varying SiN layer thicknesses was proposed to analyze on the atomic scale the AlN/SiN interfaces and understand thus the structural mechanisms occurring in the AlSiN nanocomposite. The results of this study, presented in §5.3.1 were compared with observations performed for TiN–Si_3N_4 interfaces in a multilayer system, §5.3.2 and with the findings of other authors [Hao 2006], [Söd 2006].

5.2.3 SUMMARY OF HARDNESS ENHANCEMENT THROUGH THE FORMATION OF NANOCOMPOSITES

In the above paragraph the microstructural evolution from columnar to nanocomposite structure and its influence on the mechanical properties of nanocomposites is presented. Most of the nanocomposites are formed due to a phase separation into crystalline Me-N and amorphous SiN_x phases resulting from the addition of Si, as it is the case for the TiSiN system, which shows a considerable hardness maximum. It is nevertheless possible to replace Si by Ge in TiSiN and obtain a structural refinement accompanied by a hardness enhancement as very nicely shown by Sandu [Sand 2005], [Sand 2006]. The example of TiAlSiN nanocomposite shows that some grains have very sharp interfaces, where only the lattice planes change their orientation, and some are separated by zones of a few nanometers having an amorphous aspect. On the contrary, in the AlSiN system all the nanograins are oriented in the same direction and it is difficult to determine from the HRETM images where their boundaries are. The presence of diffuse or sharp and well distinguishable interfaces between the nanograins and the amorphous matrix are one of the conditions, as will be shown in §5.3, which have to be fulfilled to obtain a nanocomposite structure showing enhanced hardness properties compared to the monolithic columnar coatings.

5.3 NANOMULTILAYERS AS MODEL SYSTEMS FOR NANOCOMPOSITES OF HARD ME-N COATINGS

The basic idea to design nanocomposites is to have a crystalline phase consisting of equiaxed grains surrounded by a very thin amorphous layer of less than 2 nm thickness. As the interface between the grains and the amorphous phase should be as sharp and abrupt as possible these two materials should be immiscible.

In the study of interfaces between the crystalline grains and the amorphous matrix by electron microscopy several problems arise for the TEM lamella preparation. Indeed, a direct identification of the deformation mechanisms in nanocomposites is virtually impossible since that would require that single grains are identified and their position is known before and after a deformation event. At grain sizes of 5 to 10 nm, which correspond to the typical crystal dimensions of nanocomposites, the sample preparation poses severe impediments. The problems are notably **1)** the production of TEM lamellae with a thickness equal to the grain size (*i.e.* several nm) in order to avoid overlapping of grains in the projected image, **2)** the amorphization of the sample during preparation, which makes the distinction of originally amorphous regions from preparation-induced amorphous ones very difficult or even impossible, and **3)** the requirement of unstrained lamellae which are stable during the preparation. Therefore 2-dimensional structures, such as multilayers with layers in the nanometer range were deposited to observe the deformation mechanism.

As already mentioned, multilayers of different materials are deposited on top of each other in the aim to prohibit the grain growth of the respective components and provide a barrier for dislocation movement in order to enhance the hardness of the coating. In order to overcome difficulties of TEM lamellae preparation from nanocomposite coatings, the three-dimensional structure of these materials is reduced to two dimensions by preparing nanomultilayers built of alternating layers. This architecture allows an independent variation of the single layer thickness and a clear identification of the nanostructure. In the paragraph below a detailed study on atomic scale of interfaces between *hcp*-AlN/*a*-SiN_x and *fcc*-TiN/*a*-SiN_x multilayers is presented. The first coating was deposited on purpose as a 2-dimensional model system for the AlSiN nanocomposite described in detail in §5.2.2, [Péli 2007] and [Péli 2009] in order to investigate the nature of the AlN-SiN_x interface and explain, why the obtained AlSiN nanocomposite does not exhibit a more significant hardness enhancement. The second system is a TiN/*a*-SiN_x multilayer where the

amorphous SiN_x layer is supposed to stop the TiN crystallites to grow out of the TiN layer [Par 2010]. Two different layouts with different layer thicknesses were investigated. It is a model system for TiN/*a*-Si_3N_4 nanocomposites.

5.3.1 AlN/SiN_x multilayer with varying SiN_x layer thickness

The AlSiN system is very interesting as it is a transparent coating, offering thus various industrial application possibilities. In §5.2.2 the attempt to produce a nanocomposite structure from AlN and SiN was presented. Unfortunately, the formation of crystalline grains having sharp boundaries with the amorphous tissue phase, as it was the case for TiAlN/SiN shown in Figure 24(a) in §5.2.1, failed. Moreover, the hardness evolution with the addition of Si into the system showed only a slight maximum. Therefore it was of crucial importance to investigate the quality of interfaces between the crystalline AlN phase and the amorphous SiN_x, as this would provide valuable scientific information about the reason, why a nanocomposite structure cannot be formed in this case and what microstructural issues are important when it comes to hardness enhancement.

For this purpose, to facilitate microstructural TEM observations on atomic scale, the $(AlN_{10\ nm}/SiN_t)$ x 4 multilayer system was deposited onto a single crystalline *hcp*-Al_2O_3 substrate oriented with the c-axis in the growth direction of the coating [Dov 1996]. The deposition conditions for the respective multilayer layouts were the same as for the nanocomposites discussed in §5.2.2 and [Péli 2007]. The AlN, grew preferentially (002) oriented along this c-axis of the Al_2O_3 substrate having thus an epitaxial relation with the latter one, Figure 27(a). In this way we obtained a single crystalline layer of AlN on top of the Al_2O_3 substrate, even though both materials have 13% lattice misfit. This misfit is however compensated by the presence of misfit dislocations every 8 to 9 atomic planes, as nicely visualized in the filtered HRTEM image in Figure 14(a) and (c). The diffraction patterns taken from the two different multilayer layouts, Figure 27(c) and (e), confirm the epitaxial growth of AlN on the Al_2O_3 substrate. On top of the first epitaxial AlN layer a SiN_x layer with a thickness of t = 0.4, 0.7, 1.2 and 2 nm was deposited. Thus the single crystalline part of the coating with the substrate could be relatively easily oriented in the TEM to observe edge-on the interfaces between the AlN and the SiN_x.

Figure 27(b) shows a dark field cross-section of the multilayer with 0.4 nm of SiN. It is clearly visible, that the columnar growth is nearly not disturbed by presence the 0.4 nm of SiN in the layer stack. Conversely, at a SiN_x thickness of 1.2 nm an apparent change in the structure is observed: as clearly visible from the dark field image in Figure 27(d), only the

first AlN layer at the substrate is single crystalline, the subsequent ones are polycrystalline and contain columnar grains.

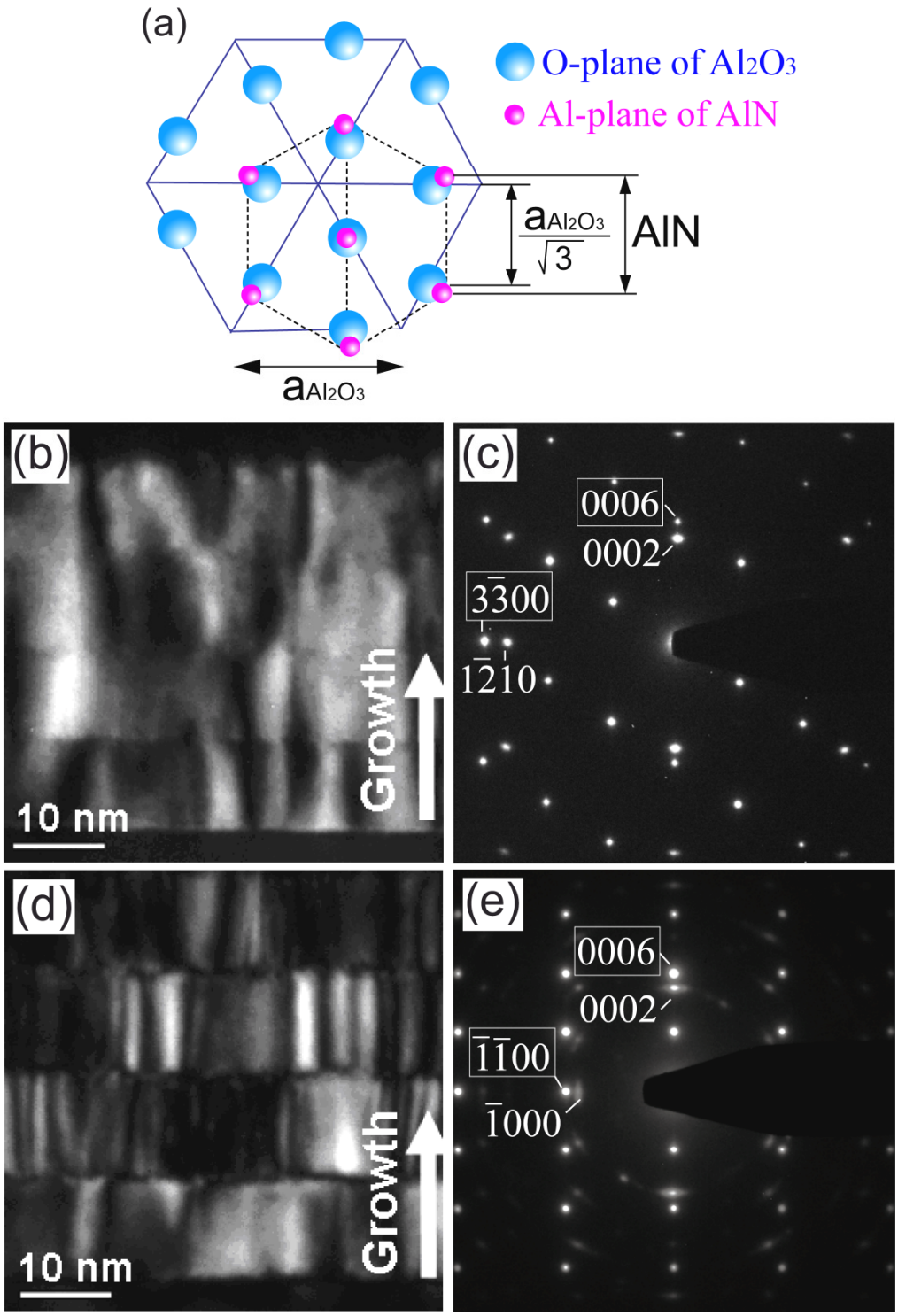

Figure 27 (a) *Schematic representation of in-plane atomic arrangement in the case of [0001] AlN film grown on [0001] Al_2O_3; Dark field cross-sections and diffraction patterns corresponding to:* **(b) & (c)** *10 nm AlN / 0.4 nm SiN_x;* **(d) & (e)** *10 nm AlN / 1.2 nm SiN_x.*

A view on the atomic scale of the interface between AlN and $SiN_{0.7\ nm}$ is presented in Figure 28(a). It can be clearly seen that the SiN layer is completely crystalline and the AlN

grows epitaxially from the substrate in the [0002] direction across the three SiN layers. The scheme representing the atomic arrangement in Figure 28(d) could be established based on the HRTEM image.

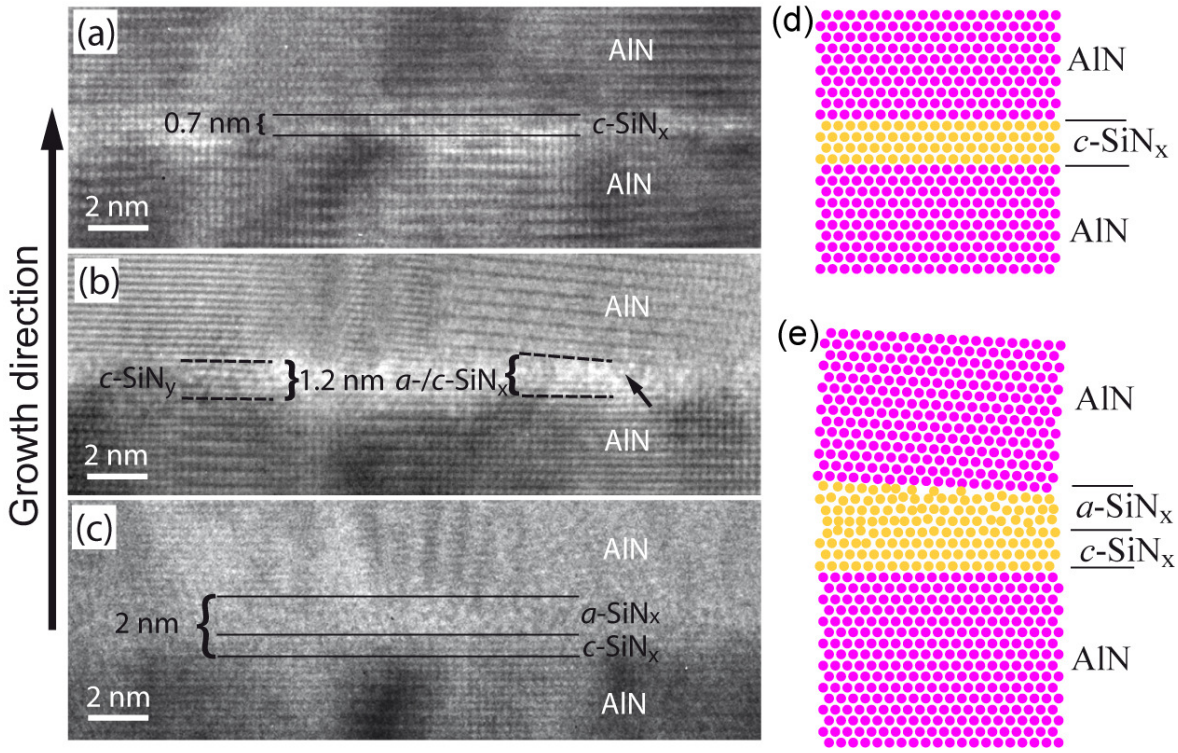

Figure 28 *HRTEM cross-sections through the AlN/SiN multilayers with varying SiN layer thicknesses:* **(a)** *0.7 nm;* **(b)** *1.2 nm;* **(c)** *2 nm; Schematic model of the atomic arrangement inside the SiN layer for the following thicknesses* **(d)** *0.4 nm and 0.7 nm;* **(e)** *1.2 nm and 2 nm.*

At a SiN_x thickness of 1.2 nm the HRTEM image in Figure 28(b) reveals a very interesting feature: the first 0.7 nm of the SiN_x layer growing directly on the epitaxial AlN is crystalline. Only the remaining 0.5 nm grow amorphous, as in the area indicated in Figure 28(b) by the arrow, causing thus breaking of the epitaxy in the multilayered structure. Indeed, the upper AlN layer is composed of grains with differently oriented atomic planes. The same behavior is observed for a 2 nm thick SiN_x layer, Figure 28(c), with the difference that the interface between the crystalline SiN_x and the amorphous SiN_x is much better visible. Therefore a schematic model, Figure 28(e), based on the HRTEM image, has been proposed. When the thickness of the SiN layer is lower than 0.7 nm it is forced to grow in a crystalline structure. Above this thickness the first 0.7-1.0 nm are crystalline and everything above this becomes amorphous. The crystalline grains formed in the next layer of AlN are almost indistinguishable, as they may be tilted out of visibility conditions due to the interruption of the epitaxy by the amorphous SiN_x layer, Figure 28(c). It is also

possible, that the lattice planes of the AlN layer above the SiN_x layer are rotated in respect to their original position in the bottom epitaxial layer, Figure 28(b).

SiN_x can indeed be deposited in crystalline form with a space group of $P6_3/m$ at temperatures above 1550°C. The only stable phase is reported with the Si_3N_4 stoichiometry. Si_3N_4 occurs in two hexagonal crystallographically stable forms α-Si_3N_4 and β-Si_3N_4 [Grün 1979], the latter one being the more stable. In pure and also amorphous Si_3N_4, Si atoms are four-fold coordinated to N atoms. Si atoms incorporated in an $Al_{1-x}Si_xN$ solid solution are expected to retain a four-fold coordination to N atoms.
According to the observations described in this paragraph and in literature, dealing with the TiN/SiN multilayers [Söd 2005], [Söd 2006] and [Hul 2007], it is possible in both systems to stabilize up to three (AlN) / two (TiN) monolayers, corresponding to about 0.7 nm / less than 0.5 nm of SiN_x, respectively, either in the wurztite structure on AlN deposited at 200°C or in cubic form on TiN deposited at 500°C or higher. However, as will be shown by conventional and HRTEM in Figure 29 and in [Par 2010], SiN_x layers of 0.5 nm thickness, deposited at 200°C, are sufficient to separate the TiN grains is the subsequent layers.

Extrapolating the findings for multilayers further to the 3D structure of nanocomposites one possible explanation for the weak hardness increase in the AlSiN nanocomposite could be related to the strong preferential growth of AlN in the (002) direction. Indeed, in the case of the nanocomposite all grains are oriented in the same direction. Additionally, as shown in this paragraph, up to 0.7 nm of SiN_x can be epitaxially stabilized on AlN. Thus the AlN/SiN/AlN interfaces would not constitute a very important barrier for dislocation movement. In the case of TiN, which does not exhibit such strong preferential growth, the nanograins are oriented randomly. Although, it is possible to stabilize about 2 monolayers of SiN in cubic structure, as shown by Söderberg [Söd 2005], [Söd 2006] and [Hul 2007], apparently the random orientation of the crystalline TiN prohibits dislocation mobility leading to a more important hardness enhancement of the TiN/SiN nanocomposite.

5.3.2 TiN/*a*-SiN_x MULTILAYERS WITH VARYING BI-LAYERS THICKNESSES

The TiN/*a*-SiN_x system was made popular due to the concept of nanocomposites where two immiscible materials are combined to form a crystalline nano-granular structure surrounded by an amorphous phase. This kind of structure impedes the formation and movement of dislocations making the material very hard. As the pure TiN film has a

columnar structure, as shown in the dark field image taken with the [002] reflection, Figure 35(a), in order to suppress the columnar growth, reduce the grain size and thus enhance hardness, two multilayered coating consisting of crystalline *fcc*-TiN layers separated by amorphous layers of SiN_x with varying bi-layer thickness have been deposited. The results of the atomic-scale structure study of the interfaces will provide important information, which can be compared with the one obtained for the AlN/SiN system helping to explain the faint hardness increase in the latter one.

The TiN/SiN_x multilayered films were deposited by reactive unbalanced magnetron sputtering from elemental titanium and silicon targets. 100 repetitions of either 5 nm TiN and 0.5 nm SiN_x or 200 repetitions of 1 nm TiN and 1 nm SiN_x were prepared resulting in a total layer thickness of 550 nm or 400 nm, respectively. The operating pressure was 0.5 Pa at a sputter gas composition of Ar/N_2 of 4:1. The deposition temperature was kept at 200°C; a negative substrate bias voltage of 70V was used to provide sufficient surface mobility of the growing film. For improved adhesion on the silicon substrates an interlayer of 50 nm TiN was applied. In order to enhance the interface smoothness at these low temperatures helium (amounting to 10% of the total gas flow) was added to the gas feed.

The TiN/SiN multilayering is clearly visible, Figure 29(a) and there seems to be no area, where a TiN column would grow epitaxially through the amorphous SiN_x layers or form long columnar structures throughout the film thickness. Both element combinations constituting the bi-layer are immiscible, consequently an amorphous layer of 0.5 nm SiN_x is sufficient to prohibit the columnar growth of crystalline TiN out of the film TiN layers at this low deposition temperature. Consequently, it is assumed that no heteroepitactic relation is present between the TiN grains of the adjacent layers. The diffraction pattern in Figure 29(b) contains strong reflections in the [200] direction, indicating texturing of the TiN. Additionally, satellite reflections originating from the multilayering are visible in the central spot.

In the HRTEM image in Figure 29(c) atomic fringes of crystalline TiN are occasionally visible in the amorphous SiN_x layers. This could be due to the fact that the sample is not perfectly perpendicularly oriented towards the incident electron beam. Although this presence of atomic fringes in the supposed amorphous SiN_x layers could indicate that some of the SiN_x is locally crystallized and consequently lead to local epitaxy between the TiN grains, in the HRTEM image, Figure 29(c), the TiN grains adjacent to the SiN_x layers have always different orientations. Even if their orientation is the same, the grain is rotated and

thus the lattice fringes occur at a different angle as shown by arrows in Figure 29(c). This is also confirmed by the FFT calculations performed on the HRTEM image of different grains numbered from 1 to 4 on the right side of Figure 29. The 5 nm high TiN grains were found to grow equiaxed: *i.e.* they are 5 nm in height and maximum 5 nm in width.

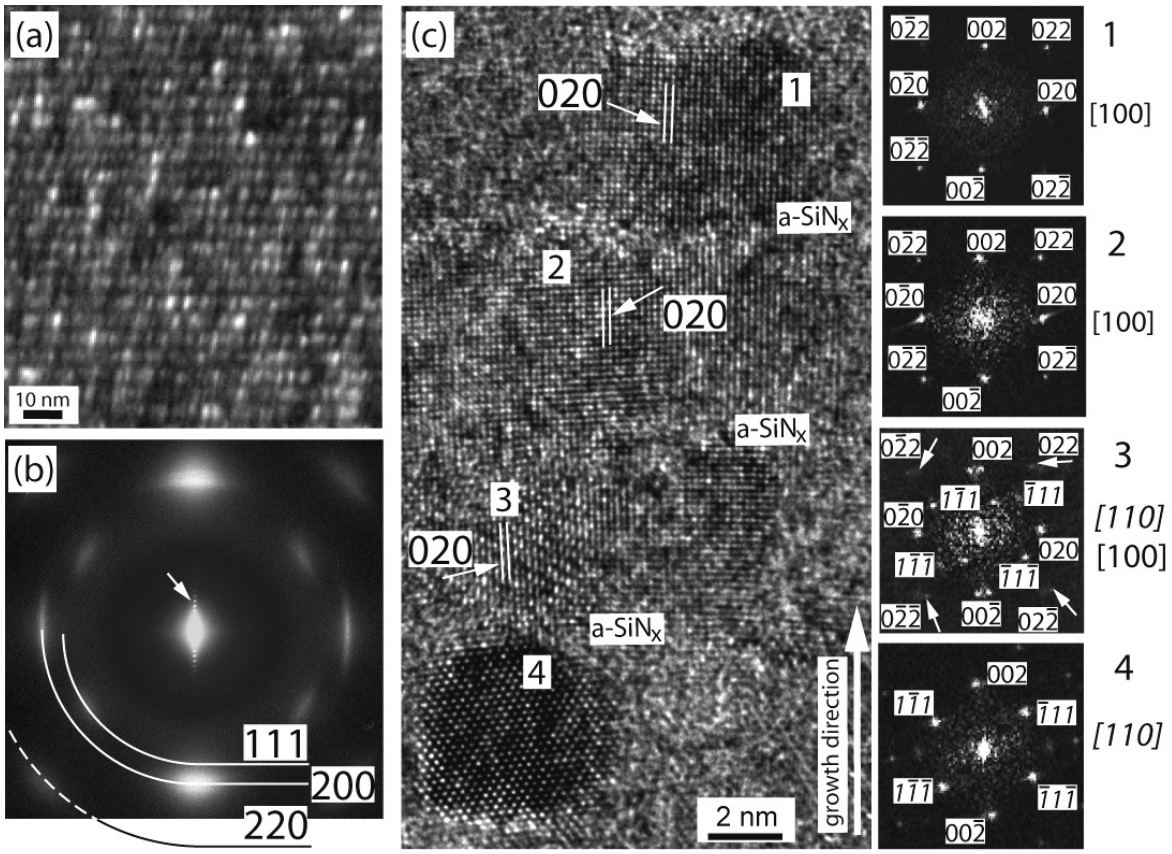

Figure 29 (a) *Dark field TEM image of the cross-section through a TiN/SiN_x multilayered coating consisting of 5 nm TiN separated by 0.5 nm SiN_x;* **(b)** *diffraction pattern inset, exhibiting preferential orientation along the [002] direction and containing satellite spots around the central transmitted beam originating from the multilayer structure;* **(c)** *High resolution TEM image showing the TiN multilayers containing differently oriented crystalline TiN grains separated by amorphous layers of SiN_x. On the right side of the figure four FFT patterns from the respective TiN grains denoted 1- 4 are presented and indexed.*

The second multilayer layout, consisting of 200 repetitions of 1 nm TiN and 1 nm *a*-SiN_x was deposited in order to verify if it is possible to reduce further the size of the TiN grains, keeping them nevertheless crystalline. The TEM investigation allowed to image the multilayer stack by bright field and dark field images shown in Figure 30(a) and (b), respectively. The TiN grains inside the 1 nm layer do not grow out of it as clearly visible from the dark field image. The diffraction pattern indexed with the lattice parameter of *fcc*-TiN, Figure 30(b), consists of sharp circles, which originate from the randomly oriented TiN nanograins. However, the ring corresponding to the [002] reflection contains large spots indicating a preferential [002] orientation of the 1 nm Ti crystallites. In the HRTEM

image, Figure 30(d), the lattice fringes in the dark TiN layers can be distinguished from the amorphous structure of the light SiN_x layers. The poor contrast is due to the too thick FIB lamella, which is about 80 nm thick, being at the limit of HRTEM imaging capacity.

There are various literature references dealing with the microstructural features of TiN/SiN multilayers depending on the thickness of both components. A very interesting study was published by Hultman et al. [Hul 2007] who found, performing molecular dynamic simulations of SiN_x deposited onto crystalline TiN, that only one monolayer of SiN_x deposited onto TiN will be crystalline and cause epitaxial growth of TiN. Already two monolayers of SiN_x deposited on TiN are sufficient to prevent crystal growth throughout the layers as these two monolayers grow amorphous.

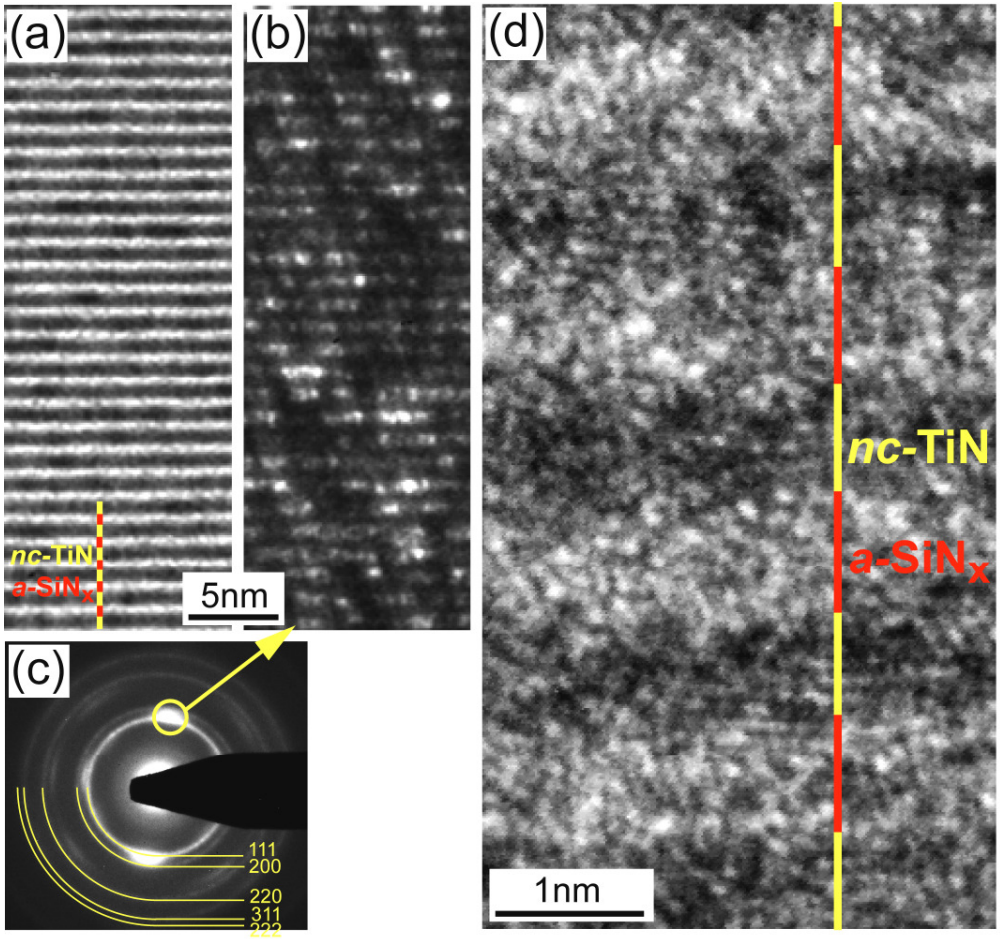

Figure 30 (a) &(b) *Bright and dark field images of the cross-section through a TiN/SiN_x multilayered coating consisting of 1 nm TiN separated by 1 nm SiN_x* **(c)** *Corresponding diffraction pattern;* **(d)** *HRTEM image of the coating.*

5.3.3 SUMMARY OF MULTILAYERS AS A MODEL SYSTEM FOR NANOCOMPOSITES

A general observation was made during the analysis of all multilayered coatings, studied in the papers [Par 2004a], [Par 2010] and [Rze 2009a], independently if they were consisting of sequences of alternating crystalline and amorphous phases or two crystalline phases: the grains inside the crystalline layer have always the height of the layer and the width adequate to their height so that they become equiaxed. This is true for crystalline layer thicknesses up to 25 nm, in particular, if they are separated by an amorphous layer. Indeed in [Par 2010], Figure 29 and Figure 30, the TiN grains in the 5 nm layers and in the 1 nm layers are equiaxed and have widths of 5 nm and 1 nm, respectively. This behavior could be due to the fact that equiaxed grains have the lowest energetic state. Moreover, the ability of grains to favor equiaxial growth in multilayers enables to produce nanocomposites from these materials. This makes multilayers suitable as two dimensional model systems for nanocomposites.

The sharpness and quality of the interfaces between the crystalline and the amorphous layers depends on the miscibility of the two constituting phases. If the two materials are immiscible, as it is the case of TiN and SiN_x, Figure 31(a), the TiN/SiN_x interface will be sharp and abrupt. SiN_x is amorphous when grown by sputter deposition at the commonly used temperatures (up to 400°C) for co-deposition with other elements.

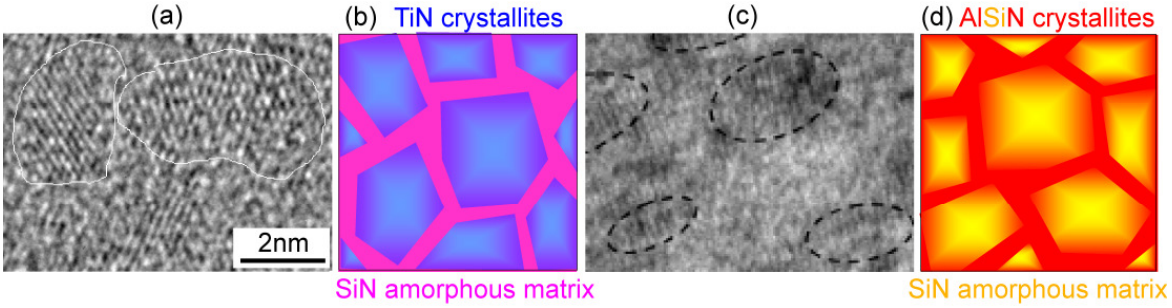

Figure 31 (a) *HRTEM image of the TiAlSiN nanocomposite coating composed of TiAlN crystalline grains surrounded by amorphous SiN_x;* **(b)** *Schematic representation of the TiAlSiN nanocomposite separated by abrupt grain boundaries from the amorphous SiN_x matrix* **(c)** *HRTEM image of the AlSiN nanocomposite;* **(d)** *Schematic representation of the AlSiN grains separated by interfaces with local epitaxy at the amorphous SiN_x matrix.*

SiN_x, when deposited at temperatures around 1500°C, grows crystalline with a hexagonal structure [Grün 1979]. Therefore when intercalated with TiN, which is cubic, there are no structural similarities between the TiN and SiN_x phases and their interface is abrupt, as represented on the schematic representation in Figure 31(b). Moreover, TiN does not grow with a pronounced preferential orientation, what causes that in the TiSiN nanocomposite

the grains are all oriented in a random way. Thus even two monolayers of the amorphous phase are sufficient to prohibit the columnar growth of the crystalline layers and form a multilayered structure. Conversely AlN and SiN are miscible *i.e.* about 6 at.% Si can be substitutionally incorporated onto the Al sites in the AlN lattice during co-deposition of Al and Si, causing some lattice distortions inside the columnar AlN grains, [Péli 2009]. Only the excess of Si forms an amorphous SiN phase around the AlSiN grains. In addition, AlN grows in a very pronounced preferential [002] orientation, which also happens in the AlSiN nanocomposite: the lattice fringes visible inside the nanograins are all oriented in the same direction, HRTEM image in Figure 31(c). Therefore in the multilayer system alternating AlN with SiN no abrupt interfaces are observed. Indeed the growth of the columnar AlN is not interrupted if the SiN_x layer is thinner than 0.7 nm in the multilayered system deposited on Al_2O_3. At the 1.2 nm SiN layer thickness locally some AlN grains are interrupted by the *a*-SiN_x layer and others grow epitaxially into the next AlN layer. If the SiN_x layer thickness exceeds 2 nm the first 1 nm of the SiN_x grow crystalline and the remaining 1 nm is amorphous. Consequently, in the AlSiN/SiN nanocomposite no substantial hardness enhancement is observed, as interfaces with local epitaxy are present, which do not obstruct dislocation mobility, as schematically shown in Figure 31(d).

6 DEFORMATION MECHANISMS IN HARD ME-N COATINGS

In order to understand the hardening effects in thin films, the mechanisms involved in plastic deformation were analyzed in detail. As the most common method to measure the hardness of materials involving plastic deformation is the nanoindentation technique, therefore detailed TEM studies were performed on cross-sections of indent imprints, to analyze the damages induced and the deformation mechanism involved in the indentation process. Indeed, the deformation process involves the nucleation and movement of dislocations. Therefore it is of crucial importance to study and understand the different processes accompanying the deformation, which will allow designing the coatings in a way to prevent the occurrence of these mechanisms, comprising among others: structural densification, microcrack propagation, shear sliding at grain boundaries in columnar coatings and grain boundary sliding in nanograined materials. Also the influence of the substrate structure and hardness has to be taken into account. The investigation of hardness-enhanced nanocomposite cracking pattern in single crystalline and columnar TiN films plastically deformed under load is expected to provide insight in the deformation mechanism through analysis of the deformed zones, in particularly by TEM.

In coatings with columns growing through the entire coating thickness, when subjected to deformation, the columns undergo shear sliding along their boundaries, which are the weakest site in the microstructure. This mechanism was demonstrated by several authors [Xie 2006], [Ma 2005], [Cai 2005], [Car 2006], [Mol 2002], [Söd 2005] and [Söd 2006] and is also observed in one of the indented reference coatings described in [Rze 2009a], [Rze 2009b] and §6.2a). Nevertheless, as will be shown in §6.2, the grain boundary shear sliding mechanism is also observed on different scales in coatings, in which the columnar growth is on purpose obstructed by the introduction of a multilayered structure. *Post-mortem* TEM observation and analysis of plastically deformed zones in multilayered coatings, can contribute to understanding the deformation behavior of such materials, provided that single grains and the amorphous tissue phase can be imaged.

First of all the influence of the substrate structure and hardness on the fracture damage generated in coatings during nanoindentation will be discussed. In the following paragraphs the *post-mortem* TEM investigations of the damages induced by nanoindentation into coatings on several examples will be presented. The first group consists of coatings containing TiN with a columnar structure [Rze 2009a] or multilayers such as *fcc*-TiN/*a*-SiN_x, [Par 2010] and *fcc*-TiN/*fcc*-NbN [Rze 2009b] and it could be shown that all the coating combinations with TiN deform by shear sliding at grain boundaries independently on the grain size. The second group does not contain TiN and thus undergoes different deformation mechanisms. It is composed of columnar *fcc*-CrN, *fcc/hcp*-NbN and *fcc*-CrN/ *fcc*-NbN multilayers, [Rze 2009a], [Rze 2009b]. The cross-sectional lamella for TEM analysis of the residual indent impressions were cut by FIB milling, described in details in §4.3.2.

6.1 INFLUENCE OF THE SUBSTRATE ON FRACTURE DAMAGE IN TiN COATINGS

Hard Me-N coatings are often deposited on various substrates, therefore it is of crucial importance to determine, if and how far the substrate influences the fracture damage generated during indentation. In the following paragraph a comparison of deformation modes and fracture patterns in single and polycrystalline TiN coatings deposited on soft and hard substrates is presented. All the cross-sectional TEM lamella through the indents were cut by FIB milling according to the scheme shown in Figure 32.

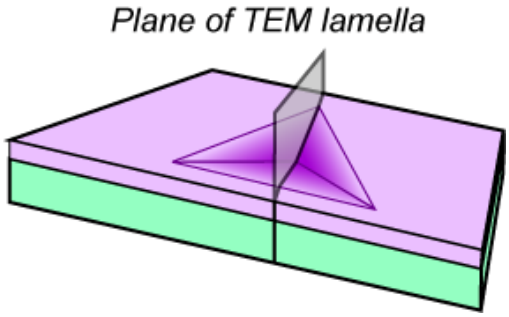

Figure 32 *Schematic of the TEM lamella orientation for the cross-section through the indent. All the TEM lamella were milled, so that the cross-section through the imprint passes across one facet and the edge on its opposite.*

6.1.1 SINGLE-CRYSTALLINE TiN COATINGS GROWN EPITAXIALLY ON MgO (001) & (111) SUBSTRATES

Single crystalline TiN coatings having a thickness of 500 nm were epitaxially grown on MgO (001) and (111) substrates at 800°C in order to study the fracture damage generated during plastic deformation upon nanoindentation. Subsequently cross-sectional TEM lamellae were cut in order to enable the visualization of the deformation damage and crack pattern. It is one of the first attempts to directly visualize and analyze by TEM the cracking patterns in single crystalline TiN coatings. First of all, the single crystalline character of the TiN films and their epitaxial growth on MgO were confirmed by TEM. After nanoindentation, it was found that the TiN (001) coating underwent compression, Figure 33(a), which is due to long range elastic deformation and local plasticity underneath the indenter tip. A conservation of volume over long range occurs and residual stress is induced. Additionally a lot of dislocations were generated in the coating, particularly well visible as dark contrast in Figure 33(c). The fracture pattern in this coating consists of a series of small, regularly spaced cracks on top of the coating following the <200>, <220> and <111> crystallographic directions, Figure 33(b) & (c). They are formed as a result of stretching of the film around the indent edge due to strong adhesion between the coating and the substrate. In the direct vicinity of the lower tip of one of the cracks generated in the <200> direction shown in Figure 33(c), another crack starts deviating along the <220> direction and then diverge back to the <200> direction. Such crack jumps and deviations are the result of having more energy in the system than the one needed to simply propagate the crack along a specific atomic plane. Hence, crack jump and deviation are ways to dissipate the excess of energy.

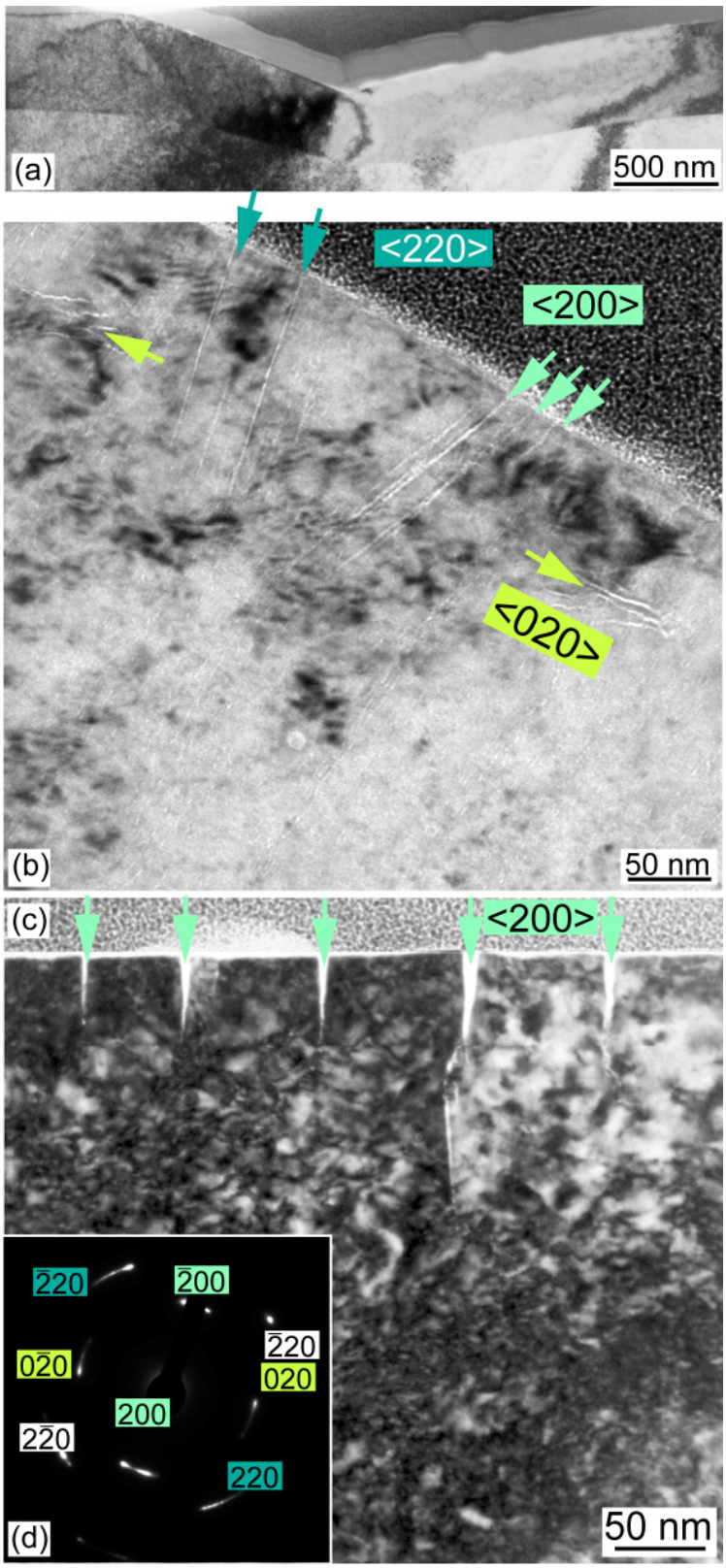

Figure 33 (a) *Cross-section through a Berkovich indent imprint performed in a 500 nm thick TiN coating grown epitaxially on MgO (001) substrate; Magnified views with generated cracks with identified crystallographic directions:* **(b)** *right side deformed by the edge of the indenter tip;* **(c)** *left side matching the facet of the indenter tip;* **(d)** *Diffraction pattern in the [100] zone axis, which allowed to determine the crystallographic directions of the cracks.*

The cracking patterns induced in the single-crystalline TiN films look similar to the ones described by Jayaram [Jay 2006], although his observations were performed by SEM in amorphous DLC coatings deposited on soft steel substrates.

The SAED pattern taken in the [100] direction, Figure 33(d), allowed identifying the crystallographic directions of the cracks generated in the coating. The elongated <220> spots of the SAED pattern, taken from a deformed area of the coating, are due to the presence of a high density of dislocations induced during plastic deformation, visible as dark contrast in the bright field image in Figure 33(c).

Attempts to identify deformation induced dislocations in single-crystalline TiN films by TEM were undertaken by Carvalho [Car 2006]. The primary slip system for dislocations glide in TiN crystals has been characterized by plastic deformation on {110} planes with slip occurring along the <110>. Due to its B1 NaCl type structure, the TiN should deform under compression along the {111} planes.

For the TiN coating grown epitaxially on the MgO (111) substrate similar results as for the TiN (001) film were obtained. Figure 34(a) shows the TEM image of the cross-section through the indent imprint performed in TiN (111) single-crystalline coating. The coating was compressed due to the local plasticity underneath the indenter tip, Figure 34(c). Also in this case a high density of deformation dislocations was generated, Figure 34(d). The diffraction pattern taken from the deformed area, Figure 34(b), has a single crystalline aspect, although some of the spots are elongated due to high density of dislocations. The cracking pattern, shown in Figure 34(c) - (e) was a little different from the one observed in TiN (001), due to the fact that it was viewed along a different crystallographic direction i.e. [110], as the substrate was oriented differently and the TEM lamella was cut accordingly. On the left side of the indent imprint, corresponding to the facet of the tip, regular, parallel cracks, along the <220> direction, reaching the entire coating thickness were generated, Figure 34(d). It is well known, that it is more favorable energetically for the material to put always a crack in the same crystallographic direction at a half distance in between the two previously induced cracks. Some of these cracks opened to form large cracks, which are not straight, but jump and deviate from the original <220> direction, Figure 34(d). Moreover, large cracks in the <200> direction, Figure 34(e), were generated. The cracks at the right side of the indent imprint, corresponding to the edge of the indenter tip, form networks looking like columnar grains. As the adhesion to the substrate is very good, the coating under tensile stress generated by the indenting tip has no choice but to crack.

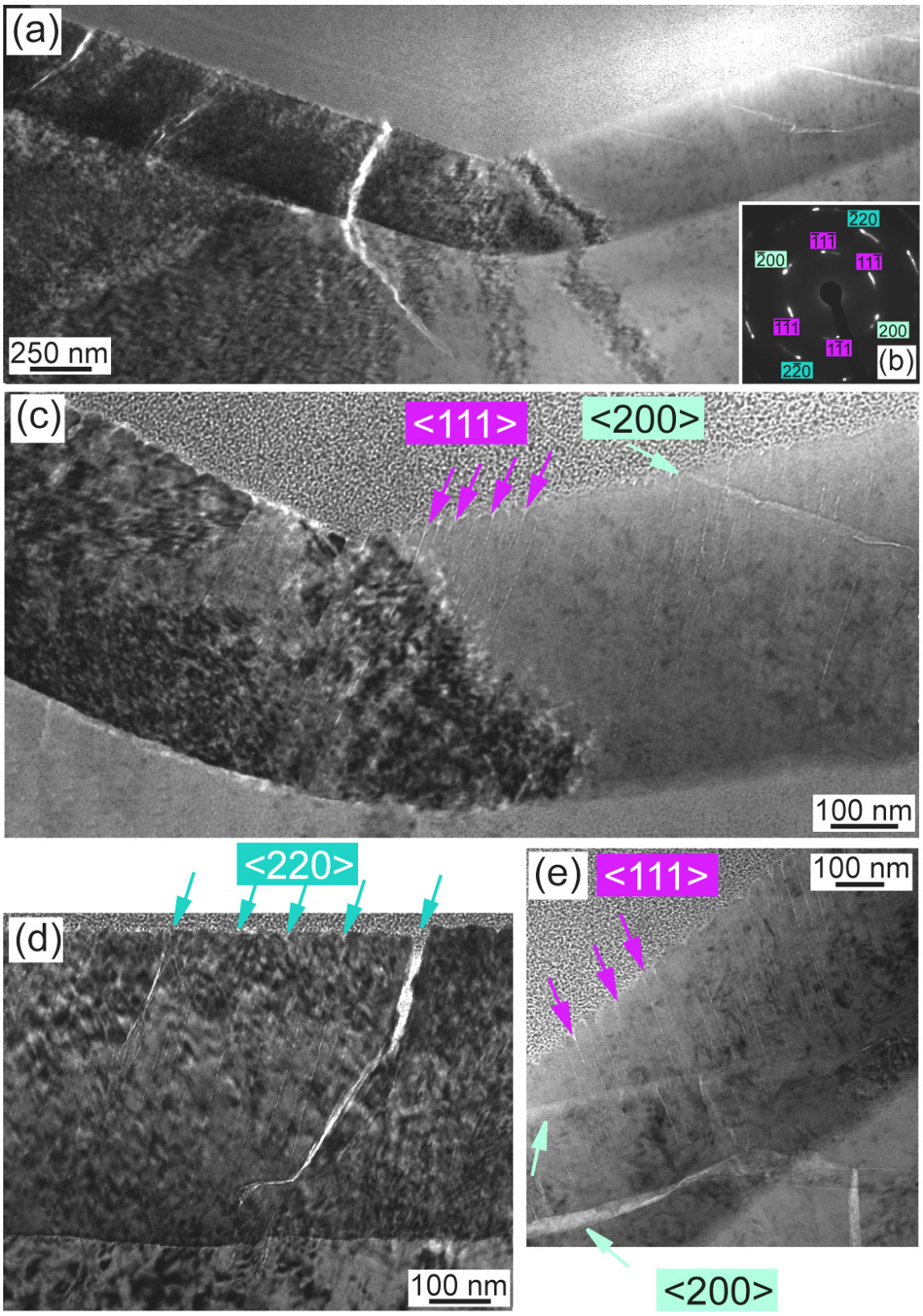

Figure 34 (a) *Cross-section through a Berkovich indent imprint performed in a 500 nm thick TiN coating grown epitaxially on MgO (111) substrate;* **(b)** *Diffraction pattern in the [110] zone axis, which allowed to determine the crystallographic directions of the cracks; Magnified views with generated cracks and identified crystallographic directions:* **(c)** *central part* **(d)** *left side deformed under the indenter tip facet;* **(e)** *right side matching the indenter tip edge.*

6.1.2 POLYCRYSTALLINE COLUMNAR TiN COATINGS – INFLUENCE OF SOFT AND HARD SUBSTRATES

A). **COLUMNAR TiN COATING GROWN ON SOFT SI SUBSTRATE**

The first TiN coating was deposited on a Si (100) substrate, which is considerably softer, than TiN. As shown in Figure 35(a) the cross-section through the as-deposited TiN coating, exhibits a columnar structure. It was, as expected, found to grow as *fcc*-TiN, with a slight [002] preferential orientation according to the left half of the diffraction pattern, Figure 35(c).

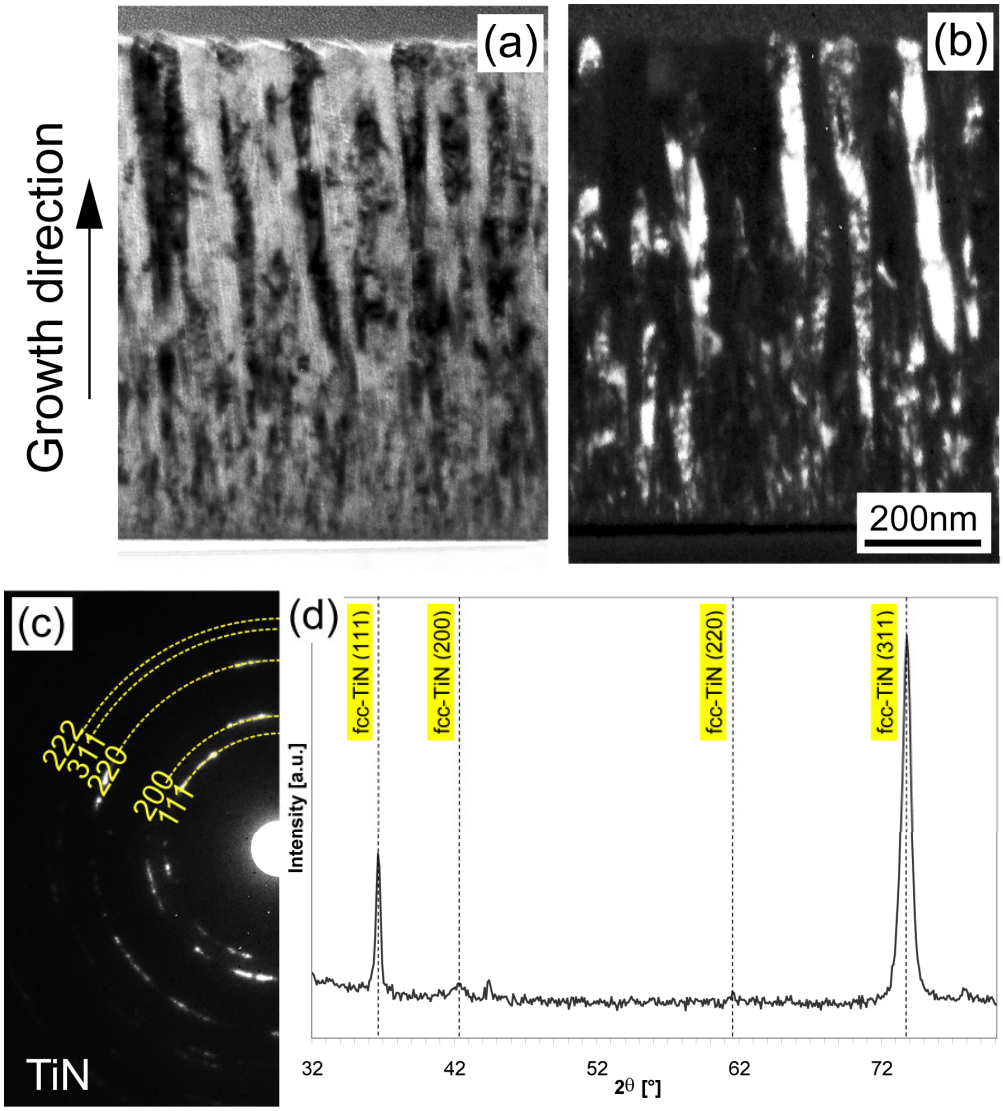

Figure 35 *TEM cross-sections through the monolithic TiN coating:* (a) *bright field;* **(b)** *dark field;* **(c)** *SAED pattern and* **(d)** *XRD diffractogram showing the presence of the fcc-TiN phase.*

The dark field image, Figure 35(b), taken with the [002] spot shows a columnar structure of the TiN with strong white and black contrast visible respectively on columns contributing to the [002] reflection and the ones out of orientation. The zones exhibiting

similar contrast level inside the columns reach almost the entire length of the latter ones, what together with a spot-like diffraction pattern strongly suggests a well crystallized material *i.e.* almost single crystalline columns.

The XRD diffractogram, Figure 35(b), shows two sharp peaks confirming the *fcc* phase and the high crystallinity of the TiN coating with a mixed (002) and (311) orientation. The hardness of the TiN coating measured by nanoindentation was at the order of 17GPa.

The TiN coating was deformed by nanoindentation with a Berkovich tip with a penetration depth limited to about 10% of the coating thickness. Further technical details of the indentation procedure can be found in [Rze 2009a] and [Rze 2009b]. The TEM bright field image of a cross-section through the indent imprint in the TiN coating, shows that the columns under the indented area are displaced vertically, Figure 36(a). The columns, as their boundaries are fractured, are literary pushed into the softer Si substrate. Thus a step-like arrangement of the columns is formed at the interface with the substrate, as visible in Figure 36(a) & (b).

At the boundaries between the columns cracks were induced as pointed out by the arrows on the magnified view, Figure 36(b). This phenomenon in the *Me-N* films is termed in literature *intergranular cracking* and *shear sliding at grain boundaries* [Ma 2005], [Cai 2005]. It is a typical deformation mechanism in coatings with a columnar structure, and particularly in TiN as will be shown in this manuscript, when the indentation load is applied in the direction parallel to the column boundaries, as the latter ones are the weakest site in the microstructure. Once the adjacent columns are separated from each other by the formation of cracks as a result of shearing deformation, the indenter tip can easily displace in the vertical direction the columns located underneath it. The shear sliding at grain boundaries *i.e.* the vertical displacement of columns can be regarded as a general deformation mechanism occurring in columnar coatings independently of the size of the columnar grains as will be shown in §6.2.

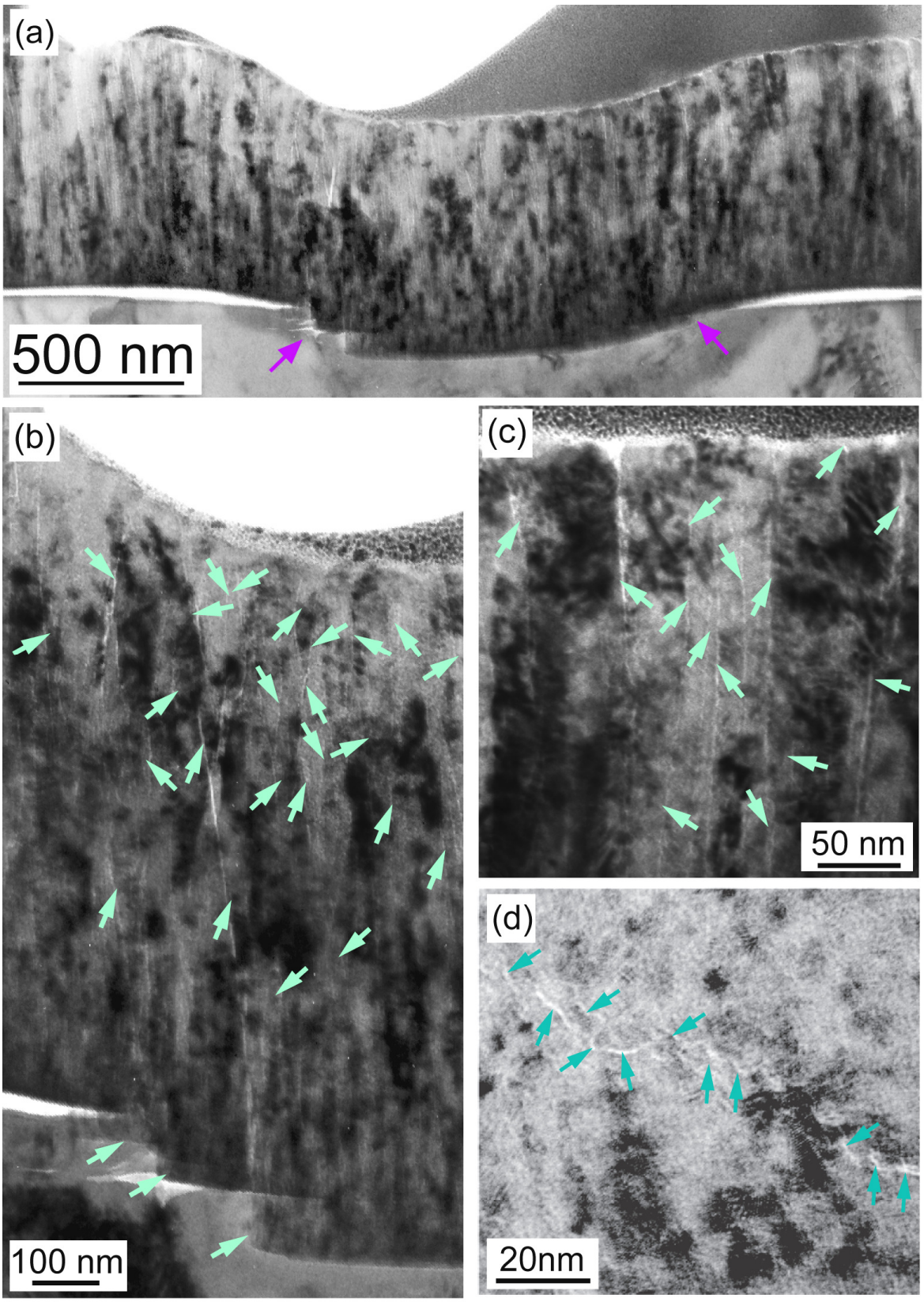

Figure 36 (a) *Indent imprint in a TiN columnar coating;* **(b)** *Steps at the interface with the Si substrate resulting from sheared TiN columns;* **(c)** *Magnified view of the cracks at the column boundaries;* **(d)** *Deformation damages in nanogranular TiSiN coating in form of irregular cracking, after Cairney [Cai 2005].*

For comparison, if the coating is fine-structured, composed of TiN nanograins of the order of 10 nm surrounded by an amorphous SiN_x matrix, Figure 36(d) after Cairney [Cai 2005], [Ma 2005], after indentation only short, irregular cracks are observed inside this kind of coatings. These authors claim that the deformation is accommodated by grain boundary sliding *i.e.* displacement of grains and short cracks. However, they succeeded only to observe by TEM intergranular cracks following tortuous paths around the grains, which were induced after the grain boundary sliding mechanism took place, as the deformation induced was much more than necessary, for grain boundary sliding to occur. Consequently, if these cracks were visible in the TEM, they must have had a depth reaching the TEM lamella thickness. Unfortunately an experimental visualization by TEM of grain boundary sliding in nanocomposites is impossible, for the following reason: the differently oriented grains have a diameter of 5-10 nm and the TEM lamella thickness is several times superior in thickness *i.e.* 50 nm and therefore the superposition of grains in the observation direction occurs, what makes the visualization of individual grains impracticable. Nonetheless attempts to reduce the three dimensional structure to two dimensions by the creation of a multilayered structure have been undertaken.

B). COLUMNAR TIN GROWN ON SINGLE CRYSTALLINE TIN COATINGS

The second TiN coating was grown on single crystalline TiN substrate having a comparable hardness to polycrystalline TiN. This very particular coating was deposited in order to unambiguously demonstrate by direct observations, that the grain boundary sliding mechanism in columnar coating is governed by the substrate hardness. In this coating 250 nm of columnar TiN was grown on 250 nm epitaxial, single-crystalline TiN deposited on MgO (001), Figure 37(a) & (b). To stop the epitaxial growth of the TiN, a 0.5 nm thin SiN_x layer was deposited, which resulted in re-nucleation of columnar TiN.

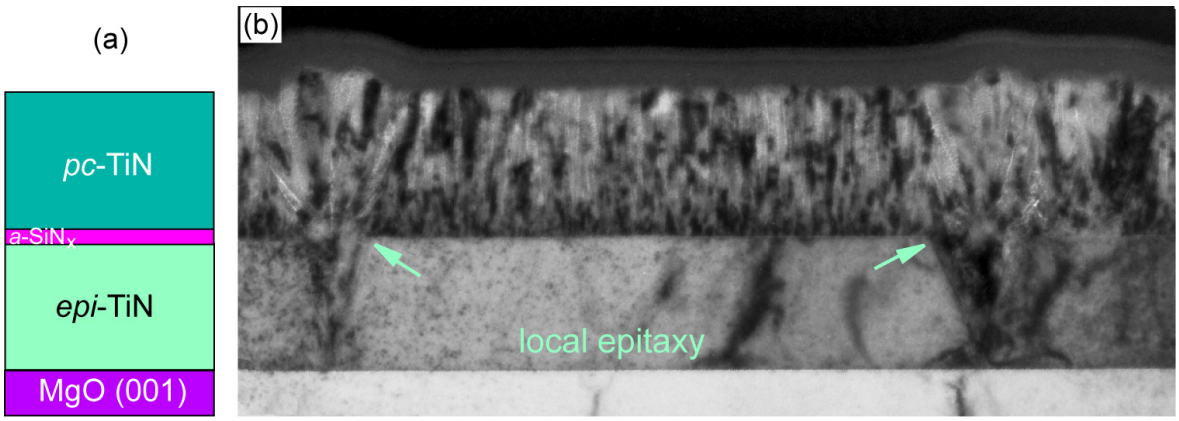

Figure 37 *Polycrystalline, columnar TiN deposited on single crystalline TiN grown epitaxially on MgO (001) substrate. At the interface between the differently structured TiN layers a 0.5 nm thin SiN_x layer was deposited to stop the epitaxy of TiN and renucleate the columnar growth.* **(a)** *Schematic representation of the coating layout;* **(b)** *TEM bright field image of the cross-section through the coating, with some local epitaxy causing the presence of large columnar grains shown by green arrows.*

After indentation, both TiN layers of the coatings underwent plastic deformation and compression, Figure 38(a). The diffraction pattern, Figure 38(b), was taken from the single crystalline part of the coating and is composed mainly of spots. Many cracks along the column boundaries following the <200> direction have been generated, Figure 38(c). After reaching the single-crystalline TiN layer, some of the cracks continue along the <200> direction and some deviate along the <111> direction, Figure 38(c). A magnified view of the interface between the columnar and the single crystalline TiN is shown in Figure 38(d). The SiN_x layer deposited at the interface was used as a marker to observe the displacement of the sliding TiN columns after indentation. Individual columns which underwent grain boundary sliding are marked by pink arrows in Figure 38(d). Pieces of broken SiN_x marker layer are also visible in the vicinity of the displaced columns.

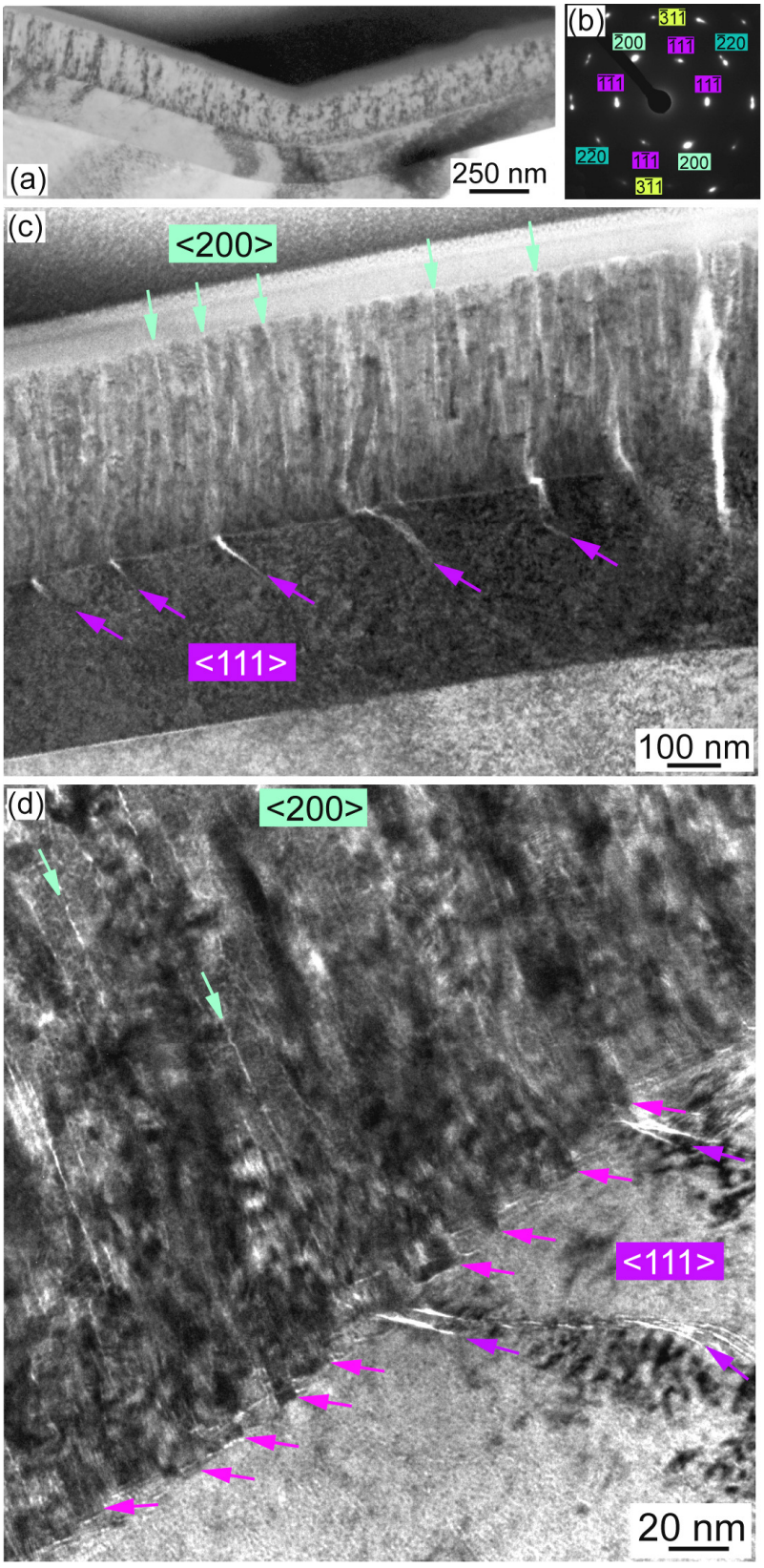

Figure 38 **(a)** *Cross-section through a Berkovich indent imprint performed in a 250 nm thick polycrystalline TiN coating deposited on 250 nm epitaxial TiN grown on MgO (001) substrate; Magnified views with generated cracks and identified crystallographic directions:* **(b)** *right side deformed by the edge of the indenter tip;* **(c)** *left side below the facet of the indenter tip;* **(d)** *Diffraction pattern which allowed to determine the crystallographic directions of the cracks.*

C). COLUMNAR TiN COATINGS GROWN ON HARD WC-Co SUBSTRATE

The last coating from this series was a polycrystalline TiN coating grown on a much harder ceramic WC-Co substrate Figure 39(a). It had a coarse columnar structure, with grains reaching the entire coating thickness.

The TEM/STEM study of the indent imprint revealed, that several mechanisms take place upon plastic deformation. The STEM image of a cross-section through an indent imprint is shown in Figure 39(b) with a clearly visible compression of the whole coating. The columns, which grow on the soft Co matrix are pushed into it, Figure 39(c).

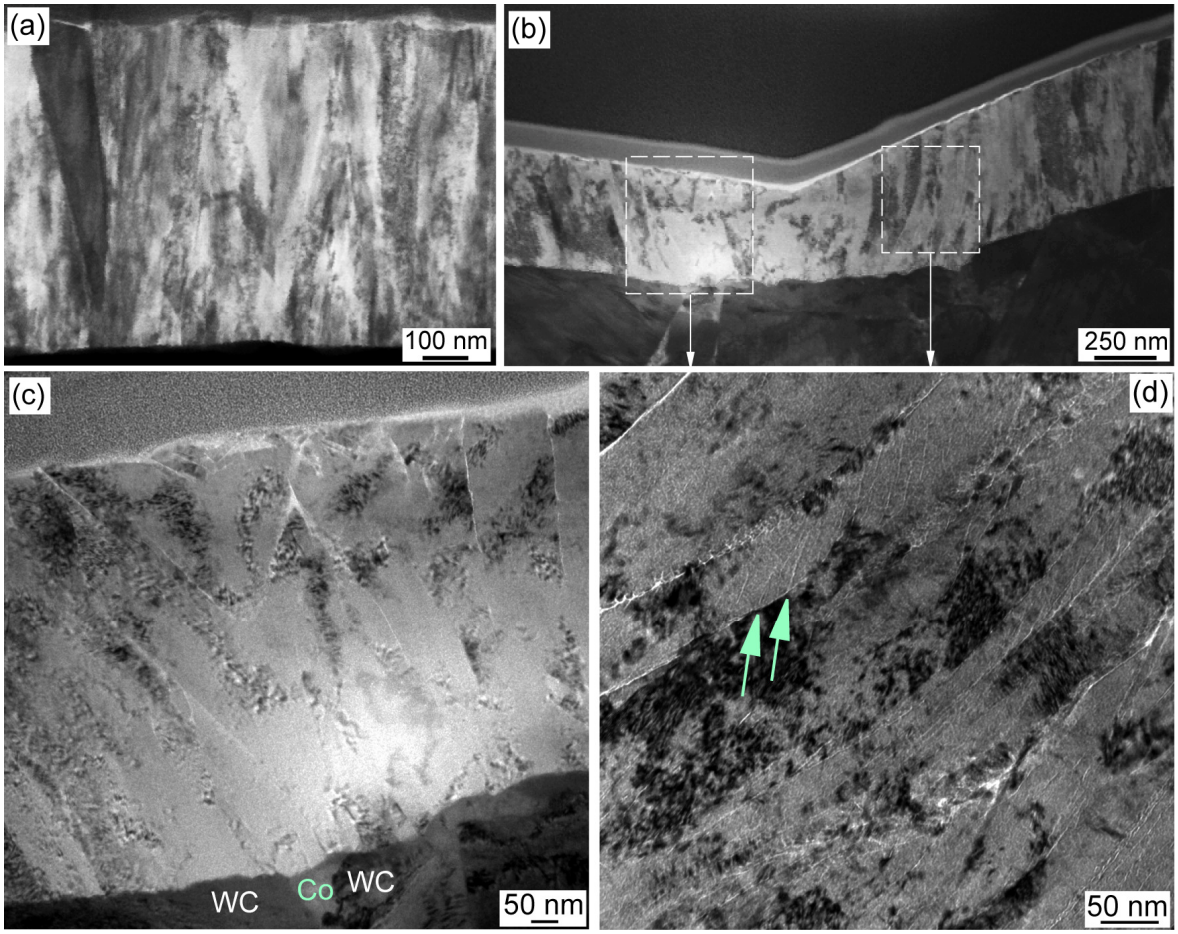

Figure 39 (a) *STEM image of a cross-section through an as-deposited polycrystalline TiN film grown on WC-Co* **(b)** *STEM image of a cross-section through the indent imprint, the whole coating is compressed and on the right side the grains are bent;* **(c)** *Magnified view of the left side of the indent imprint, matching the edge of the indenter tip, with cracks formed along grain boundaries. The TiN grain above the soft Co matrix is pushed into it, while interface between the TiN grains and the hard WC grains is straight;* **(d)** *Magnified view of the right side of indent cross-section, corresponding to the facet of the indenter tip, with cracks generated inside the columns and at their boundaries.*

The deformation of the polycrystalline TiN coating growing on hard WC grains can be regarded as the deformation of a single TiN column (pillar) [Mic 2007] – first it undergoes sliding at the grain boundary, which is the weakest part of the system. When it is further compressed and the critical stress is reached, fractures inside the columnar grains are formed starting from the column boundary towards the inside of the grain. These cracks follow the typical crystallographic slip planes i.e. <111> direction, Figure 39(d).

The bending of the columns originates from long-distance stretching of the surface material, Figure 39(b), resulting from the bending of columns at the bottom due the excellent adhesion to the substrate. The deformation of the poly-TiN coating takes place by material flow, but no pile up occurs due to low toughness of the coating.

6.1.3 SUMMARY OF INFLUENCE OF THE SUBSTRATE ON FRACTURE DAMAGE IN TiN COATINGS

TEM observations of fracture damage induced during nanoindentation in single crystalline TiN coatings epitaxially grown on MgO (001) and (111) substrates revealed compression of the film and a high density of deformation dislocations. The main deformation damage was fracture along the main crystallographic directions i.e. <200>, <220> and <111>. The cracks form a pattern looking similar to the columnar structure. Moreover, some cracks jump and deviate from their original direction, what shows that there is an excess of energy brought into the system that has to be dissipated.

The analysis of polycrystalline TiN coatings grown on substrates with different hardness shows unambiguously that grain boundary sliding is the main deformation mechanism in columnar coatings. The extent of sliding is nevertheless dependent on the substrate hardness. Coatings deposited on substrate being either softer or having a comparable hardness to TiN i.e. polycrystalline TiN deposited on Si or single crystalline TiN, undergo only grain boundary sliding, however the columns are not internally destroyed. If the substrate hardness exceeds the hardness of the coating, as it is the case for the WC-Co substrate, the columns are bent and internally fractured as they cannot be pushed into the substrate as it is the case of the TiN columns growing on WC grains.

All three examples of plastic deformation of columnar TiN coatings grown on substrates with different hardness i.e. Si, single crystalline TiN and WC-Co unambiguously show that

the substrate strongly influences and even governs the fracture damage generated in the coating during plastic deformation during indentation.

6.2 DEFORMATION BY SHEAR SLIDING AT GRAIN BOUNDARIES IN MULTILAYERED COATINGS CONTAINING TiN

Depending on the constituent materials in the multilayer coating, polycrystalline nanolaminate structures are reported to deform by different mechanisms. The most commonly observed are shear sliding at grain boundaries for TiN/NbN, TiN/SiN and TiN/(Ti,Al)N [Mol 2002], [Car 2006] and densification underneath the indentation imprint for TiN/NbN [Chu 1995], [Long 2006].

However, as will be shown in the section below, even the same class of materials *i.e.* metal nitrides, can behave very differently at both: the micro- and nanoscales with regard to material pile-up and sink-in around the tip during indentation. These types of behaviors can greatly affect both: the calculated hardness and modulus values and are not apparent by observing only the load-displacement response. On the other hand, thin film fracture is generally seen in instrumented indentation as a pop-in [Bor 2008]. However, this may also be misleading, as it is shown in [Rze 2009b], that crack initiation is not always associated with pop-in events. These issues can be addressed by *in – situ* indentation performed inside a scanning electron microscope (SEM), since this technique allows for the pile–up, sink–in crack initiation and propagation and shear band formation [Mos 2006] to be observed at the scale of interest in real time. This provides additional information on fracture toughness and strain hardening behavior, which facilitates proper quantitative data evaluation enabling a more accurate calculation of contact area and the establishing of an improved mechanical model. This information, when combined with *post-mortem* TEM studies of the film cross-sections beneath the indents, increases the understanding of the underlying deformation mechanisms of the studied coatings.

In the following paragraphs it will be experimentally shown by TEM analysis that all multilayered coatings containing TiN, deform by shear sliding at grain boundaries at nanoscale with grains of the order of one nanometer.

6.2.1 SHEAR SLIDING AT GRAIN BOUNDARIES AT NANOSCALE IN TiN/*a*-SiN$_X$ MULTILAYERS

TiN/SiN$_x$ multilayered coatings with two layouts i.e. TiN$_{5\ nm}$/SiN$_{0.5\ nm}$ and TiN$_{1\ nm}$/SiN$_{1\ nm}$ were grown on a 50 nm thick buffer layer deposited on Si (001) substrates. The alternating layers of nc-TiN and amorphous SiN$_x$ allow an independent variation of the single layer thickness and a clear identification of the nanostructure in particular after being plastically deformed. In the latter case, the intercalating SiN$_x$ layer helps as a marker to retrieve the original position of the multilayer segment. The TiN$_{5\ nm}$/SiN$_{0.5\ nm}$ multilayer was indented to four different initial depths: 100 nm, 250 nm, 500 nm and 1000 nm in order to observe the deformation mechanisms occurring in nanostructured coatings.

At initial indentation depth of about 20% of the total film thickness, which corresponds to 100 nm the layers directly under the indent imprint are titled out of visibility condition by about 8°, Figure 40(a) and (b). The first sign of failure was the destruction of the multilayer continuity by cracking at the TiN/TiN crystallite boundaries perpendicular to the layer and displacement of either individual TiN grains, Figure 40(e) & (e'), or pieces containing several multilayers, Figure 40(b) by about half period of the multilayer. This failure mode is independent on the TiN/SiN layer thickness, as demonstrated for two samples with different TiN and SiN layer thicknesses: *i.e.* TiN$_{5\ nm}$/*a*-SiN$_{0.5\ nm}$ and TiN$_{2\ nm}$/*a*-SiN$_{1\ nm}$, Figure 40(g). Furthermore a sequence of the deformation mechanisms occurring in nanostructured multilayers during nanoindentation has been proposed.

For initial indentation depths of 250 nm, 500 nm and 1000 nm all the features *i.e.* shear sliding at TiN/TiN grain boundaries of pieces of multilayers as well as the tilting out of visibility condition of the multilayering occurring for the 100 nm indent are present. For the 250 nm indent additionally to these mechanisms completely open cracks at the lower part of the coating, Figure 40(d), corresponding most probably to areas of maximum stress accumulation, occur. The lateral cracks are due to shear stresses exceeding the shear strength of the coating. Moreover, at the coating-substrate interface in the direct vicinity of the latter cracks a beginning of delamination is observed.

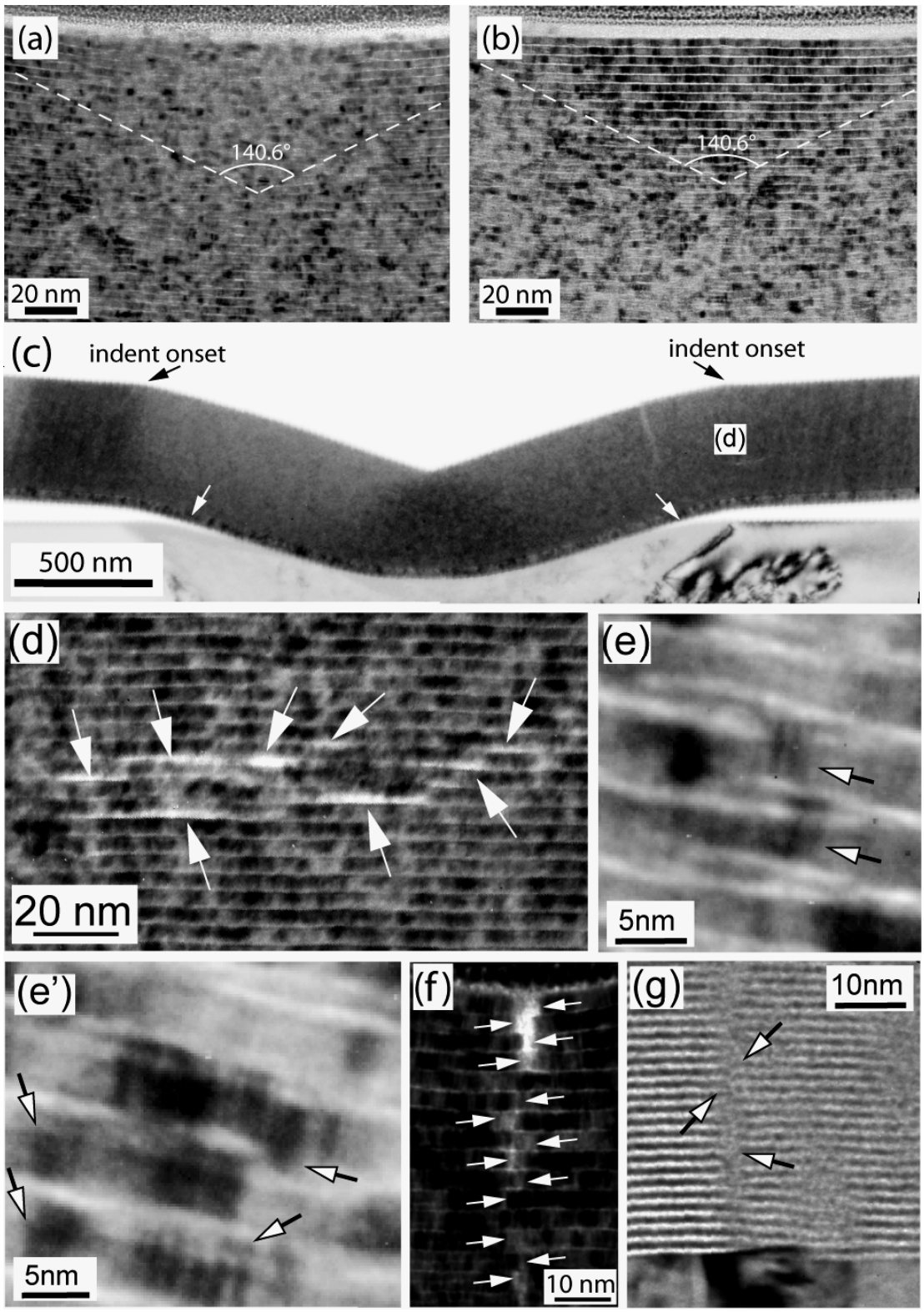

Figure 40 (a) *Cross-section through the 100 nm deep indent with the multilayering tilted out of visibility conditions;* **(b)** *The multilayering is visible again after tilting the sample by 8° around an axis in plane with the layers;* **(c)** *Cross-section through the 1000 nm deep indent: delamination from the substrate as well as vertical cracks at the indent onsets are visible;* **(d)** *Cracks at the TiN/SiN_x interfaces, located at the bottom of the film;* **(e) & (e')** *Magnified view of individual grains displaced due to shear sliding at grain boundaries;* **(f)** *Traces of shear sliding of entire multilayer pieces in the $TiN_{1\ nm}/SiN_{1\ nm}$ coating.*

By indenting further down to 500 nm, the fully open cracks and the delamination become more pronounced. Additionally a vertical crack following the TiN/TiN grain boundaries directly underneath the indenter tip was generated, which is connected with the delamination process controlling the stress distribution inside the coating, Figure 40(f).

The indentation to 1000 nm, Figure 40(c), leads to an almost complete delamination of the film, which has a consequence in stress relaxation inside the coating and resulting in disappearance of the fully open cracks. Also the vertical crack underneath the indenter tip is not visible anymore, most probably because the side parts outside the pile-ups are almost free-standing after the delamination and the deformation stress is thus relaxed. This indicates that the film under these excessive loads delaminates from the substrate due to the high substrate deformation before the lateral cracks can form and split open. At the pile-ups vertical cracks, following tortuous paths along TiN grain boundaries are observed, Figure 40(c).

The main finding from the TEM analysis is a direct observation of the fracture mechanism occurring in multilayers subjected to plastic deformation in form of individual TiN grains, Figure 40(e) & (e'), or multilayer pieces with a width of about 20 nm, Figure 40(g), which are vertically displaced in the plane of the lamella, without being internally destroyed.

6.2.2 Shear sliding at grain boundaries at two different scales in TiN/NbN multilayers

The TiN/NbN multilayer was deposited on a Si (001) substrate, with individual layer thickness of 25 nm for TiN and 25 nm for NbN, respectively. In the NbN reference coating in the diffraction pattern, Figure 23(c), two phases were identified: cubic δ and hexagonal δ' phase, see §5.1.2 for details. The diffraction pattern of the multilayered coating, visible in Figure 41(d), is composed of sets of rings corresponding to *fcc*-TiN and *fcc*-NbN, which is the cubic δ-NbN phase. No rings or even single spots matching δ'-NbN could be identified. Therefore it is assumed that the layered structure constrains the NbN to grow in the cubic δ-NbN phase suppressing the presence of the hexagonal δ'-NbN. This absence of the hard, covalent δ'-NbN phase would explain the hardness decrease in the multilayered coating in respect to the pure NbN reference coating (26.5 GPa) as the hardness values found for the TiN/NbN multilayer varied from 15 GPa measured by nanoindentation to 19 GPa measured with *in-situ* picoindentation. Moreover, as only one

phase is present in the NbN layers, no nanocomposite structure was formed inside the layer as it was the case for the bulk NbN coating, which would in addition enhance the hardness.

The bright field cross-sectional TEM micrograph taken from the TiN/NbN coating, Figure 41(a) reveals very wavy interfaces between the respective layers. It seems that the columnar growth mechanism dominates the multilayer structure, which is most probably caused by competitive growth of strongly misoriented columns.

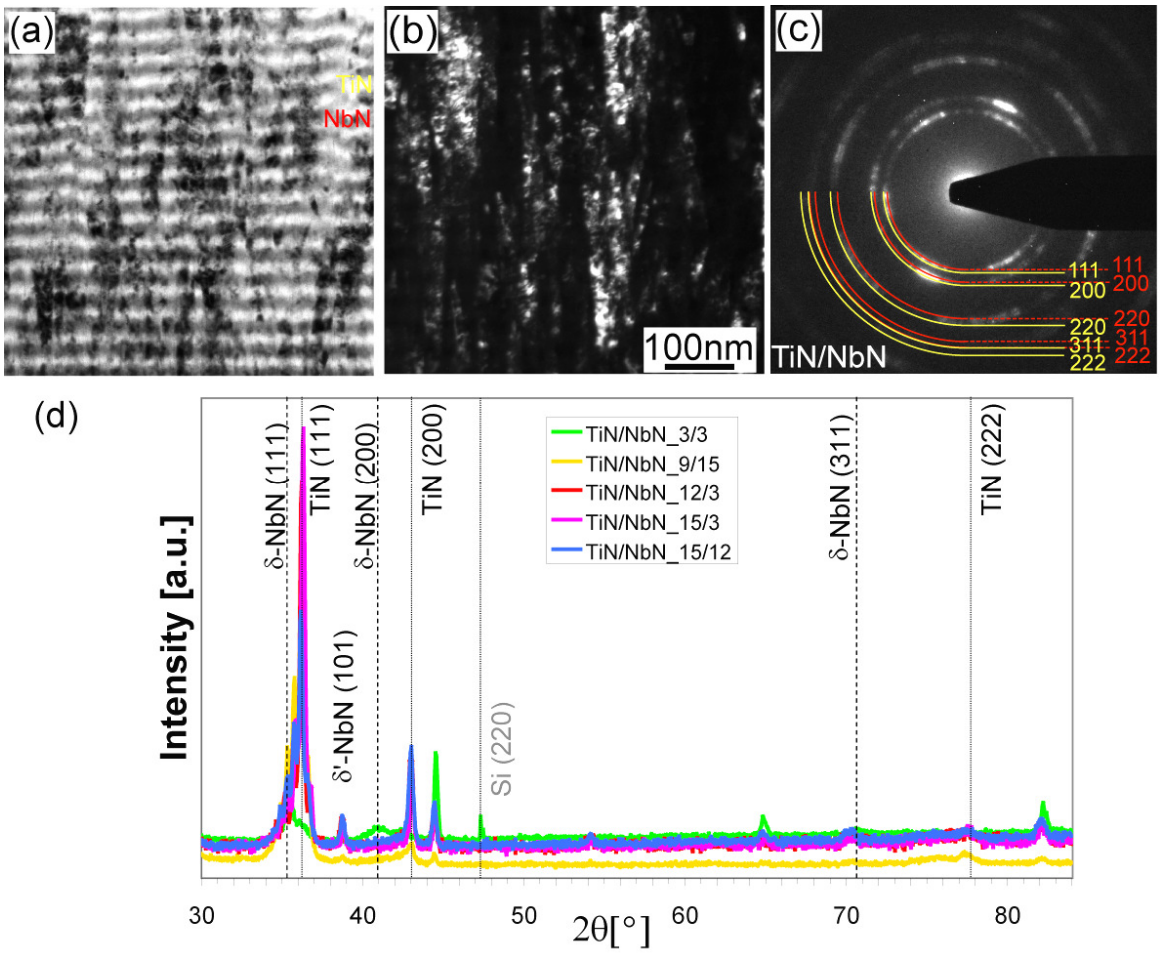

Figure 41 *TEM cross-sections through the TiN/NbN coating:* **(a)** *bright field;* **(b)** *dark field image taken with the [200] spot;* **(c)** *Corresponding SAED pattern and* **(d)** *XRD diffractograms of five different multilayer layouts. The thicknesses of the respective layers are given in nanometers.*

The column boundaries seem to be well defined, which is not astonishing, as sharp columns were present in both monolithic TiN and NbN coatings. Indeed, in the dark field image, Figure 41(b) the interfaces between the layers cannot be distinguished and large columns grow across the coating apparently not disturbed by the multilayering. Therefore partial, local epitaxy between the TiN and NbN is supposed. This local epitaxy is related to the compression of the NbN lattice due to the compressive stresses arising in the coating

during the deposition procedure. The NbN, having a slightly larger lattice parameter than the TiN, Table 3, due to the compressive stress matches the lattice parameter of TiN, enabling it to grow epitaxially on top of NbN. Conversely, if the NbN with its larger lattice parameter would like to grow epitaxially on top of the TiN, the TiN lattice would have to expand, which is not possible due to the compressive stresses present in the coating generated during the deposition process. This particularity of locally semi-coherent and incoherent interfaces, which are respectively invisible and visible on the TEM images, is even more pronounced for the NbN/CrN coating described in §6.3.3.

Table 3 *d -values for the fcc-TiN, fcc-CrN, metallic bcc-Cr, primitive cubic Cr (p-Cr), fcc-δ-NbN and hcp-δ'-NbN. All values are given in Å.*

d_{fcc}	*fcc*-TiN	*fcc*-CrN	$d_{bcc\text{-}Cr}$	*bcc*-Cr	$d_{p\text{-}Cr}$	*p*-Cr	*fcc δ*-NbN	d_{hcp}	*hcp δ'*-NbN
[111]	2.4492	2.394	[110]	2.039	[200]	2.300	2.536	*[002]*	*2.74*
[200]	2.1207	2.068	[200]	1.4419	[210]	2.049	2.196	*[100]*	*2.55*
[220]	1.4997	1.463	[211]	1.1774	[220]	1.873	1.553	*[101]*	*2.307*
[311]	1.2789	1.249	[220]	1.0195	[310]	1.611	1.324	*[102]*	*1.872*
[222]	1.2245	1.197	[310]	0.912	[311]	1.441	1.268	*[103]*	*1.487*

The cross-section through the indent imprint in the TiN/NbN coating is depicted in Figure 42(a). During indentation the deformation occurs mainly by shear sliding between the columns, what is apparently not prohibited by the multilayering, as clearly illustrated by Figure 42 (b). This is confirmed by the magnified view, Figure 42(b), revealing intergranular cracking between the big columns and individual grains. On the surface of the coating shear steps were formed due to vertical displacements of entire packages of multilayers. Inside these packages cracks at grain boundaries can be observed, caused by individual grains, which underwent shear sliding at grain boundaries, white arrows in Figure 42(c).

The TiN/NbN multilayer is a very particular combination of materials, as the mechanism of shear sliding at grain boundaries occurs in this system at two scales:

– The *microscale*, in which columnar-shaped pieces of multilayers having sizes comparable to TiN columnar coatings: 200 nm in width and reaching the entire coatings thickness are vertically displaced over distances up to a double layer period *i.e.* 50 nm, Figure 42(b).

– The *nanoscale*, where individual nanograins of about 10 nm in diameter are vertically displaced over distances of half of a layer thickness, Figure 42(c).

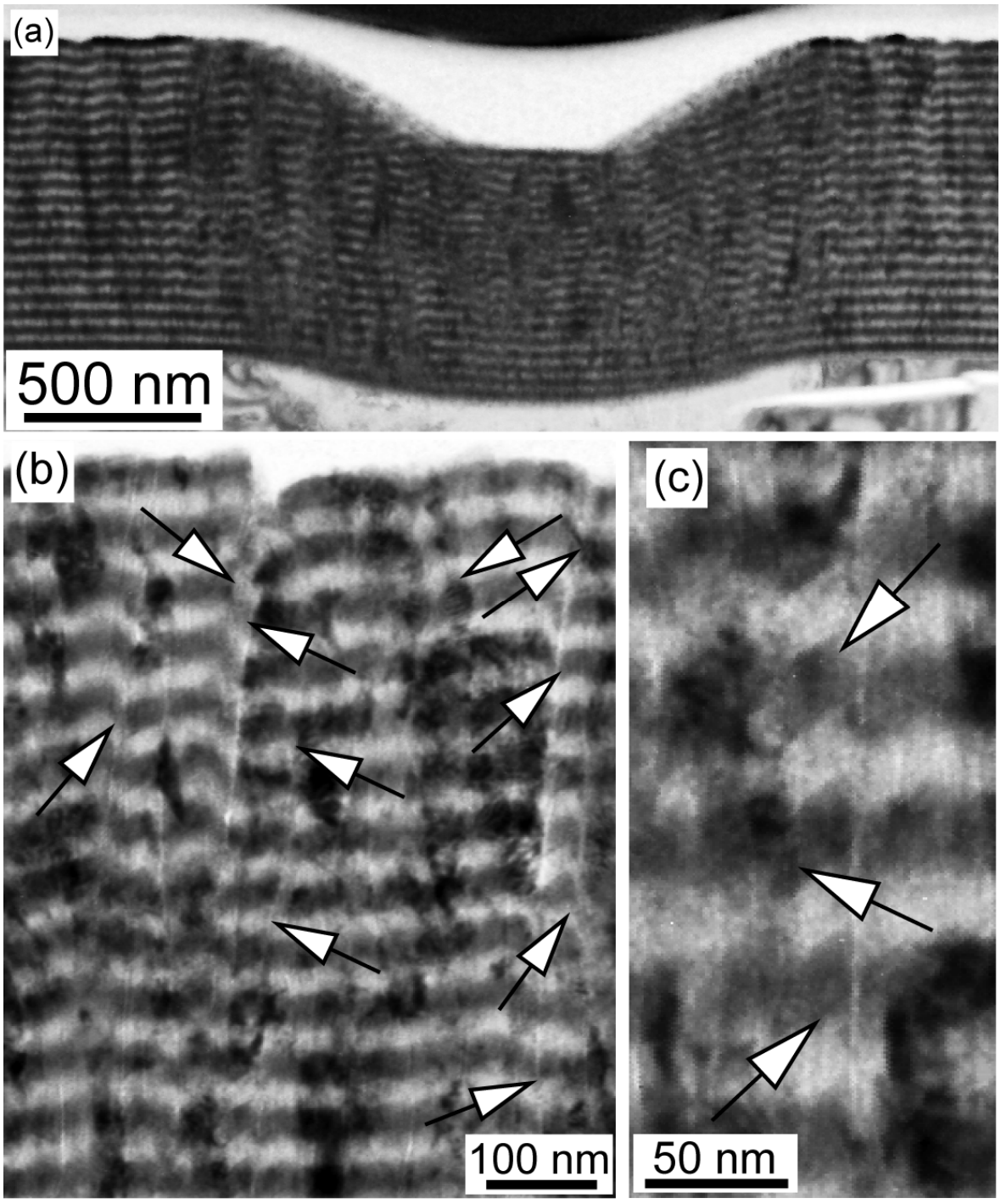

Figure 42 (a) *TEM cross-sectional image through the indent in the TiN/NbN multilayer; Magnified view of* **(b)** *the cracks along the column boundaries and* **(c)** *displaced grains, see text for details.*

Most probably these failure modes are favored by the high degree of crystallinity of both materials and their high hardness. The plastic deformation *i.e.* the thickness decrease of the multilayers below the indent imprint was estimated to ~20%.

6.2.3 ACCOMMODATION OF SHEAR SLIDING AT GRAIN BOUNDARIES IN TIN/CRN

The TiN/CrN multilayer consists of 20 repetitions of 25 nm thick *fcc*-TiN alternated with 25 nm of *fcc*-CrN deposited on a Si substrate, Figure 43(a). The diffraction pattern, Figure 43(c), clearly shows two sets of rings corresponding to *fcc*-TiN and *fcc*-CrN. No additional rings indicating the formation of a solid solution of TiCrN were present. Both materials have the same *fcc*-B1 structure [Yang 2002] and the calculated lattice mismatch between TiN and CrN is in the range between 1.8 to 3.3%. These structural characteristics could easily promote partial epitaxial growth [Mus 1998], [Mus 1999], however, epitaxy of entire interfaces between CrN and TiN in the multilayer structure was not observed.

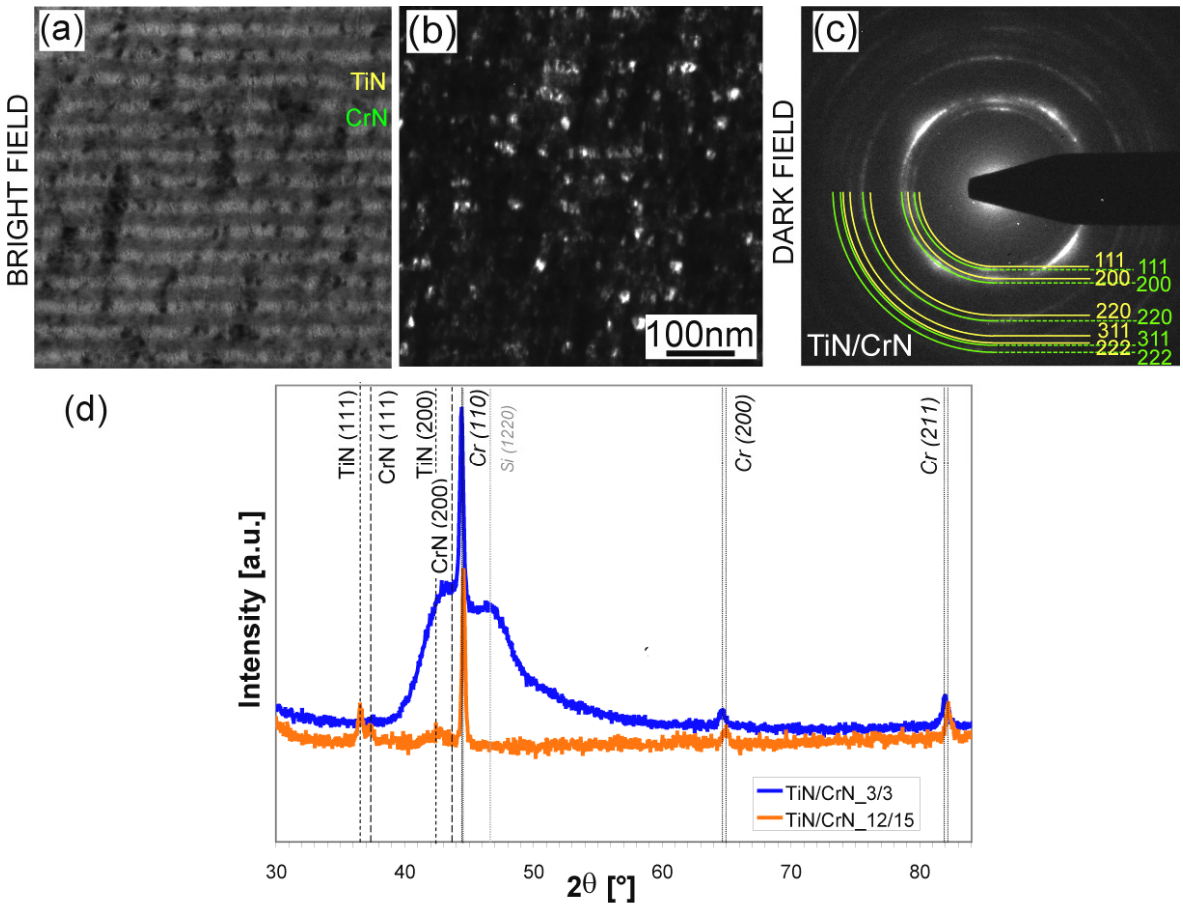

Figure 43 *TEM cross-sections through the TiN/CrN coating:* **(a)** *bright field;* **(b)** *dark field image taken with [200] spot;* **(c)** *Diffraction pattern;* **(d)** *XRD diffractogramms of two different multilayer layouts. The thicknesses of the respective TiN and CrN layers are given in nanometers.*

The absence of epitaxy could be related to the presence of a certain volume fraction of metallic Cr in the CrN layers, identified by XRD, Figure 43(d). The XRD diffractogram, taken for two different multilayer thicknesses shows peaks from *fcc*-TiN, *fcc*-CrN. Additionally, it contains some peaks originating from metallic Cr, which is softer than CrN. Metallic Cr has a much smaller lattice parameter compared to TiN, Table 3, which makes epitaxy at the interface impossible. The majority of the TiN and CrN grains are equiaxed growing up to the thickness of the respective layers. However, locally columns growing over a distance of 3-4 layers are visible.

In the dark field image taken with the (002) reflection, Figure 43(b) mainly crystalline TiN grains, with very strong white uniform contrast are visible [Nor 1998]. Conversely, the CrN grains are hardly distinguishable as well as the multilayer interfaces.

The TEM image of the indented cross-section through the TiN/CrN multilayer is shown in Figure 44(a). The multilayering is still visible and the coating directly underneath the indent imprint underwent compression. At the contact edge of the indenter tip, left side of Figure 44(a), the multilayering is less visible. This is related to the fact that due to the indentation, the multilayers are tilted out of visibility conditions. Indeed, to be observable by TEM, the interfaces of the multilayers have to be oriented perpendicular to the electron beam. After tilting the sample around an axis parallel to the multilayering, the layers come into visibility conditions. The plastic deformation *i.e.* the thickness decrease of the multilayers below the indent imprint was estimated to ~20%.

As the coating contains TiN layers it was expected to deform by shear sliding at grain boundaries. A closer look to the columnar grain boundaries reveals a large amount of microcracks, shown by the light green arrows in Figure 44(b). Locally, vertically displaced individual grains or packages of multilayers could be seen, purple arrows in Figure 44(b), but they were not as clearly visible as for example in TiN/SiN_x coatings (§6.2.1 and [Par 2010]). A step at the substrate interface, purple arrow in Figure 44(a), strongly suggests that shear sliding indeed occurs, but the sliding TiN grains are accommodated by the CrN layers, containing a certain volume fraction of soft, metallic Cr, as identified by XRD.

Another interesting feature is a relatively sharp limit between the areas where the multilayering is visible and not visible, see the light green arrow in Figure 44(a). It seams like the TiN/CrN coating underwent local shearing during indentation. This is an example of a coating, in which mixed deformation mechanisms take place i.e. grain boundary sliding and shear band formation.

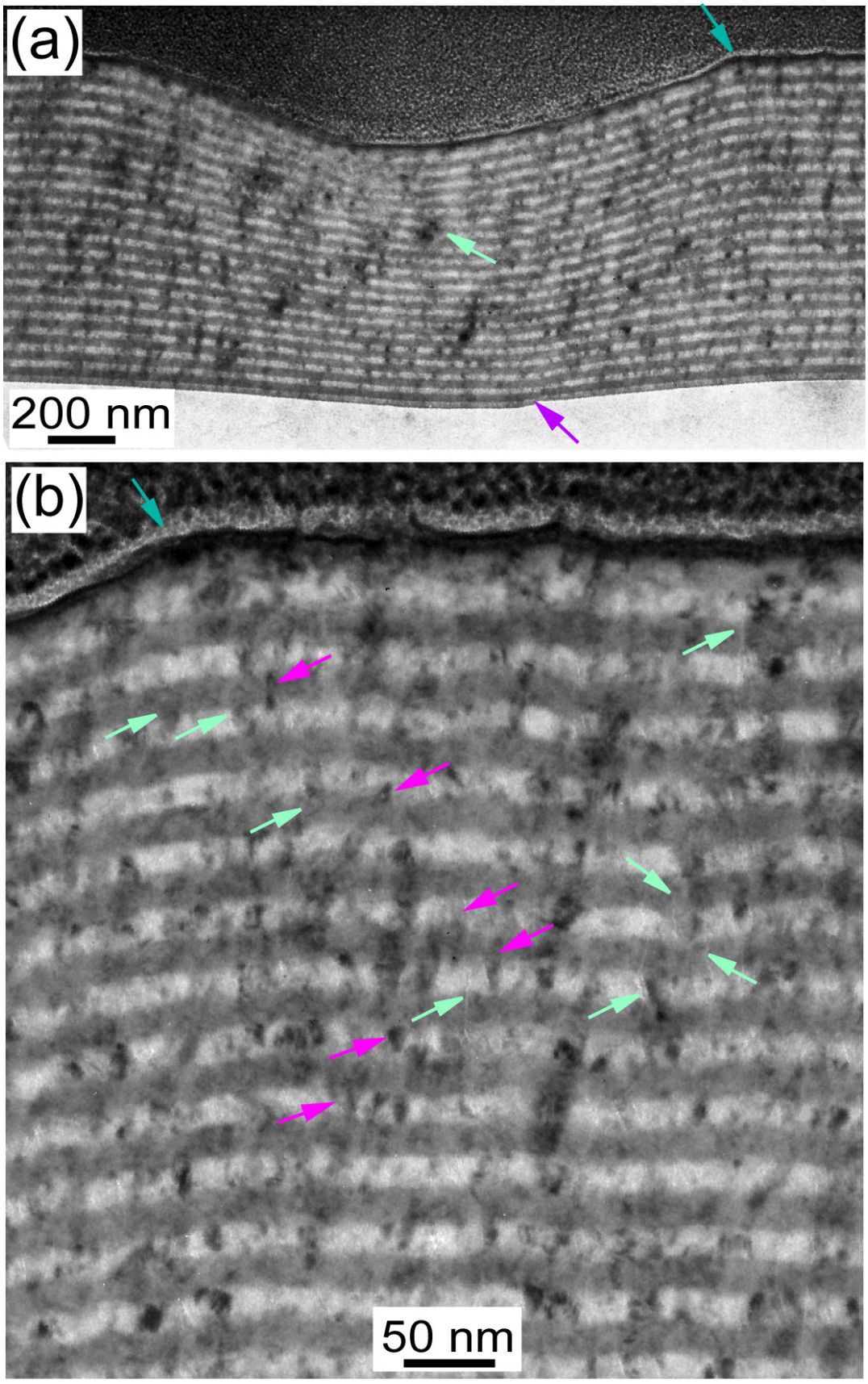

Figure 44 (a) *TEM cross-section image through the indent imprint in the TiN/CrN coating;* **(b)** *Magnified view of cracks (light green arrows) and displaced individual TiN grains (purple arrows).*

6.3 OTHER DEFORMATION MECHANISM IN COATINGS WITHOUT TiN

As will be shown in the paragraphs below not all columnar coatings deform by pure shear sliding at grain boundaries to such extent as TiN, but involve also other mechanisms. These exceptions include: NbN and CrN columnar coatings and their combination into a multilayer NbN/CrN, which deform by densification or shearing forming shear bands underneath the indent imprint.

6.3.1 DEFORMATION BY DENSIFICATION AND MATERIAL FLOW IN CrN

The monolythic CrN coating was deposited on a Si (001) substrate and exhibits a coarse columnar structure, Figure 45(a). The diffraction pattern, shown in Figure 45(c), has a rather spot-like appearance than a circular one, and according to the *d*-values given in Table 3, corresponds to the *fcc*-CrN phase. Additionally very strong preferential orientation in the [002] direction is observed. Indeed, the dark field image, Figure 45(b) taken with the [002] spots reveals large zones of similar crystallographic orientations, all with comparable light contrast, suggesting the presence of low angle grain boundaries. The columns in the dark field image Figure 45(b) have a dot-like structure inside, which could be due to the presence of a large density of dislocations. The CrN coating was found to be the softest among the three studied films with H = 15.8 GPa. This low value is most probably due to the presence of a certain volume fraction of soft metallic Cr, which is identified by XRD. The XRD diffractogram of the CrN coating, Figure 45(d), exhibits one sharp peak at $2\theta = 28.5°$corresponding to the {111} family of planes of the silicon substrate. Between $2\theta = 40°$-$60°$ a very large diffraction peak is present. It is composed of several peaks corresponding to different phases of Cr, however it is impossible to unambiguously deconvolute these peaks. At $2\theta = 47.42°$ the (220) peak from the Si substrate is present. As for the other peaks they could correspond to *fcc*-CrN (200) at $2\theta = 43.7°$ or to metallic *bcc*-Cr (110) at $2\theta = 44.4°$.

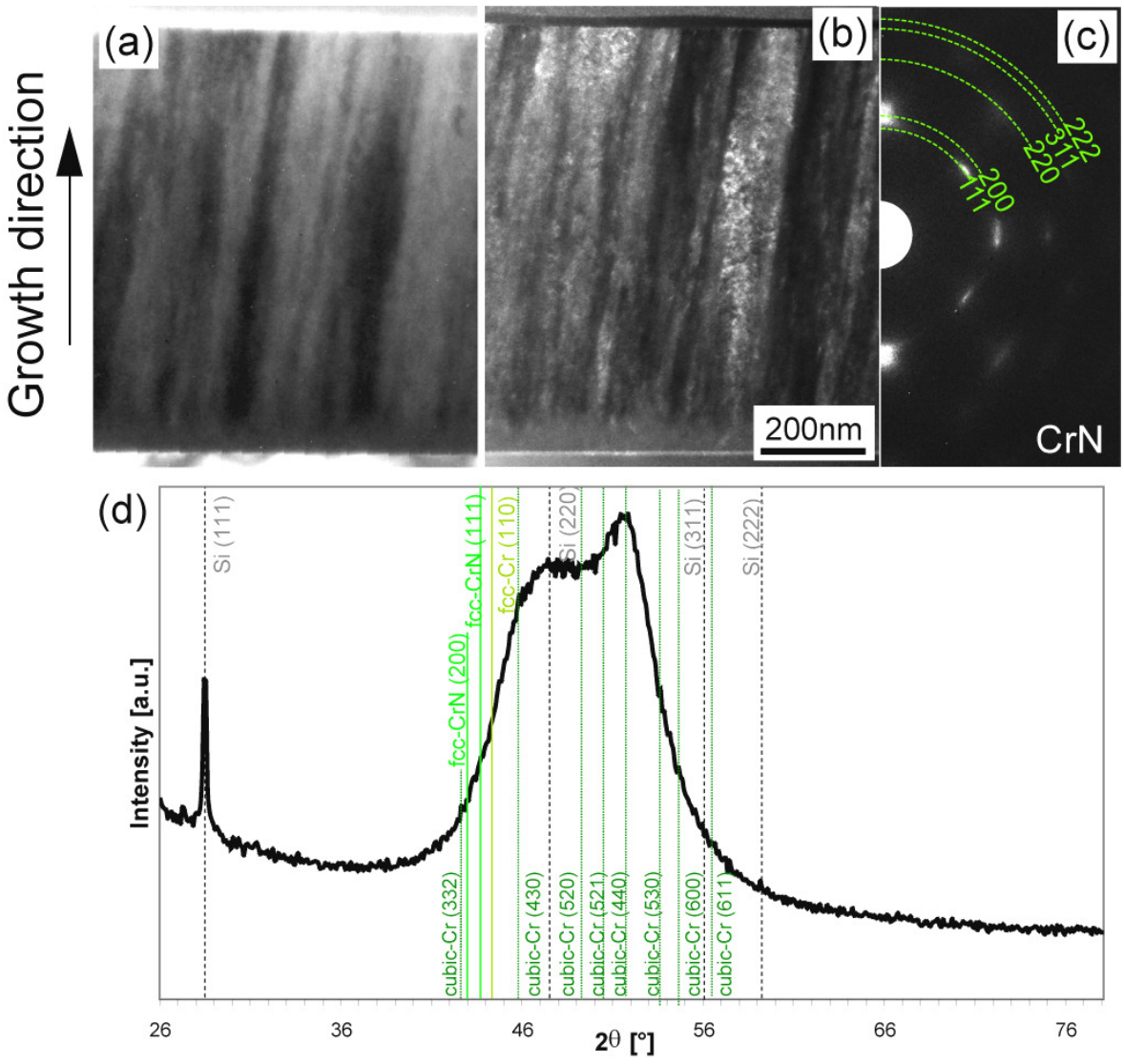

Figure 45 *TEM cross-sections through the monolithic CrN coating:* ***(a)*** *bright field;* ***(b)*** *dark field;* ***(c)*** *SAED pattern and* ***(d)*** *XRD diffractogram showing the presence of three phases: fcc-CrN, bcc-Cr and p-Cr.*

Another possibility would be a cubic primitive phase of metallic Cr (JCPDF file n°190323), which exhibits several peaks in the range of 2θ = 40°-60° or an oxide phase with chromium (ex. Cr_2O_3 or Cr_3O_4), as the sample surface could have been oxidized with time. In the diffraction pattern taken by TEM no diffraction rings originating from an oxide phase were observed, most probably due to the fact, that the TEM sample was freshly prepared as a cross-section and that the contribution of the oxide phase, eventually present on the coating surface, is negligible. Moreover, it is impossible to identify the presence of neither of the metallic Cr phases due to the almost identical d-spacings of these phases and the *fcc*-CrN phase, as apparent from Table 3. The two possible reflexions, which would be distinguishable in the diffraction pattern of CrN, Figure 45(c), are the [220] and [310], were not observed in the related diffraction pattern.

The bright field TEM image of the indent cross-section of the CrN coating is shown in Figure 46. Except a reduction of the coating thickness underneath the indent imprint no other damages could be observed in the TEM micrograph. No intercolumnar cracking or vertical displacement of the columns, as it was the case for the TiN coating having also a columnar structure, could be identified. The CrN coating is the only coating among the observed ones, for which no visual damage in form of deformation twinning or amorphization, was induced into the Si substrate during indentation. Neither delamination between the coating and the substrate nor cracks in the substrate, were observed. Most probably it is due to the fact, that the deformation of the CrN coating under indentation occurred by densification and material flow, which is proven by the formation of pile-up at the indent onsets, Figure 46. In this coating the plasticity is most probably due to the presence of soft, metallic Cr. Furthermore, material flow uses a significant part of the total energy in the system and therefore no crack in the substrate is generated. No deepening of the coating into the substrate is observed, which suggests that all the deformation is confined within the coating.

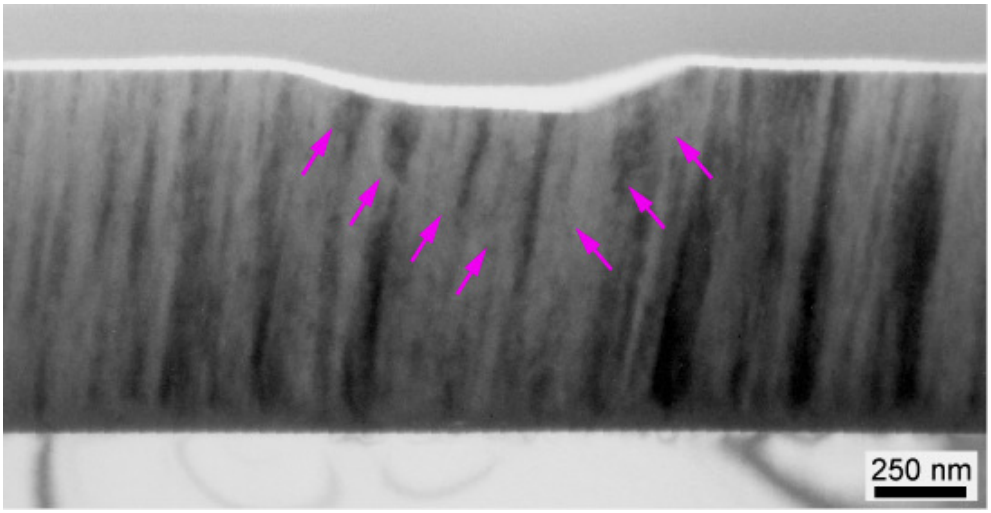

Figure 46 *TEM cross-sectional image through the indent in the columnar CrN coating. The plastic zone below the indent imprint is delimited by purple arrows.*

At the right edge of the indent imprint corresponding to the area below one of the Berkovich tip facets, the TEM image of the columnar structure is not sharp. This is due to the presence of a shear bands delimiting a plastic zone directly below the indent imprint, as shown in Figure 46 by the purple arrows. It is not as well visible as in the multilayered combinations with CrN, most probably because in addition to shearing there are other more dominating deformation mechanisms present like densification and material flow described above. These shear bands are rather not perpendicular to the grain boundaries and are

related most probably to the crystallographic {111} planes in *fcc* materials, which are the gliding planes for dislocations.

6.3.2 DEFORMATION BY COMPRESSION OF NBN

The microstructure of the as-deposited NbN coating has been presented in detail in §5.1.2. The TEM image of the cross-section through the indent imprint performed in the NbN coating is shown in Figure 47. The NbN film behaves like an elastic plate and thus the majority of the plastic deformation is confined within the substrate. The amount of plastic deformation in the NbN film could be estimated to 3.8% from the indentation curves. No apparent cracks along the columnar boundaries were found. However, it seems that the NbN deforms to a certain extent by shear sliding at grain boundaries. The amount of deformation involved is not enough to form cracks, however the grains at the contact surfaces of the indenter tip are better distinguishable, as shown by the purple arrows in Figure 47 and the coating surface is rougher than in the undeformed areas: the columns are arranged in a step-like manner.

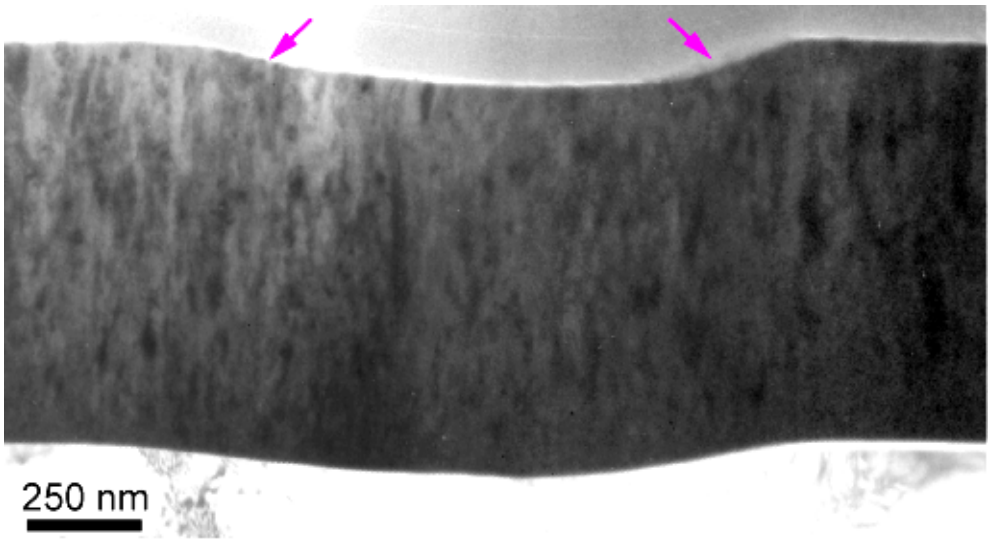

Figure 47 *TEM cross-sectional image through the indent in the columnar NbN coating. Purple arrows show the well distinguishable column tips at the edges of the indent imprint.*

An additional reason indicating for shear sliding at grain boundaries is the fact that the NbN coating is composed of two phases: the cubic δ-NbN and the hexagonal δ'-NbN. The columns thus have a so called two phase nanocomposite structure, with cubic or hexagonal grains forming boundaries inside the columns. These boundaries form a barrier for dislocation movement as they are not only differently oriented crystallographically, but they also have different structures. Thus the weakest parts of the microstructure are the column boundaries.

6.3.3 DEFORMATION BY SHEAR BAND FORMATION IN NBN/CRN MULTILAYERS

Multilayered NbN/CrN coatings composed of 20 repetitions of 25 nm of NbN alternated with 25 nm of CrN and 20 repetitions of 3 nm of NbN alternated with 3 nm of CrN were deposited on Si (100) substrate. The TEM bright field image of the cross-section through the multilayer, Figure 48(a) shows smooth layers with very sharp and straight interfaces.

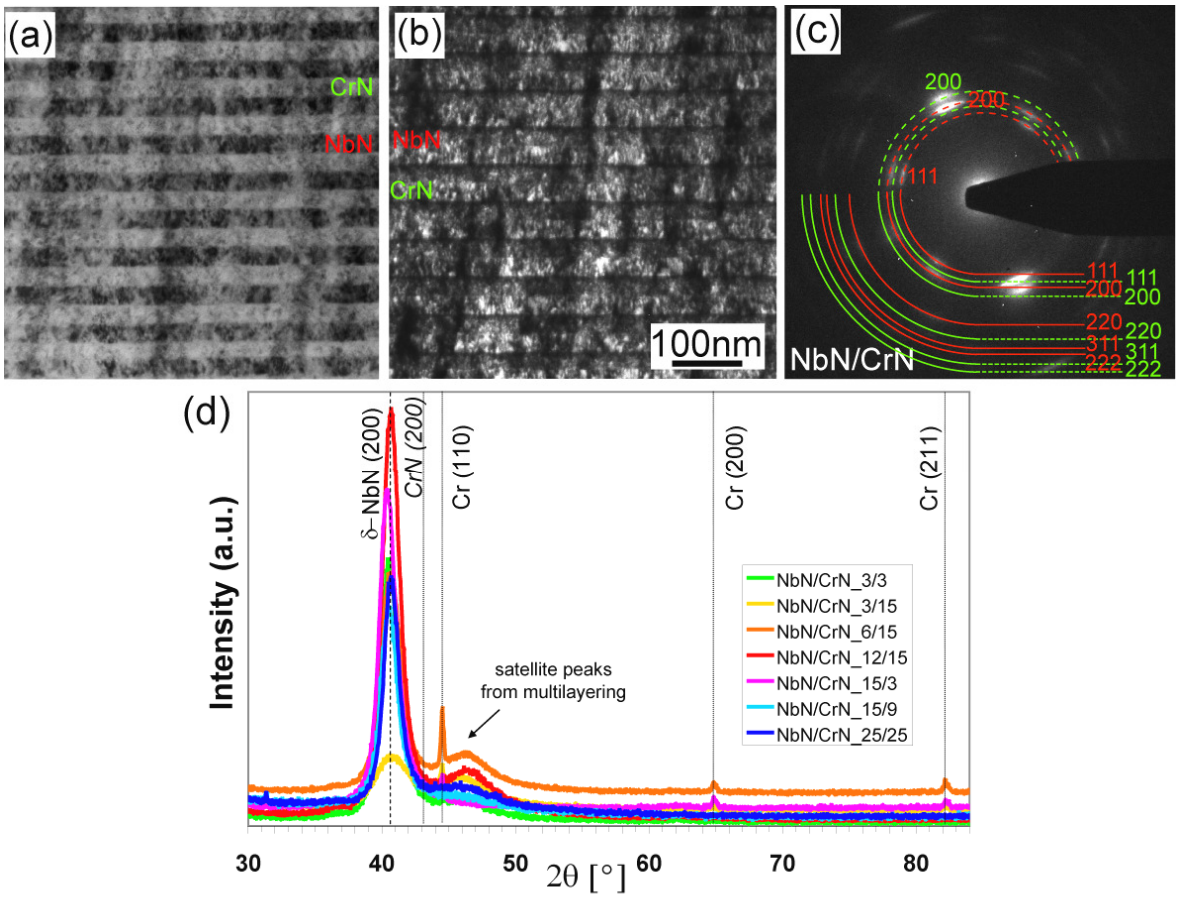

Figure 48 *TEM cross-sections through the NbN/CrN coating:* **(a)** *bright field;* **(b)** *dark field image taken with the mixed [111]/[200] spots;* **(c)** *XRD diffractograms of seven different multilayer layouts. The thicknesses of the respective layers are given in nanometers.*

The columns grow partially through the multilayering and contain an internal structure in form of zones of different crystallographic orientation. The diffraction pattern taken from the multilayered coating, Figure 48(c), contains two sets of rings matching the *fcc*-CrN and *fcc*-NbN. No presence of the hexagonal δ'-NbN phase could be detected. Additionally the diffraction pattern shows strong [111] and [002] texturing. The NbN/CrN coating is the only one in which the multilayered structure is clearly distinguishable in the dark field image, Figure 48(b). A very interesting feature, which has to be mentioned, is that only one of the interfaces is well visible, while the other one is invisible. The visible interfaces are

the NbN/CrN in the growth direction contrary to the non-distinguishable CrN/NbN interface. A closer look onto the dark field image allows perceiving local epitaxial growth of NbN grains situated above the CrN ones, which thus have the same light or dark contrast. Conversely, the CrN grains growing on top of the NbN grains very rarely show epitaxy. This is most probably related to the stress state of the coating. Indeed, most of the *Me-N* coatings deposited by sputtering processes exhibit residual compressive stresses up to several GPa. These stresses arise during the deposition procedure. Consequently, as the deposited NbN layer has a lattice parameter larger than the one of CrN, Table 3, its lattice is compressed favoring epitaxial growth on CrN having a smaller lattice parameter. It is however impossible in the opposite way, as the smaller CrN lattice would have to be stretched to form a semi-coherent interface with NbN. Nevertheless, during deposition CrN layer with a smaller lattice parameter is compressed, so that the NbN with a larger lattice parameter cannot grow epitaxially and a non-coherent interface, which is thus very well visible, is formed. The hardness of the multilayered NbN/CrN coating is about 38GPa measured by the picoindenter similarly to the columnar phase modulated nanocomposite NbN coating. As the NbN layers were formed by the *fcc* δ-NbN phase, it is assumed, that the high hardness values originate from the stress induced by the multilayering. Indeed, due to the compressive stress generated during the deposition procedure and epitaxy between the NbN/CrN interfaces it is possible. Most probably, as only one interface is epitaxial and the CrN/NbN interface is non-coherent, it is an important barrier for dislocations therefore this multilayered coating is very hard.

The TEM image of the cross-section through the indent imprint performed with the Berkovich tip in the NbN/CrN multilayered coating with the respective layer thicknesses of 25 nm is depicted in Figure 49(a).

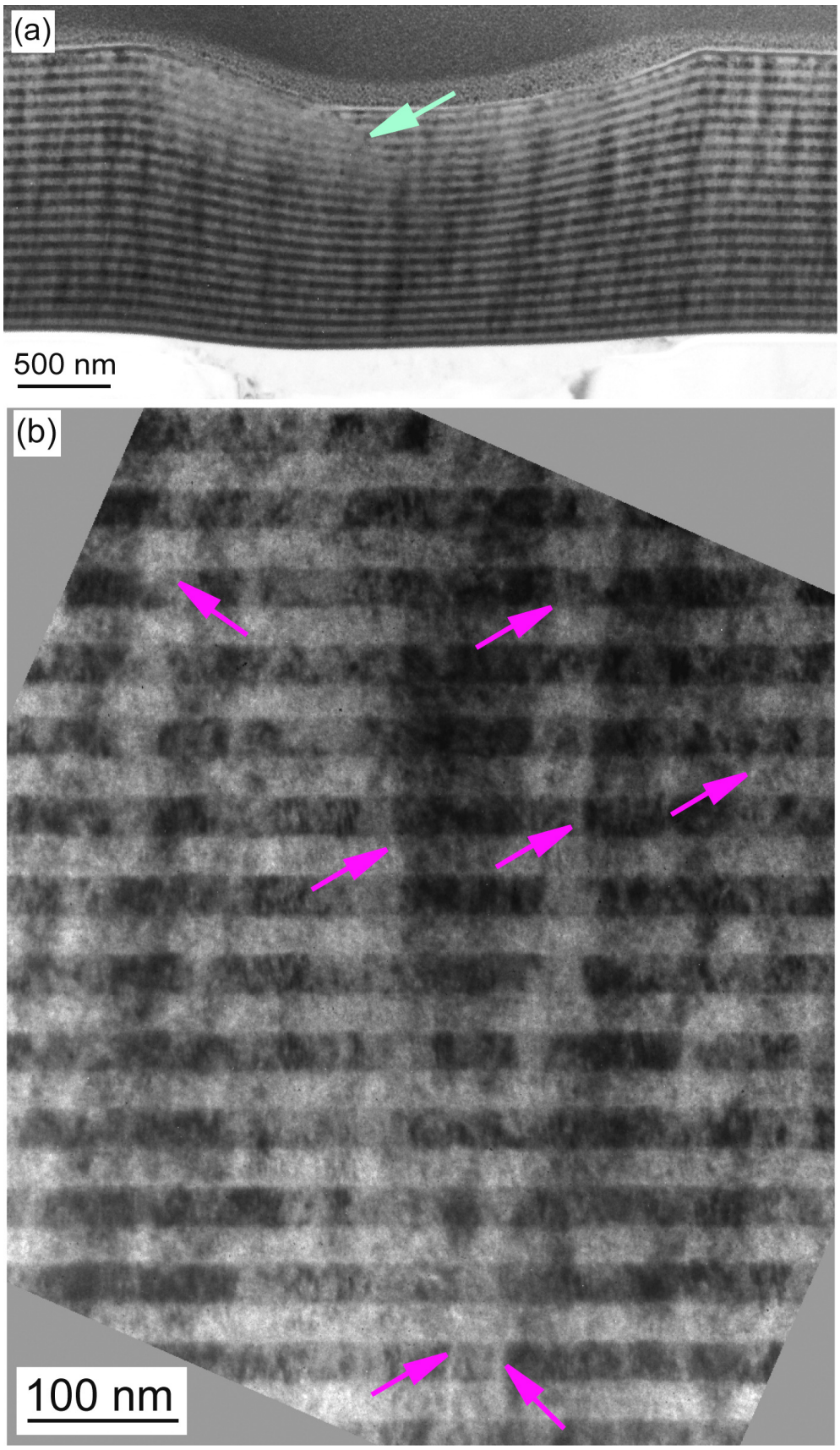

Figure 49 (a) *Bright field TEM cross-section through the indent imprint in the NbN/CrN 25/25 coating with a shear band shown by the light green arrow;* **(b)** *Magnified view of the undestroyed columns underneath the indent imprint. Very tiny intergranular cracks are highlighted by purple arrows.*

At first glance the multilayering is not destroyed, however underneath the facettes of the Berkovich tip the multilayering is tilted out of visibility conditions. This area is separated by a shear band, shown by the light green arrow in Figure 49(a), from the zone directly underneath the imprint, where the multilayers underwent only compression. The plastic deformation *i.e.* the thickness decrease of the multilayers below the indent imprint was estimated to ~16%. On the magnified view of the damaged NbN/CrN multilayers, very tiny intercolumnar cracks are distinguishable, as highlighted by the purple arrows in Figure 49(b). Contrary to TiN, NbN does not have such a pronounced tendency to grain boundary sliding under plastic deformation, Figure 47(a). Therefore in combination with CrN containing soft, metallic Cr, which accommodates most of the plastic deformation, only shear band are formed upon indentation of the NbN/CrN coating.

Conversely, when the thickness of the individual NbN/CrN layers is reduced down to 3 nm, it seems that shear sliding mechanisms act in the coating, Figure 50(a). The TEM image of the indent imprint cross-section in the $NbN_{3\ nm}/CrN_{3\ nm}$ coating revealed, that pieces of the entire film are pushed into the substrate forming steps at the interface with the substrate, as shown by purple arrows in Figure 50(b). From this observation it is evident shear sliding occurs in this system when the thickness of the individual layers is reduced to 3 nm. It is also visible as a step in the multilayering generated at the pile-up, green arrow in Figure 50(c). One possible explanation could be related to the very small thickness of the coating (20 repetitions of $NbN_{3\ nm}/CrN_{3\ nm}$ = 120 nm compared to 1 μm for the $NbN_{25\ nm}/CrN_{25\ nm}$ coating). The 120 nm thin coating is indented to a depth, which is by far exceeding its thickness. Moreover, as no delamination in any of the monolythic NbN, CrN or combined NbN/CrN coatings was observed, it is assumed that the adhesion with the substrate is very good. The coating under indentation has no choice but to crack. The cracks cannot be induced along the main crystallographic directions, like in a single crystalline coating, due to the presence of many grains having the size of 3 nm. Instead vertical shearing occurs in form of displaced layers marked by light green arrows in Figure 50(d), which is also observed in single crystalline TiN coatings as cracks forming a columnar-like fracture pattern. Also the upper part of the sliding layers underwent compression, dark green arrow in Figure 50(d). Apparently the volume fraction of the soft, metallic Cr in CrN layers was not sufficient to accommodate the excessive plastic deformation after indentation.

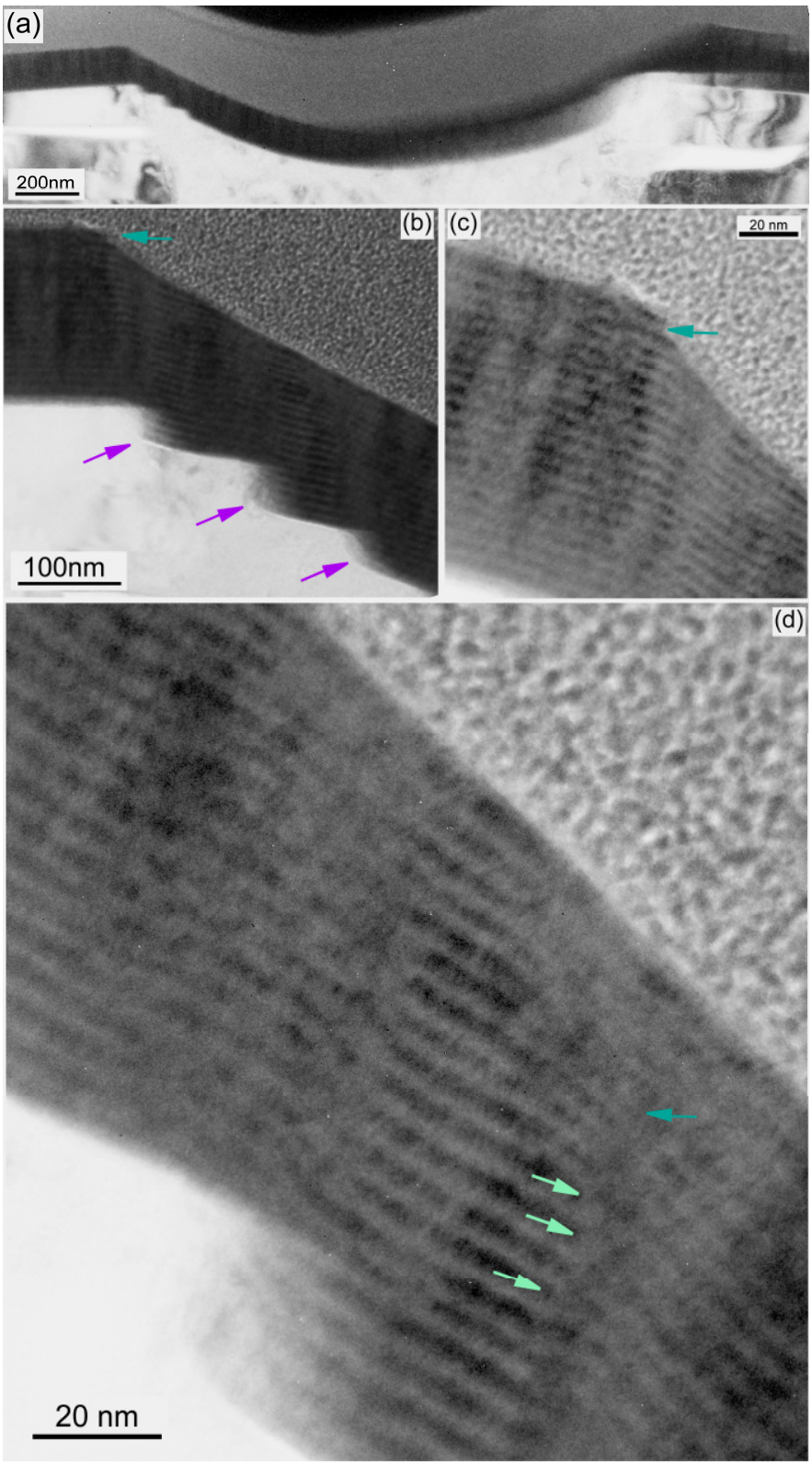

Figure 50 (a) *Bright field TEM cross-section through the indent imprint in the NbN/CrN 3/3 coating;* **(b)** *Magnified view of pieces of the multilayering, which underwent sliding. Steps were formed at the interface with the Si substrate. No intergranular cracks are visible;* **(c)** *Magnified view of the pile-up with a step in the coating due to the displaced multilayers marked by a green arrow;* **(d)** *Magnified view of the interface between pieces of multilayering, which underwent sliding. Displaced layers are marked by light green arrows. Compressed layers in the upper part of the coating are marked by dark green arrow.*

6.3.4 SUMMARY OF DEFORMATION MECHANISMS OCCURRING IN MULTILAYERED COATINGS

In multilayered structures the deformation process during nanoindentation is complicated and depends on the multilayer composition. A general conclusion, which can be made from the microstructural investigations performed by TEM, is that all multilayer coatings containing TiN deform by shear sliding at grain boundaries, independently on the thickness of the layers. In the TiN/SiN_x system it involved cracking along the vertical TiN/TiN crystallite boundaries and entire packages of multilayers containing several TiN grains in width and 3-4 multilayers in height were displaced. This observation shows that the involvement of an amorphous SiN_x layer only in two dimensions as a horizontal separator is not enough to prevent shear sliding at crystallite boundaries even at a scale of 1 nm.

Through very careful and detailed TEM studies of indented multilayer systems it was possible to visualize that the shear sliding at grain boundaries mechanism occurs at two scales in the TiN/NbN system: the micro and the nanoscale. At microscale entire pieces of TiN/NbN multilayers are vertically displaced, accompanied by the formation of boundary cracks between columns located within individual layers. Simultaneously steps occur at the coatings surface and/or the substrate interface because pieces of the displaced multilayers are pushed into the soft substrate. At nanoscale individual grains, with sizes of 25 nm, are displaced resulting in fractures in the multilayer structure.

In multilayer combinations with CrN mixed deformation mechanisms occur simultaneously. In the TiN/CrN coating grain boundary sliding is observed to a very small extent by steps formed at the coating-substrate interface and individual displaced grains. Below the indent imprint a shear band was generated. This mixed deformation mode is most probably due to the presence of soft, metallic Cr in the CrN layers, which accommodates the sliding grains and the plastic deformation of the whole coating allowing the formation of shear bands.

Observation of the deformation of the NbN/CrN combination showed that this coating, deformed only by shearing at an individual layer thickness of 25 nm. When the layer thicknesses were reduced to 3 nm mixed deformation modes by grain boundary sliding and shear band formation occurred.

7 OXIDATION RESISTANCE OF HARD ME-N COATINGS

For many applications the oxidation resistance of the *Me-N* coating is of particular interest. Especially during high-performance metal cutting operations, in addition to the mechanical properties the chemical stability has to be assured. The degradation of the coating occurs by wear related to oxidation or diffusion, when, due to friction, locally temperatures high enough to activate chemical or structural changes are reached. The addition of Al but also of Cr and Y in the form of solid solution has been shown to increase the oxidation resistance. The volume of the worn material is proportional to the energy dissipated in the contact with the formation of the oxidized debris.

Additionally, from the electron microscopy observations performed by the author it seems that the oxidation resistance depends not only on the chemical composition of the coating, but also on its microstructure *i.e.* grain size, which is presented in detail in [Par 2004b]. In the paragraphs below it will be demonstrated that coatings with a smaller grain size are more resistant to oxidation than coatings with large, columnar grains. The oxidation resistance of *Me-N* coatings will be presented and discussed in detail on the following examples: $Ti_{1-x-y}Al_xSi_yN$ coatings [Par 2004b] with two different compositions and consequently different microstructures and on $Zr_{1-x}Al_xN$ coatings [Lam 2006], as they have a very interesting oxidation mechanism different from other coatings.

7.1 INFLUENCE OF MICROSTRUCTURE ON OXIDATION RESISTANCE

The industrially deposited $Ti_{1-x-y}Al_xSi_yN$ coatings described in detail in [Par 2004a] and in §5.1.1 and §5.2.1, which are known to have a good resistance to oxidation, were heat treated at atmospheric pressure under N_2 at 1000°C for 1 hour. Two coatings have been chosen for comparison of their resistance to oxidation: the criterion of choice was their difference in microstructure. The first chosen coating was a Ti-rich $Ti_{1-x}Al_xN$ film exhibiting a columnar structure with the ratio of (Al+Si)/Ti = 0.5. The second one was an Al+Si-rich $Ti_{1-x}Al_xSi_yN$ nanograined film ((Al+Si)/Ti = 1.63). The cross-sections through the coatings were observed by conventional TEM, which revealed the growth of oxide film on the top of both samples, Figure 52.

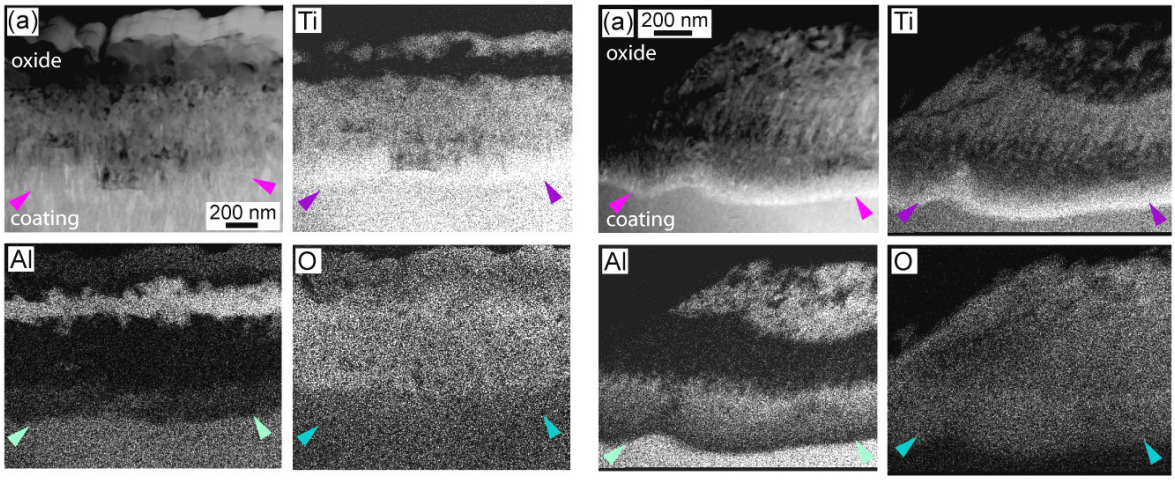

Figure 51 *Dark STEM images of cross-sections through the oxide layer on top of the coating with the corresponding EDX maps of Ti, O, Al and N for:* **(a)** *the Ti-rich columnar TiAlSiN coating;* **(b)** *the Al+Si-rich nanocomposite TiAlSiN coating. The arrows indicate the oxide (top) / coating (bottom) interface.*

The chemical analysis performed by EDX, Figure 51, revealed a non-uniform composition of oxides layers on both samples. The oxide thickness growing on top of the *Ti*-rich sample was about 1.0 µm thick and consisted of two regions: the first one having 750 nm growing directly on top of the film, consisted of Al_2O_3 and TiO_2 crystallites having a random distribution, followed by a second layer composed of discrete, relatively large (150–350 nm in diameter) TiO_2 particles on top, Figure 51(a). It has to be pointed out, that the interface between the coating and the oxide layer is not straight, but seems to follow the columnar structure of the coatings. The columns are rounded at their tops and the oxide is not only growing on these tops but also surrounding them, Figure 52(a). Additionally the white lines along the column boundaries reaching up to 250 nm deep into the coating, marked by white arrows in Figure 52(a), were assumed to be oxygen diffusion channels. These features at were not observed in as-received coatings described in detail in [Par 2004a] and [Par 2004b]. Indeed, the EDX mapping performed on these lines, Figure 52(c), shows a depletion in Ti, Al and N, but the presence of oxygen. Also the two EDX spectra taken in one of the oxygen diffusion channels and in the coating show a reduction of Ti and Al concentration in these channels compared to the coating, Figure 52. The oxygen content increases from about 7 at.% in the upper part of the coating to 14 at.% in the channels.

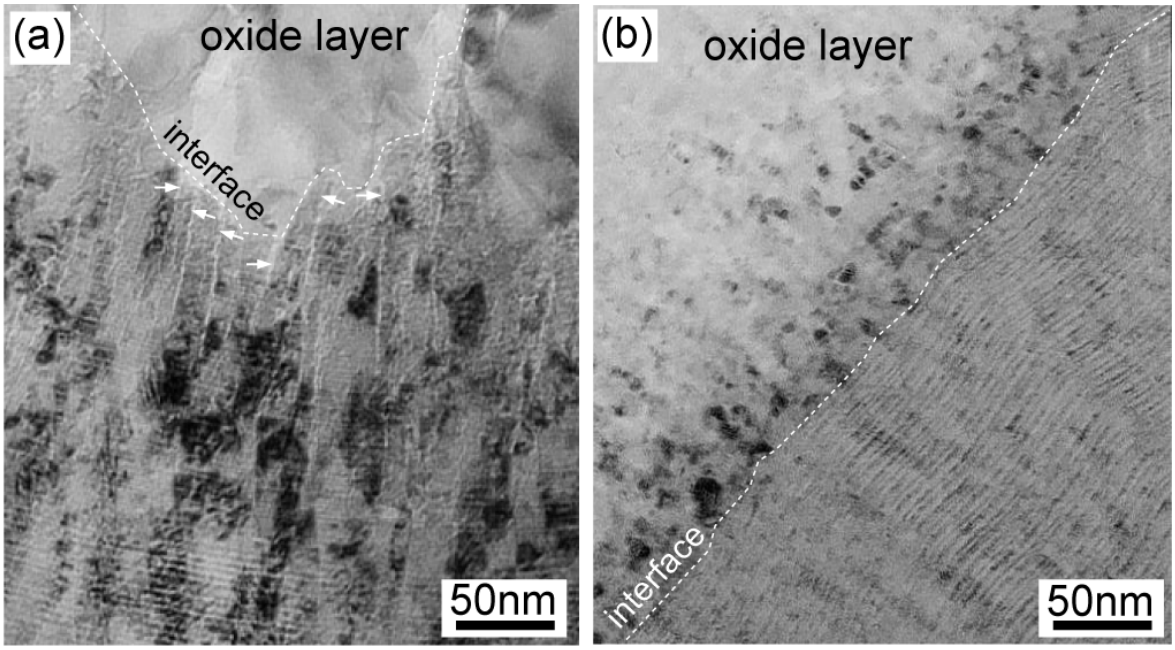

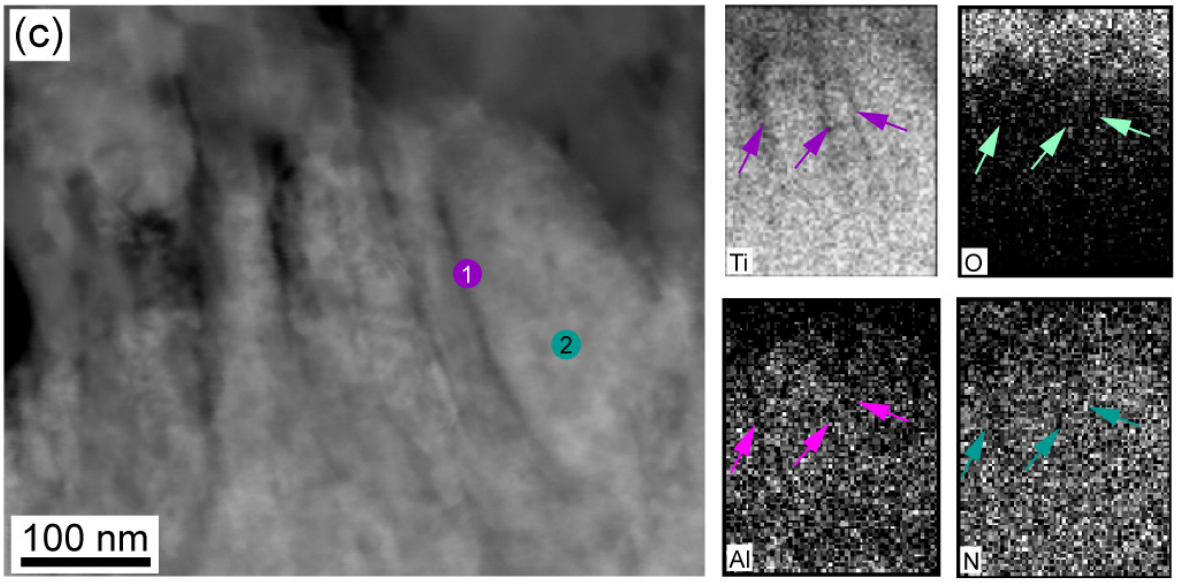

[at.%]	Ti	O	Al	N	Si
Spectrum 1	60	14	4	18	4
Spectrum 2	65	7	4	21	3

Figure 52 *Dark STEM bright field images of cross-sections through the coating-oxide layer interface:* **(a)** *Ti-rich TiAlSiN film with pronounced columnar structure. The white lines at the grain boundaries correspond to channels facilitating the oxygen diffusion into the coating;* **(b)** *AlSi-rich TiAlSiN film exhibiting a fine grained nanocomposite structure. The interface with the oxide layer is straight and abrupt prohibiting the diffusion of oxygen into the coating;* **(c)** *Dark STEM image and the corresponding EDX maps of Ti, O, Al and N showing the depletion of Ti and the presence of O along the column boundaries (arrows).*

On the HRTEM image of two adjacent TiAlN grains, denoted A and B in Figure 53, an amorphous region with a light contrast, delimited by white dotted lines, between the differently oriented grains is clearly visible. It corresponds most probably to an oxidized

grain boundary, for the two following reasons. The first one is that amorphous structures with this particular shape were not observed in as received samples of this composition. Additionally there is not enough Si in this sample therefore an amorphous precipitation of a SiN_x phase at the grain boundary is impossible, which is the second reason. Furthermore the shape of this amorphous region is different from regions corresponding to the amorphous SiN_x phase, shown in Figure 24(c) and (d), which has a somewhat regular half-moon shape, contrary to the feature visible in Figure 53, which is irregular with branches. This image, together with the EDX analysis, lead to the conclusion that the white lines at grain boundaries are indeed oxygen diffusion channels.

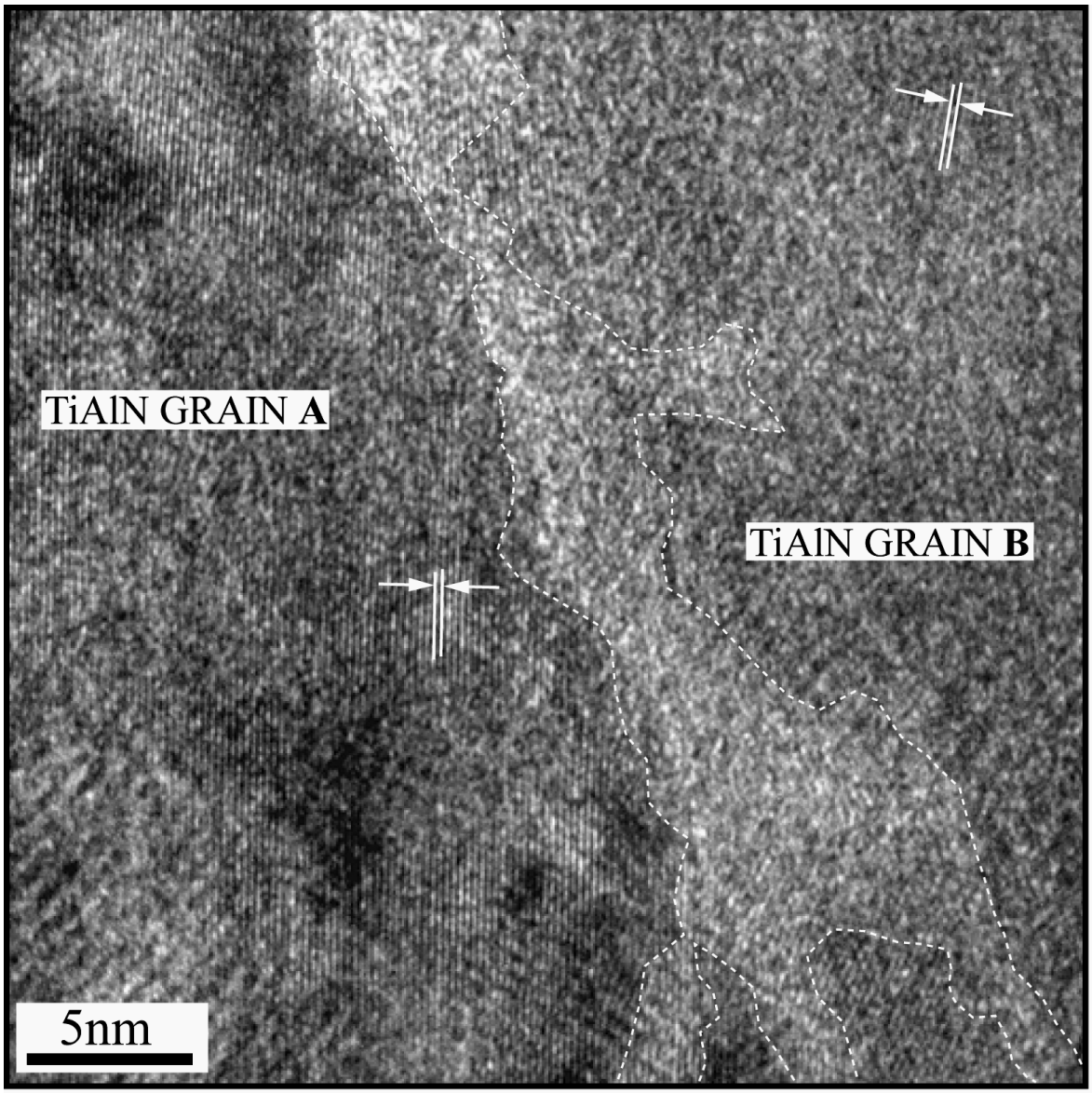

Figure 53 *HRTEM image of an oxide channel at grain boundary between two adjacent TiN crystalline columns. The white dashed lines are added artificially for sake of clarity.*

The oxide layer grown on the Al-rich film was around 0.7 μm thick and exhibited a non-uniform chemical composition: it consisted of three sub-layers identified by EDX, Figure 51(b). The layer adjacent to the non-oxidized coating was composed of nano-crystalline alumina particles having an approximate thickness of 190 nm, followed by mainly TiO_2, with a thickness of about 320 nm. The outermost layer of 210 nm was composed of large, randomly distributed crystallites, which could be identified as Al_2O_3 and TiO_2 particles. Both oxides were found to be crystalline with different grain sizes: ~20 nm for alumina and up to ~60 nm for titania. The interface between the very fine-grained oxide and the coating is straight and abrupt, white dotted line in Figure 52(b), contrary to the columnar film. No white lines along the nanograin boundaries, suggesting the presence of oxygen diffusion channels, could be observed at any magnification. Differences in oxidation resistance of differently structured coating were also observed by other authors in other systems [Cas 2007], [Cas 2008].

7.2 INFLUENCE OF CHEMICAL COMPOSITION ON THE OXIDATION MECHANISMS

It is known that rapid oxidation of ZrN occurs already at very low temperatures [Lam 2006]. Therefore Al was co-deposited to improve the chemical stability and increase the hardness. Details about the deposition procedure can be found in [Lam 2005] and [Lam 2006]. The samples were heat-treated at atmospheric pressure under air in a quartz tube at temperatures between 350°C and 650°C. The oxidation time was varied between 16 and 240 minutes and it was expected, that a protective oxide layer grows at the surface of the coating. This layer is formed at the initial state of oxidation and should act subsequently as a barrier against diffusion of oxygen into the coating.

The as deposited [Lam 2005] and oxidized $Zr_{0.73}Al_{0.27}N$ sample was imaged by conventional and HRTEM, [Lam 2006]. Figure 54(a) shows a cross-section through the as received coating exhibiting a columnar structure throughout the whole coating thickness. The columns are slightly finer at the substrate than in the upper part of the coating. After the heat-treatment almost half of the coating is oxidized, Figure 54(b). Comparing the thickness increase of the oxidized coating, Figure 54(b), with the thickness of the not oxidized on, Figure 54(a), the oxide layer grown on the top of the coating is only 150 nm.

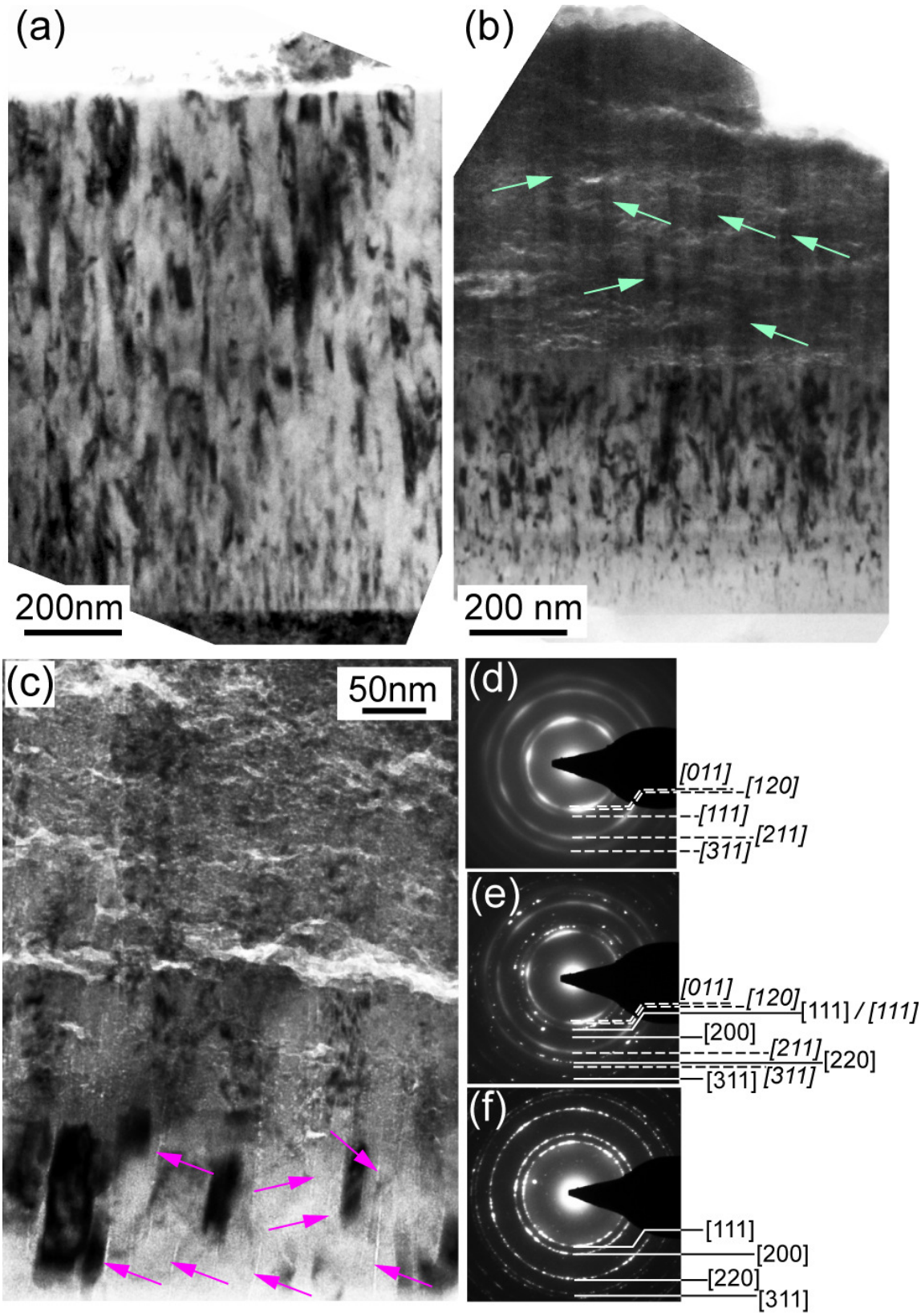

Figure 54 *TEM bright field image of a cross-section through a Zr0.73Al0.27N* **(a)** *as-deposited;* **(b)** *oxidized at 650°C under air for 240 minutes;* **(c)** *magnified view of the interface with the corresponding SAED patterns taken in the:* **(d)** *oxide layer;* **(e)** *interface comprising the oxidized layer and the coating;* **(f)** *coating.*

From this TEM image it seems, that the oxide layer is not really growing on top of the $Zr_{0.73}Al_{0.27}N$ coating, but it penetrates into the coating itself, which is thus oxidizing. Indeed, if the oxide layer would grow on top of the film, the total thickness of the film would increase, which is not the case, as evident from Figure 54(b), where both images have the same scale bar. Another indication for this particular behavior is that the oxide layer is full of horizontal cracks, which means that the material is subjected to major stress resulting from the oxidation process occurring inside the coating. If the oxide layer would grow on top, there would be no reason to have so much stress to cause such a dense cracking. But the most important indication for the oxidation into the coating is that in Figure 54(b) the columnar structure is still visible inside the oxidized region (light green arrows).

The magnification of the interface between the oxidized and non-oxidized part of the coating, visible in Figure 54(c), clearly shows that the passage from the region unaffected by the oxide to the oxidized one is not abrupt, but rather smooth. Additionally oxygen diffusion channels along the columnar grain boundaries, favoring the oxidation process, are clearly visible, indicated by purple arrows in Figure 54(c). Thus it is clear, that the oxide is not growing on top of the coating, as it is the case for other nitride coatings, but is penetrating into the film. The mechanism is the following: first the grain boundaries are oxidizing, which is confirmed by the presence of oxygen channels, Figure 54(c), and then the whole columnar structure is oxidized, and the oxide is penetrating deeper and deeper into the coating with time.

This particular behavior of ZrN-based coating originates from metallic zirconium, which is known to oxidize in a particular way [Abo 2003]. As seen from Figure 54, this oxidation mechanism is also found in coatings after nitriding the Zr. According to the TEM observations of a cross-section through an oxidized Zr alloy, preformed by Abolhassani *et al.* [Abo 2003], the oxide film does not only grow on the surface but also into the Zr alloy and cracks parallel to the surface are formed inside the oxidized zone of Zr, black arrow in Figure 55(a), similarly to what is observed for the ZrAlN coating, Figure 54(b). Such cracks have been often observed and as Abolhassani explains, could be due to stress build-up in the oxide layer.

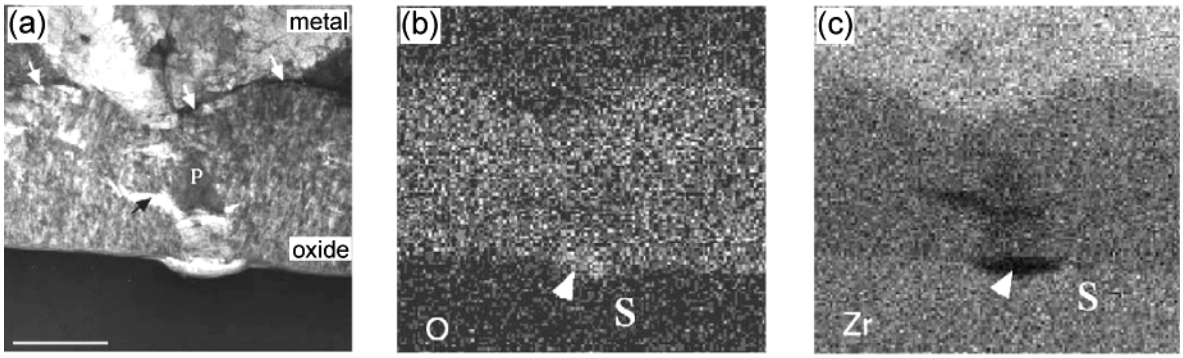

Figure 55 (a) *TEM bright field image of the metal-oxide interface showing a CrFe precipitate P in the oxide region with a crack in its vicinity (black arrow), white arrows indicate the metal-oxide interface;* **(b)** *Oxygen map taken by EDX, the oxide region is well visible (lighter contrast);* **(c)** *Zr EDX map, showing the presence of Zr not only in the metal, but also in the oxide part; S indicates the oxide surface. After Abolhassani et al. [Abo 2003].*

Based on the EDX analysis of CrFe precipitates which are present in the Zr, it can be concluded that the oxide layer formed during oxidation does not only grow on the top of Zr but also into the metal, see EDX maps of oxygen and zirconium in Figure 55(b) & (c), as some of the precipitates, which were present in the Zr alloy prior to oxidation, are found inside the oxide layer. In their vicinity lateral cracks in the oxide layer are formed, due to stress build-up, similarly to the dense network of lateral cracks observed in the ZrAlN film, black arrow in Figure 54(b) & (c).

SUMMARY OF OXIDATION BEHAVIOR OF HARD COATINGS

The above paragraphs show, that the oxidation mechanisms depends strongly as well on the chemical composition of the coating as on its microstructure. The microstructure plays a key-role in oxidation resistance as coarse, columnar grains favor the penetration of oxygen deep into the coating, as their boundaries serve as a diffusion channels for oxygen. This mechanism is related to the columnar structure of the coatings as it is present in the Ti-rich TiAlSiN coating as well as in the ZrAlN coating. Conversely the nanograined Al-rich TiAlSiN coating has an abrupt interface with oxide layer and no traces of penetration of oxygen into the coating inside could be evidenced by TEM.

However, the oxidation mechanism is different in TiAlN-based coatings than in the ZrN-based coating. The TiAlSiN coatings, independently on their microstructure and composition grow an oxide layer on top. This oxide layer has a mixed composition, which could be determined by EDX analysis. It is coarse-grained in the case of the Ti-rich coating

and fine-grained for the Al-rich coating. In addition, for the Al-rich coating a protective Al_2O_3 layer is grown at the interface with the coating prohibiting further oxidation of the coating. This is not possible in the case of the Ti-rich coating as it does not contain enough Al and the Ti is very reactive with oxygen.

Conversely to TiAlSiN coatings, the ZrAlN coatings grow only a very thin layer of oxide on top, but mainly the existing coating is oxidizing. The columnar structure of the coating is still visible in the oxidized region. The interface with the not oxidized film region is rather graded and oxygen diffusion channels are visible at the column boundaries. The oxidized part of the coating is subjected to high stresses, which cause the occurrence of a dense network of cracks parallel to the coating surface. This very unusual behavior of the oxide layer penetrating progressively into the ZrAlN coating originates from the oxidation mechanism of metallic Zr, as nicely shown by Abolhassani *et al.* [Abo 2003].

8 CONCLUSIONS

Me-nitride films are widely investigated materials, as they allow adapting the properties of the coated substrate, such as: enhanced hardness, strength, fracture toughness, thermal stability and conductivity, friction and oxidation resistance, to the application. Thus hardness enhancement of protective coatings is an important issue in materials engineering, as it increases lifetime of a material. There are two origins of the high hardness. The first one originates from the microstructure and is stable upon annealing. The second is related to the residual stresses introduced into the coating during the deposition process. As soon as these stresses are released, for example by a heat treatment, the hardness drops. Therefore, a lot of efforts are put into the design of particularly structured coatings exhibiting high hardness. One method is to artificially introduce interfaces either in form of grain boundaries to obtain nanocomposites or as layers resulting in a multilayered structure.

In this work it was attempted to determine, which type of interface structure, introduced into Me-N coatings, would enhance the hardness values and the oxidation resistance. It is a novel approach, proposed in this work, to design materials on atomic scale to obtain specific macroscopic properties.

The aim of this study was the analysis of the atomic scale structure of different types of interfaces and boundaries by TEM and determination of their impact on hardness, deformation mechanisms, fracture damage and oxidation resistance. It could be shown, that all types of interfaces: i.e. those introduced inside the columns in monolythic coatings, those between crystalline grains and the amorphous matrix in nanocomposites or those between respective layers resulting in multilayer coatings, resulted in higher hardness values. Moreover, in this study it could be experimentally established, that non-coherent and semi-coherent interfaces were the most favorable to obtain a more considerable hardness enhancement.

By inducing deformation into the material it is possible to determine the deformation mechanisms taking place and define the parameters, which contribute to the hardening effects. This was done by nanoindentation used to deliberately induce plastic deformation into the coatings. In the frame of this habilitation thesis the deformation mechanisms occurring in various types of coatings, after being observed experimentally by TEM, could be identified. Intergranular cracks at micro and nanoscale result from shear sliding at grain boundaries, which was found to be the dominant deformation mechanism in Me-N

coatings. It could be also shown, that coatings deposited on hard substrates exhibit more fracture damage, than the ones growing on substrates undergoing mainly shear sliding at grain boundaries. Consequently substrate hardness and structure determines to which extent the deformation and fracture damage occuring in coatings.

The interfaces play a key role in the oxidation resistance of coatings. As could be shown, a compact, nanocomposite structure is much more resistant to oxidation: it forms a flat, straight and abrupt interface with the fine-grained oxide on film surface prohibiting oxygen penetration into the structure. Conversely, coatings having a coarse columnar structure form a rough interface with the oxide growing as large grains. Hence the column boundaries are diffusion channels for oxygen. This mechanisms is independent on the chemical composition of the coating, it is indeed related to the structure since it was observed in different films.

Based on the results obtained in the frame of the investigation the following detailed conclusions could be drawn:

1. Nanostructuration is not the only way to obtain hard films: columnar coatings can also be very hard, if they contain intentionally designed interfaces, which provide a barrier for dislocation movement. These barriers are not the boundaries between the columns. They are either compositionally graded multilayers, often found in for example TiAl(Si)N industrially deposited coatings, which do not disturb the columnar growth, or zones inside the columns formed by different phases of the same material like *fcc* δ-NbN and hexagonal δ'-NbN, resulting in formation of a so-called compositionally graded nanocomposite.
2. The formation mechanism of the nanocomposite structure was proposed based on TEM investigation of a particular compositionally graded TiAlSiN coating. Images taken on atomic scale level of interfaces between grains having different compositions, revealed the formation of initially crystalline and subsequently, with increasing Si content, amorphous zones at these grain boundaries. By further increasing the Si concentration, the coating was completely nanocrystalline having crystalline grains surrounded by an apparently amorphous matrix. This observation of a progressive appearance first of crystalline and then amorphous zones at grain boundaries would strongly suggest that the nanocomposite structure is indeed composed of crystalline grains surrounded by an amorphous matrix.

3. For the first time it was experimentally demonstrated by HRTEM images, that the nanocomposite structure with an amorphous tissue phase, can only be formed with two phases having very different crystallographic structures such as TiN and SiN_x. A trial was given to produce an AlSiN nanocomposite, as AlN being transparent offers wide application possibilities. However, it was shown that, although the addition of Si into AlN leads to the formation of a nanocomposite-like structure, no considerable hardness enhancement is observed, conversely to the TiSiN system. A detailed investigation of an AlN/SiN multilayer model system, in comparison to a TiN/SiN_x multilayer showed that the interfaces between the hexagonal AlN and the SiN_x are semi-coherent. Indeed, the first 2 monolayers (0.7 nm) of SiN_x grow epitaxially as a crystalline phase on top of the *hcp*-AlN. Additionally the AlN crystallites have a very strong (002) preferential orientation. This causes that all nanograins in the nanocomposite are oriented in the same direction, what, combined with the local epitaxy of the crystalline SiN_x, results in interfaces which are not sharp enough, to prevent dislocation movement. Consequently, the AlSiN system shows only a moderate hardness enhancement.
4. Single crystalline TiN coatings grown on MgO (001) and (111) substrates were found to deform by fracture along the main crystallographic directions. Some cracks jumped or deviated form their original directions, which showed that there was an excess of energy induced to the system, which had to be dissipated. Additionally, fracture patterns looking similar to the columnar structure were observed.
5. A novel idea was to deposit 500 nm of columnar TiN on various substrates i.e. soft Si, equally hard single crystalline TiN and hard, ceramic WC-Co to study the influence of the substrate hardness and structure on the deformation mechanisms of the coating. The outcome of this investigation was that the substrate governs the fracture damage of the coating. Columnar TiN coatings grown on a soft Si substrate underwent grain boundary shear sliding, similarly to the columnar TiN grown on single-crystalline TiN having a comparable hardness. The extent of sliding depends on substrate hardness, however it occurs only for substrates being softer or equally hard as the coating itself. For substrates harder than the coating like ceramic WC-Co compression, bending as well as intergranular and internal fracture of the individual columns occurs.
6. Monolythic NbN underwent also grain boundary sliding, but to such a small extent, that it was hardly identifiable by TEM. This is most probably due to the fact, that NbN had a phase modulated nanocomposite structure containing two phases: *fcc* δ-NbN and

hexagonal δ'-NbN, what resulted in a harder structure less prone to fracture, which could accommodate more elastic deformation.

7. All multilayered coatings containing TiN layers deformed by grain boundary sliding independently on the column size (1 nm or 100 nm) and scale. Depending on the alternating layer composition individual grains or entire multilayer packages were displaced. The extent of the column displacement depends on the multilayer layout, individual layer thickness and indentation depth.
8. In the TiN/*a*-SiN_x combinations ($TiN_{5\ nm}$/*a*-$SiN_{0.5\ nm}$ and $TiN_{1\ nm}$/*a*-$SiN_{1\ nm}$) the mechanism of grain boundary sliding upon plastic deformation was the most spectacular, as pieces of multilayers reaching a size of 20 nm were vertically displaced by about half of the multilayer period on a scale of 5 nm or even 1 nm.
9. The shear sliding mechanisms in TiN/NbN multilayer coatings occurs simultaneously at two different scales. At microscale columnar-shaped pieces of multilayers were vertically displaced over distances up to a double layer period. At nanoscale, inside the displaced multilayer pieces individual nanograins were vertically shifted over distances of half of a layer thickness. Most probably these failure modes are favored by the high degree of crystallinity of both materials and their high respective hardnesses.
10. In the TiN/CrN multilayer system were the CrN layers contained soft, metallic Cr, the sliding TiN grains were accommodated by the softer interlayers. The monolythic CrN coating was deformed only by compression and shearing due to the presence of the soft, metallic Cr.
11. Observations performed for the NbN/CrN coating showed that the coatings without TiN layers deform only by formation of shear bands and not grain boundary sliding. Only very tiny intercolumnar cracks were observed, due to the fact, that most of the plastic deformation was accommodated by the CrN layers containing some soft, metallic Cr. Moreover, contrary to TiN, NbN does not have a tendency to grain boundary sliding to such extent under plastic deformation. An exception was the $NbN_{3\ nm}$/$CrN_{3\ nm}$ coating, which after indentation exceeding by far its thickness underwent shear sliding and entire pieces of the multilayers were pushed into the soft Si substrate.
12. It could be proved that interfaces play a key role in the oxidation resistance of coatings. An innovative TEM study of cross-sections through oxidized films showed that, a compact, nanocomposite structure is much more resistant to oxidation: it forms a flat,

straight and abrupt interface with the fine-grained oxide on film surface prohibiting oxygen penetration into the structure.

13. Conversely, coatings having a coarse columnar structure form a rough interface with the oxide growing as large grains. Hence the column boundaries are diffusion channels for oxygen. This mechanisms is independent on the chemical composition of the coating, it is indeed related to the structure since it was observed in Ti-rich TiAlSiN and in ZrAlN films.
14. The growth of the oxide layer on top of the surface of the coating or into it depends on the oxidation mechanism of the pure metal composing the coating. This could be demonstrated by TEM observations of TiAlSiN and ZrN columnar coatings. In the case of the Ti-based film the oxide was growing on top of the coating, and the coating surface was depleted of Ti to form TiO_2. Conversely, in ZrN the oxygen penetrated into the coating, and "covered" its columnar structure, which is the consequence of the oxidation mechanism of pure Zr.

From the microstructural study performed by conventional TEM and by HRTEM down to the atomic scale it is clearly visible that the interfaces, independently if they are inside or between the respective grains or between different layers play a key role in the mechanical performance of the coating. They influence not only the hardness, but also the deformation mechanisms as well as the oxidation resistance of the coatings. Therefore it is extremely important to take into account the structural features of the interfaces when designing a new coating.

References

[Abo 2003] S. Abolhassani, M. Dardas, M. Leboeuf, D.Gavillet *"In situ study of the oxidation of Zircaloy-4 by ESEM"* Journal of nuclear materials 321 p.70 (2003)

[Ada 1962] M.A. Adams, G.T. Murray *"Direct Observations of Grain-Boundary Sliding in Bi-Crystals of Sodium Chloride and Magnesia"* J. Appl. Phys. 33(6) p. 2126 (1962)

[Alm 1984] E.A. Almond *"Aspects of various processes for coating and surface hardening"* Vacuum 34 p.835 (1984)

[And 1995] P.M. Anderson, C. Li *"Hall-Petch relations for multilayered materials"* Nanostr. Mater. 5 (3) p.349 (1995)

[Aou 2001] S.M. Aouadi, D.M. Schultze, S.L. Rohde, K.-C. Wong, K.A.R. Mitchell *"Growth and characterization of Cr2N/CrN multilayer coatings"* Surf. & Coatings Technol. 140(3) p.269 (2001)

[Arzt 1998] E. Arzt *"Size effects in materials due to microstructural and dimensional constraints: a comparative review"* Acta Mater., 46 (16) p.5611 (1998)

[Ash 1976] N.W. Ashcroft & N.D. Mermin "*Solid State Physics"* (Holt, Rinehart & Winston, New York) p.387 (1976)

[Ban 2002] R. Banerjee, R. Chandra, P. Ayyub *"Influence of the sputtering gas on the preferred orientation of nanocrystalline titanium nitride thin films"* Thin Solid Films 405 p.64 (2002)

[Barn 1988] S.A. Barnett, L. Hultman, J.-E. Sundgren, F. Ronin *"Epitaxial growth of ZrN on Si (100)"* App. Phys. Letters 53 (5) p.400 (1988)

[Bour 2007] O. Bourbia, S. Achour, N. Tabet, M. Parlinska and A. Harabi, "*Effect of tantalum addition on microstructure and optical properties of TiN thin films",* Thin Solid Films, 515, 17, 6758-6764, (2007).

[Bee 1978] W. Beere, *"Stresses and deformation at grain boundaries"* Phil. Trans. R. Soc. Lond. A288 p. 177 (1978)

[Benk 2004] M. Benkahoul, C.S. Sandu, N. Tabet, M. Parlinska-Wojtan, A. Karimi and F. Lévy, *"Effect of Si incorporation on the properties of niobium nitride films deposited by DC reactive magnetron sputtering"* Surf. & Coat. Technol. *188-189,* p. 435-439, (2004).

[Bho 2004] S. Bhowmick, Z.H. Xie, M. Hoffman, V. Jayaram S.K. Biswas *"Nature of contact deformation of TiN films on steel"* J. Mater. Res. 19(9) p.2616 (2004)

[Bla 1973] A.G. Blachman *"dc bias-sputtered aluminium films"* J. Vac. Sci. Technol. 10 p. 299 (1973)

[Bor 2008] O. Borrero-Lopez, M. Hoffman, A. Bendavid, P.J. Martin *"A simple nanoindentation-based methodology to asses the strength of brittle thin films"* Acta Mater. 56 p. 1633 (2008)

[Bull 2001] S.J. Bull *"Interface engineering and graded films: Structure and characterization"* J. Vac. Sci. Technol. A19 p.1404 (2001)

[Cahn 1962] J. W. Cahn. *"The Impurity-Drag E_ect in Grain Boundary Motion"*, Acta Metallurgica, 10, p.789 (1962)

[Cai 2005] J.M. Cairney, M.J. Hoffman, P.R. Munroe, P.J. Martin, A. Bendavid *"Deformation and fracture of Ti–Si–N nanocomposite films"* Thin Solid Films 479 p.193 (2005)

[Call 1985] Callister, William Jr, *"Materials Science and Engineering, An Introduction"*. (John Wiley & Sons NY), NY (1985 [Kub 1988] F. Kubel, W. Lengauer, K. Yvon, , K. Knorr, A. Junod, *"Structural phase transition at 205^{o}K in stoichiometric vanadium nitride"* Phys. Rev. B 38, 18, p.12908 (1988)

[Cam 1986] R.C. Cammarata *"The supermodulus effect in compositionally modulated thin films"* Scripta Metall. 20(4) p.479 (1986)

[Car 2003] N.J.M. Carvalho, E. Zoestbergen, B.J. Kooi, J.T.M. De Hosson *"Stress analysis and microstructure of PVD monolayer TiN and multilayer TiN/(Ti,Al)N coatings"* Thin Solid Films 429 p.179 (2003)

[Car 2006] N.J.M. Carvalho, J.Th.M. De Hosson *"Deformation mechanisms in TiN/(Ti,Al)N multilayers under depth-sensing indentation"* Acta Mater. 54 p.1857 (2006)

[Cas 2007] L. Castaldi, D. Kurapov, A. Reiter, V. Shklover, P. Schwaller, J. Patscheider *"High temperature phase changes and oxidation behavior of Cr–Si–N coatings"* Surf**.** & Coat**.** Technol**.** 202 (4-7), p.781 (2007)

[Cas 2008] L. Castaldi, D. Kurapov, A. Reiter, V. Shklover, P. Schwaller, J. Patscheider *"Effect of the oxygen content on the structure, morphology and oxidation resistance of Cr-O-N coatings"* Surf**.** & Coat**.** Technol**.** (2008)

[Cho 1985] A.H. Chokshi, T.G. Langdon, *"The role of interfaces in superplastic deformation"* In *Superplasticity*, eds. B. Baudelet and M. Suery, p. 1-15. Centre Nationale de la Recherche Scientifique 2 (1985)

[Chu 1995] X. Chu, S.A. Barnett *"Model of superlattice yield stress and hardness enhancements"* J. Appl. Phys. 77 (9) p.4403 (1995)

[Cros 1975] F.W. Crossman, M.F. Ashby, *"The non-uniform flow of polycrystals by grain-boundary sliding accommodated by power law creep"* Acta Metall. 23 p.425 (1975)

[Csel 2005] T. Cselle, *"Application of coatings for tooling quo vadis2005?"* Vakuum in Forschung und Praxis, 17, p.33 (2005)

[Csel 2007] T. Cselle, M. Morstein, A. Lümkemann, J. Prohazka*"3(+1)Kathoden – 30 Schichten -300 Chargen"* Schweizer Präzisions-Fertigungstechnik, p.1 (2007)

[D'Heu 1970] F.M. D'Heurle *"Aluminum films deposited by rf sputtering"* Metall. Trans. 1 p.725 (1970)

[Ding 2000] J. Ding, Y. Meng, S.Wen *"Mechanical properties and fracture toughness of multilayer hard coatings using nanoindentation"* Thin Solid Films 371 p.178 (2000)

[Dir 1977] A.G. Dirks, H.J: Leamy *"Columnar microstructure in vapor-deposited thin films"* Thins Solid Films 47, p.219 (1977)

[Dov 1996] K. Dovidenko, S. Oktyabrsky, J. Narayan, M. Razeghi *"Aluminum nitride films on different orientations of sapphire and silicon"* J. Appl. Phys. 79 (5) p.2439 (1996)

[Edi 1974] J.W. Edington *Monographs 1-5*, London, Macmillan, Philips Technical Library, (1974)

[Erni 2009] R. Erni, M.D. Rossell, C. Kisielowski, U. Dahmen *„Atomic-resolution imaging with a sub-50-pm electron probe"* Phys. Rev. Lett. 102 p. 096101 (2009)

[Fisc 2000] A. C. Fischer-Cripps. *"A review of analysis methods for sub-micron indentation testing"*, Vacuum, 58(4), p.569 (2000)

[Gall 2003] D. Gall, S. Kodambaka, M.A. Wall, I. Petrov, J.E. Greene *"Pathways of atomistic processes on TiN(001) and (111) surfaces during film growth: an ab initio study"* J. Appl. Phys. 93 p.9086 (2003)

[Gif 1976] R.C. Gifkins, *"Grain-boundary sliding and its accommodation during creep and superplasticity"*. Met. Trans. 7A p. 1225 (1976)

[Gil 1970] J.J. Gilman *"Hardnesses of carbides and other refractory hard metals"* J. Appl. Phys. 41 p. 1664 (1970)

[Glas 2007] A. Glaser, S. Surnev, F.P. Netzer, N. Fateh, G.A. Fontalvo, C. Mitterer *"Oxidation of vanadium nitride and titanium nitride coatings"* Surf. Science 601(4) p.1153 (2007)

[Gre 1995] J.E. Greene, J.E. Sundgren, L. Hultman, I. Petrov, D.B. Bergstrom *"Development of preferred orientation in polycrystalline TiN layers grown by ultrahigh vacuum reactive magnetron sputtering"* Appl. Phys. Lett. 67 p.2928 (1995)

[Grün 1979] R. Grün*"The crystal structure of β-Si_3N_4; structural and stability considerations between α- and β-Si_3N_4*" Acta Cryst. B35 p.800 (1979)

[Hall 1951] O.E. Hall *"The Deformation and Ageing of Mild Steel: III Discussion of Results"* Proc. R. Lond. B64 p.474 (1951)

[Hao 2006] S. Hao, B. Delley, S. Vepřek, C. Stampfl *"Superhard Nitride-Based Nanocomposites: Role of Interfaces and Effect of Impurities"* Phys. Rev. Lett. 97 086102–1 (2006)

[Has 2006] A. Hasnaoui, P. M. Derlet, H. van Swygenhoven *"Interaction between dislocations and grain boundaries under an indenter – a molecular dynamics simulation"* Acta Mater. 52(8) p.2251 (2006)

[Helm 1985] U. Helmersson, B.O. Johansson, J.-E. Sundgren, H.T.G. Hentzell & P. Billgren *"Adhesion of titanium nitride coatings on high-speed steels"* J. Vac. Sci. Technol. A 3 p.308 (1985)

[Her 2005] M. Hermann, F. Furtmayr, A. Bergmaier, G. Dollinger, M. Stutzmann, M. Eickhoff *"Highly Si-doped AlN grown by plasma-assisted molecular-beam epitaxy"* Appl. Phys. Lett. 86, 192108 p.1 (2005)

[Hof 1966] R.W. Hoffmann *"Physics of Thin Films"* edited by G. Hass & R.E. Thun (Academic, New York, 1966) Vol.3 p.211

[Holl 1986] H. Holleck *"Material selection for hard coatings"* J. Vac. Sci. Technol. A 4(6) p.2661 (1986)

[Holl 1988] H. Holleck *"Metastable coatings – prediction of composition and structure"* Surf. & Coat. Technol. 3 p.151 (1988)

[Holu 1999] P. Holubar, M. Jilek, M. Sima *"Nanocomposite nc-TiAlSiN and nc-TiN-BN coatings: their applications on substrates made of cemented carbide and results of cutting tests"* Surf. & Coat. Technol. 120, p.184 (1999)

[Hul 1995] L. Hultman, J.-E. Sundgren, J.E. Greene, D.B. Bergstrom and I. Petrov *"High-flux low-energy (≅20 eV) N2+ ion irradiation during TiN deposition by reactive magnetron sputtering: Effects on microstructure and preferred orientation"*J. Appl. Phys. 78(9) p.5395 (1995)

[Hul 2000] L. Hultman *"Thermal stability of nitride thin films"* Vacuum 57(1) p.1 (2000)

[Hul 2007] L. Hultman, J. Bareno, A. Flink, H. Söderberg, K. Larsson, V. Petrova, M. Oden, J.E. Greene and I. Petrov *"Interface structure in superhard TiN-SiN nanolaminates and nanocomposites: Film growth experiments and ab-initio calculations"* Phys. Rev. B 75(15) p.155437 (2007)

[Hum 1998] W. Hume-Rothery, B.R. Coles *"Atomic theory for students of metallurgy"*, 6th ed, Maney Publishing, London UK (1998)

[Jay 2006] V. Jayaram, S. Bhowmick, Z.-H. Xie, S. Math, M. Hoffman, S.K. Biswas, *"Contact deformation of TiN coatings on metallic substrates"* Mat. Sci. Eng. A 423 p.8 (2006)

[John 1999] W.L. Johnson, *"Bulk Glass-Forming Metallic Alloys: Science and Technology"* MRS Bull. 24 (10) p.42 (1999)

[Kas 1985] B.P. Kashyap, A. Arieli, A.K. Mukherjee, *"Review: microstructural aspects of superplasticity"* J. Mat. Sci. 20 p.2661 (1985)

[Kato 1980] M. Kato, T. Mori, L.H. Schwartz *"Hardening by spinodal modulated structure"*, Acta Metall. 28(3) p.285 (1980)

[Kle 1987] S.J. Klepeis, J.P. Benedict & R.M. Anderson, *Mat. Res. Soc. Proc*. 115, Pittsburgh, PA. USA p.179, (1987)

[Klo 1968] E. Klockholm & B.S. Berry, J. Electrochem. Soc. 115 p.823 (1968)

[Kni 1989] J.C. Knight, T.F. Page, I.M. Hutchings, *""*Surf. Eng. 5 p.213 (1989)

[Koe 1970] J.S. Koehler *"Attempt to design a strong solid"* Phys. Rev. B. 2 (2) p.547 (1970)

[Kra 1983] B. Kramer *"Requirements for wear-resistant coatings"* Thin Solid Films 108 p.117 (1983)

[Kuhl 1989] D. Kuhlmann-Wilsdorf, *"Theory of Plastic Deformation"* Mat. Sci. & Eng. A, 113, p. 1 (1989)

[Kurz 2010] K. Kurzydłowski et al. *„Nanomateriały inżynierskie, konstrukcyjne i funkcjonalne"* Wydawnictwo Naukowe PWN, Warszawa (2010)

[Kut 2005a] K. Kutschej, P.H. Mayrhofer, M. Kathrein, P. Polcik, R. Tessadri, C. Mitterer *"Structure, mechanical and tribological properties of sputtered Ti1–xAlxN coatings with 0.5≤x≤0.75"* Surf. & Coat. Technol. 200 (7) p. 2358 (2005)

[Kut 2005b] K. Kutschej, N. Fateh, P.H. Mayrhofer, M. Kathrein, P. Polcik, C. Mitterer *"Comparative study of Ti1−xAlxN coatings alloyed with Hf, Nb, and B"* Surf. & Coat. Technol 200(1-4) p.112 (2005)

[Lam 2006] R. Lamni, PhD. Thesis n°3238, EPFL, Switzerland, *« Propriétés physiques et chimiques des couches minces de ZrN, Zr-Al-N et Zr-Cr-N déposées par pulvérisation magnétron réactive »*, http://library.epfl.ch/en/theses/?nr=3238 (2006)

[Lam 2005] R. Lamni, R. Sanjinés, M. Parlinska-Wojtan, A. Karimi, and F. Lévy, *"Microstructure and nanohardness properties of Zr–Al–N and Zr–Cr–N thin films"* J. Vac. Sci. Technol. A 23, 593 (2005). [Li 2002] T.Q. Li, S. Noda, Y. Tsuji, T. Ohsawa, H. Komiyama *"Initial growth and texture formation during reactive magnetron sputtering of TiN on Si(111)"* J. Vac. Sci. Technol., A 20 p.583 (2002)

[Lan 1975] T.G. Langdon, *Grain boundary deformation processes* in *"Deformation of Ceramic Materials"*, eds. R. C. Bradt and R. E. Tressler, p. 101-126. Plenum, New York. (1975)

[Lan 1981] T.G. Langdon *Deformation of polycrystalline materials at high temperatures* in "*Deformation of Polycrystals: Mechanisms and Microstructures"*, eds. N. Hansen, A. Horsewell, T. Leffers and H. Lilholt, pp. 45-54. (1981)

[Lan 1983] T.G. Langdon, D. Simpson, R.C. Gifkins *"Cyclic grain boundary migration during high temperature fatigue—II. Measurements of grain boundary sliding"* Acta Metall., 31(6) p. 939 (1983)

[Lan 1994] T.G. Langdon, *"A unified approach to grain boundary sliding in creep and superplasticity"* Acta Metall. et Mater., 42(7) p. 2437 (1994)

[Ley 2004] A. Leyland, A. Matthews, *"Design criteria for wear-resistant nanostructured and glassy-metal coatings"* Surf. & Coat. Technol. 177-178 p.317 (2004)

[Li 1997] J. Li, T. Chow, *""* Int. J. Solids Struct. 34 p.4463 (1997)

[Lim 2003] S.H. Lim, D.G. McCulloch, M.M.M. Bilek, D.R. McKenzie *"Relation between microstructure and stress in titanium nitride films grown by plasma immersion ion implantation"* J. Appl. Phys. 93 p.4283 (2003)

[Long 2006] Y. Long, F. Giuliani, S.J. Lloyd, J.M. Molina-Aldareguia, Z.H. Barber, W.J. Clegg *"Deformation processes and the effects of microstructure in multilayered ceramics"* Composites: PartB 37, p.542 (2006)

[Löf 1994] F.H.W. Löffler, *"Systematic approach to improve the performance of PVD coatings for tool applications"* Surf. & Coat. Technol. 68/69 p.729 (1994)

[Ma 2000] C.-H. Ma, J.-H. Huang and Haydn Chen *"A study of preferred orientation of vanadium nitride and zirconium nitride coatings on silicon prepared by ion beam assisted deposition"* Surf. & Coat. Technol. 133-134 p.289 (2000)

[Ma 2005] L.W. Ma, J.M. Cairney, M. Hoffman, P.R. Munroe *"Deformation mechanisms operating during nanoindentation of TiN coatings on steel substrates"* Surf. & Coat. Technol. 192 p.11 (2005)

[Mad 1997] A. Madan, I.W. Kim, S.C. Cheng, P. Yashar, V.P. Dravid, S.A. Barnett *"Stabilization of Cubic AlN in Epitaxial AlN/TiN Superlattices*" Phys. Rev. Lett. 78 (9) p.1743 (1997)

[Mah 2005] S. Mahieu, P. Ghekiere, G. De Winter, S. Heirwegh, D. Delpla, R. De Gryse, O.I. Lebedev, G. Van Tendeloo *"Mechanism of preferential orientation in sputter deposited titanium nitride and yttria-stabilized zirconia layers"* J. Cryst. Growth 279 p.100 (2005)

[Mart 2005] P.J. Martin, A. Bendavid, J.M. Cairney, M. Hoffman, *"Nanocomposite Ti-Si-N, Zr-Si-N, Ti-Al-Si-N, Ti-Al-V-Si-N thin film coatings deposited by vacuum arc deposition"* Surf. & Coat. Technol. 200(7) p.2228 (2005)

[Matt 1989] D.M. Mattox *"Particle bombardment effects in thin film deposition: a review"* J. of Vac. Sci. & Technol. A 7(3) p. 1105 (1989)

[Mayr 2003] P.H. Mayrhofer, A. Hörling, L. Karlson, J. Sjölén, T.Larsson, C. Miterer, L. Hultman, *"Self-organized nanostructures in the Ti-AL-N system"* Appl. Phys. Lett. 83(10) p.2049 (2003)

[Mayr 2006a] P.H. Mayrhofer, C. Mitterer, J.G. Wen, I. Petrov and J.E. Greene *"Thermally induced self-hardening of nanocrystalline Ti-B-N thin films"* J. Appl. Phys., 100 p. 044301 (2006)

[Mayr 2006b] P.H. Mayrhofer, D. Music and J.M. Schneider *"Ab initio calculated bimodal and spinodal of cubic TiAlN"* Appl.Phys Lett. 88, 071922 (2006)

[Mayr 2007] P.H. Mayrhofer, D. Music and J.M. Schneider *"Erratum: Ab initio calculated bimodal and spinodal of cubic TiAlN [Appl.Phys Lett. 88, 071922 (2006)]"* Appl. Phys. Lett. 90 p.029902 (2007)

[Maz 1997] A. Mazel, P. Marti, F. Henry, B. Armas, R. Bonnet, M. Loubradou *"Nanostructure and local chemical composition of AlN-Si3N4 layers grown by LPCVD"* Thin Solid Films 304 p.256.(1997)

[Män 2001] H.D. Männling, D.S. Patil, K. Moto, M. Jilek, S. Veprek *"Thermal stability of superhard nanocomposite coatings consisting of immiscible nitrides"* Surf. Coat. Technol. 146–147 p.263 (2001)

[Mean 1986] W.D. Means, M.W. Jessell, *"Accommodation migration of grain boundaries"*, Tectonophysics 127 p.67 (1986)

[Mich 1999] A. Michels, C. E. Krill, H. Ehrhardt, R. Birringer, and D. T. Wu. *"Modelling the influence of grain-size-dependent solute drag on the kinetics of grain growth in nanocrystalline materials",* Acta Materialia, 47(7) p.2143 (1999)

[Mic 2007] J. Michler, K. Wasmer, S. Meier, F. Oestlund, K. Leifer *„Plastic deformation of gallium arsenide micropillars under uniaxial compression at room temperature"* Appl. Phys. Lett. 90(4) p.043123 (2007)

[Mir 1990] P.B. Mirkarimi, L. Hultman, S.A. Barnett *"Enhanced hardness in lattice-matched single-crystal TiN/$V_{0.6}Nb_{0.4}N$ superlattices"* Appl. Phys. Lett., 57 p.2654 (1990)

[Mir 1992] P.B. Mirkarimi, M. Shinn, L. Hultman, S.A. Barnett *"An ultrahigh vacuum magnetron sputtering system for the growth and analysis of nitride superlattices"* J. Vac. Sci. Technol. A 10, p.75 (1992)

[Mit 1998] C. Mitterer, P. Losbichler, F. Hofer, P. Warbichler, P.N. Gibson, W. Gissler *"Nanocrystalline hard coatings within the quasi-binary system TiN-TiB2"* Vacuum 50 (3-4) p.313 (1998) [Mos 2007] M. Moser and P.H. Mayrhofer *"Yttrium-induced structural changes in sputtered Ti1-xAlxN thin films"* Scripta Mat. 57 p.357 (2007)

[Mit 1999] C. Mitterer, P.H. Mayrhofer, M. Beschliesser, P. Losbichler, P. Warbichler, F. Hofer *et al.* *"Microstructure and properties of nanocomposite Ti-B-N and Ti-B-C coatings"* Surf. & Coat. Technol. 120-121 p.405 (1999)

[Mol 2002a] J.M. Molina-Aldareguia, S.J. Lloyd, S.J. Oden, T. Joelsson, L. Hultman, W.J. Clegg *"Deformation structures under indentations in TiN/NbN single-crystal multilayers deposited by magnetron sputtering at different bombarding ion energies"* Phil. Mag. A 82 p. 1983 (2002)

[Mol 2002b] J. M. Molina-Aldareguia, S.L. Lloyd, M. Oden, T. Joelsson, L. Hultman, W.J. Clegg *"Deformation structures under indentations in TiN/NbN single-crystal multilayers deposited by magnetron sputtering at different bombarding ion energies"* Phil. Mag. A 82/10 p.1983 (2002)

[Mos 2006] B. Moser, J.F. Löffler, J. Michler *"Discrete deformation in amorphous metals: an in-situ SEM indentation study"* Phil. Mag. 86 p. 5715 (2006)

[Murr 1975] L.E. Murr *"Interfacial Phenomena in Metal and Alloys"* (Addison Wesley, Reading) p.258 (1975)

[Mus 1998] J. Musil, J. Vlicek *"Magnetron sputtering of films with controlled texture and grain size"* Mater. Chem. Phys. 54 p116 (1998)

[Mus 1999] J. Musil, P. Zeman, H. Hrubý, P. H. Mayrhofer *"ZrN/Cu nanocomposite film—a novel superhard material"* Surf. & Coat. Technol. 120-121 p.179 (1999)

[Mus 2000] J. Musil *"Hard and superhard nanocomposite coatings"* Surf. & Coat. Technol. 125 p.322 (2000)

[Mus 2001] J. Musil and J. Vlcek. *"Magnetron sputtering of hard nanocomposite coatings and their properties",* Surf. & Coat. Technol. 142 p. 557 (2001)

[Münz 2001] W.D. Münz, D.B. Lewis, P.E. Hovsepian, C. Schönjahn, A. Ehisarian, I.J. Smith **"***Industrial scale manufactured superlattice hard PVD coatings"* Surf. Eng. 17(1) p.15 (2001)

[Nied 1999] A. Niederhofer, P. Niesladek, H.D. Männling, K. Moto, S. Veprek, M. Jilek *"Structural properties, internal stress and thermal stability of nc-TiN/a-Si_3N_4, nc-TiN/SiN_x and ($TiN_{1-x}Al_ySi_x$)N superhard nanocomposite coatings reaching the hardness of diamond"* Surf. & Coat. Technol. 120 p.173 (1999)

[Nor 1998] B. North *"Six issues for the hard coatings community",* Surf. & Coat. Technol. 106 p.129 (1998)

[Nord 1998] M. Nordin, M. Larsson, S. Hogmark *"Mechanical and tribological properties of multilayered PVD TiN/CrN, TiN/MoN. TiN/NbN and TiN/TaN coatings on cemented carbide"* Surf. & Coat. Technol. 106 p.234 (1998)

[Oh 1993] U.C. Oh, J.H. Je *"Effects of strain energy on the preferred orientation of TiN thin films"* J. Appl. Phys. 74 p. 1692 (1993)

[Pan 1982] A. Pan & J.E. Greene *"Interfacial chemistry effects on the adhesion of sputter-deposited TiC films to steel substrates"* Thin Solid Films 97 p.79 (1982)

[Par 2004a] M. Parlinska-Wojtan, A. Karimi, T. Cselle and M. Morstein, *"Conventional and high resolution TEM investigation of the microstructure of compositionally graded TiAlSiN thin films"*, Surf. & Coat. Technol., 177-178, p. 376-381, (2004).

[Par 2004b] M. Parlinska-Wojtan, A. Karimi, M. Morstein and T. Cselle, *"Characterization of thermally treated TiAlSiN coatings by TEM and nanoindentation",* Surf. & Coat. Technol. *188-189*, p. 344-350, (2004).

[Par 2010] M. Parlinska-Wojtan, S. Meier and J. Patscheider *"TEM characterization of TiN/SiN_x multilayered coatings plastically deformed by nanoindentation"* Thin Solid Films 518 (17) p.4890–4897, (2010).

[Pat 2001] J. Patscheider, T. Zehnder, M. Diserens *"Structure–performance relations in nanocomposite coatings"* Surf. & Coat. Technol. 146-147 p.201 (2001)

[Pat 2003] J. Patscheider *"Nanocomposite hard coatings for wear protection"* MRS bulletin 28(3) p.180 (2003)

[Pats 2004] P. Patsalas, C. Gravalidis, S. Logothetidis *"Surface kinetics and subplantation phenomena affecting the texture, morphology, stress, and growth evolution of titanium nitride films"* J. Appl. Phys. 96 p.6234 (2004)

[Pel 1991] J. Pelleg, L.Z. Zevin, S. Lungo, N. Croitoru *"Reactive-sputter-deposited TiN films on glass substrates"* Thin Solid Films 197 p.117 (1991) [Pet 1953] J.N. Petch, Iron Steel Inst. 174, p.25 (1953)

[Péli 2007] A. Pélisson, M. Parlinska-Wojtan, H.J. Hug, J. Patscheider, *"Microstructure and properties of Al-Si-N transparent hard coatings deposited by magnetron sputtering"*, Surf. & Coat. Technol. 202, p. 884-889, (2007).

[Péli 2009] A. Pélisson PhD. Thesis, University of Basel, Switzerland, (2009) *"Al-Si-N transparent hard nanostructured hard coatings"* http://edoc.unibas.ch/view/year/2009.html

[Pen 1962] J.N. Pendle & P.J. Gielisse *"Hardness of Nonmetallic Solids on an Atomic Basis"* Phys. Rev. B 125(3) p. 828 (1962)

[Petc 1953] N.J. Petch *"The cleavage strength of polycrystals"* J. Iron Steel. Inst. 174(1) p. 25 (1953)

[Petr 2003] I. Petrov, P. B. Barna, L. Hultman, and J. E. Greene *"Microstructural evolution during _lm growth",* J. of Vac. Sci. & Technol. A, 21 p. S117 (2003)

[Pow 1966] C.F. Powell, J.H. Oxley and J.M. Blocher Jr.*"Vapor deposition"* (1966)

[Rogl 1992] P. Rogl, J.C. Schuster *"Phase Diagrams of Ternary Boron Nitride and Silicon Nitride Systems"* ASM International, Materials Park, OH, p.131 (1992)

[Raj 1971] R. Raj, M.F. Ashby, *"On grain boundary sliding and diffusional creep"* Met. Trans. 2 p.1113 (1971)

[Ree 2000] J.-H. Ree, *"Grain boundary sliding in experimental deformation of Octachloropropane"* In: Stress, Strain and Structure, A volume in honor of W D Means. Eds: M.W. Jessell and J.L. Urai. 2, Journal of the Virtual Explorer http://virtualexplorer.com.au/journal/ (2000)

[Rov 2008] F. Rovere, P.H. Mayrhofer, A. Reinholdt, J. Mayer, J.M. Schneider *"The effect of yttrium incorporation on the oxidation resistance of Cr–Al–N coatings"* Surf. & Coat. Technol. 202(24) p.5870 (2008)

[Rze 2009a] K. Rzepiejewska – Malyska, M. Parlinska – Wojtan, K. Wasmer, K. Hejduk, J. Michler, *"In – situ SEM indentation studies of the deformation mechanisms in TiN, CrN and TiN/CrN",* Micron 40 (1), p. 22-27, (2009).

[Rze 2009b] K.A. Rzepiejewska-Malyska, W.M. Mook, M. Parlinska-Wojtan, J. Hejduk, J. Michler *"In – situ SEM indentation studies on multilayer nitride films: methodology and deformation mechanisms"* JMR 24(3), p.1208, (2009).

[Sand 2005] C.S. Sandu, R. Sanjinés, M. Benkahoul, M. Parlinska-Wojtan and F. Lévy, *Structural and chemical properties of sputter-deposited Ti–Ge–N thin films*, Surf. & Coat. Technol. 200(5-6) p.1483 (2005)

[Sand 2006a] C.S. Sandu, R. Sanjine´s, M. Benkahoul, M. Parlinska-Wojtan, A. Karimi, F. Lévy, *"Influence of Ge addition on the morphology and properties of TiN thin films deposited by magnetron sputtering",* Thin Solid Films, 496 p. 336 – 341, (2006)

[Sand 2006b] C.S. Sandu, M. Benkahoul, M. Parlinska-Wojtan, R. Sanjinés, F. Lévy, *"Morphological, structural and mechanical properties of NbN thin films deposited by reactive magnetron sputtering"* Surf. & Coat. Technol. 200 p. 6544–6548, (2006)

[Sanj 2006] R. Sanjinés, C.S. Sandu, R. Lamni and F. Lévy *"Thermal decomposition of $Zr_{1-x}Al_xN$ thin films deposited by magnetron sputtering"* Surf. & Coat. Technol. 200(23-24) p. 6308 (2006)

[Schi 1998] J. Schiotz, F.D. di Tolla and K.W. Jacobsen *"Softening of nanocrystalline metals ate very small grain sizes"* Nature 391(6667) p.561 (1998)

[Sen 2004] U. Sen, *"Thermo reactive diffusion vanadium nitride coatings on AlSi 1020 steel"* Key Engineering Materials 264-268 p.577 (2004)

[Shi 1982] P. Shirat, R.B. Vastava, T.G. Langdon *"An evaluation of the roles of intercrystalline and interphase boundary sliding in two-phase superplastic alloys"* Acta Metall. 30(1) p.285 (1982)

[Shii 2010] T. Shiino, K. Todoroki, N. D. Minh, L. Jiang, S. Shiba, Y. Uzawa, H. Maezawa, N. Sakai and S. Yamamoto *"Improvement of Critical Temperature of Superconducting NbN and NbTiN Thin Films Using an AlN Buffer Layer"* Supercond. Sci. Technol. **23** 045004 (2010)

[Sol 2008] J. Soldán, J. Neidhardt, B. Sartory, R. Kaindl, R. Čerstvý, P.H. Mayrhofer, R. Tessadri, P. Polcik, M. Lechthaler, C. Mitterer *"Structure–property relations of arc-evaporated Al–Cr–Si–N coatings"* Surf. & Coatings Technol. 202(15) p.3555 (2008)

[Söd 2005] H. Söderberg, M. Oden, J.M. Molina-Aldareguia and L. Hultman *"Nanostructure formation during deposition of TiN/SiN_x nanomultilayers films by reactive dual magnetron sputtering"* J. Appl. Phys. 97/11 p.114327, (2005)

[Söd 2006a] H. Söderberg, Ph.D. Thesis, Lulea University of Technology, Sweden, (2006) ISSN: 1402-1544 *"Growth and characterization of TiN/SiN_x multilayer thin films"* http://epubl.ltu.se/1402-1544/2006/59/LTU-DT-0659-SE.pdf

[Söd 2006b] H. Söderberg, M. Oden, T. Larsson, L. Hultman and J. M. Molina-Aldareguia *"Epitaxial stabilization of cubic SiNx in TiN/SiNx multilayers"* Appl. Phys. Lett. 88 p.191902, (2006)

[Sun 2008] Qian Sun, Zheng-Wen Fu *"Vanadium nitride as a novel thin film anode material for rechargeable lithium batteries"* Electrochimica Acta 54(2) p.403 (2008)

[Swy 2002] H. van Swygenhoven *"Polycrystalline Materials: grain boundaries and dislocations"* Science 296(5565) p.66 (2002)

[Swy 2006a] H. van Swygenhoven, J. Weertman *"Deformation in nanocrystalline metals"* Mater. Today 9(5) p.24 (2006)

[Swy 2006b] H. van Swygenhoven, P.M. Derlet, A.G. Frøseth *"Nucleation and propagation of dislocations in nanocrystalline fcc metals"* Acta Mater. 54(7) p.1975 (2006)

[Szlu 2005] I. Szlufarska, A. Nakano ans P. Vashishta *„A crossover in the mechanical response of nanocrystalline ceramics"* Science 309(5736) p.911 (2005)

[Tan 2001] Y. Taniyasu, M. Kasu, N. Kobayashi "*Lattice parameters of wurtzite $Al_{1-x}Si_xN$ ternary alloys*" Appl. Phys. Lett. 79 p.4351 (2001)

[Tho 1993] C.V. Thompson *"Texture evolution during grain growth in polycrystalline films"* Scripta Metall. et Mater. 28(2) p.167 (1993)

[Thor 1977] J. A. Thornton. *"High Rate Thick Film Growth"* Annual Reviews of Materials Science 7(1) p. 239 (1977)

[Tjon 2004] S.C. Tjong nad H. Chen *"Nanocrystalline materials and coatings"* Mat. Sci. Eng. R, 45(1-2) p.1 (2004)

[Turn 1949] D. Turnbull, J.C. Fisher, *"Rate of nucleation in condensed systems"* J. Chem. Phys 17 (1) p.71-73 (1949).

[Vepr 1995] S. Veprek, S. Reiprich *"A concept for the design of novel superhard coatings"* Thin Solid Films 268 p.64 (1995)

[Vepr 1996] S. Veprek, M. Haussmann, S. Reiprich, L. Shizhi, J. Dian *"Novel thermodynamically stable and oxidation resistant superhard coating materials"* Surf. & Coat. Technol. 86–87 p. 394 (1996)

[Vepr 1999] S. Veprek *"The search for novel, superhard materials"* J. Vac. Sci. Technol. A17 p.2401 (1999)

[Vepr 2004] S. Veprek, H.D. Männling, M. Jilek, P. Holoubar *"Avoiding the high temperature decomposition and softening of $(Al_{1-x}Ti_x)N$ coatings by the formation of stable superhard nc-$(Al_{1-x}Ti_x)N$/a-Si_3N_4 nanocomposite"* Mat. Sci. Eng.A 366 p. 202 (2004)

[Vepr 2005] S. Veprek, M.G.J. Veprek-Heijman, P. Karvankova and J. Prochazka *"Different approaches to superhard coatings and nanocomposites"* Thin Solid Film 476(1) p.1 (2005)

[Vepr 2008] S. Veprek, M.G.J. Veprek-Heijman, R.F. Zhang *"Chemistry, physics and fracture mechanics in search for superhard materials, and the origin of superhardness in nc-TiN/a-Si3N4 and related nanocomposites"* J. Phys. & Chem. Sol. 68(5-6) p.1161 (2008)

[Wen 2008] M. Wen C.Q. Hu, C.Wang, T. An, Y.D. Su, Q.N. Meng and W.T. Zheng *"Effects of substrate bias on the preferred orientation, phase transition and mechanical properties for NbN films grown by direct current reactive magnetron sputtering"* J. of Appl. Phys. 104 p.023527 (2008)

[Wen 2009] M. Wen C.Q. Hu, Q.N. Meng, Z.D. Zhao, T. An, Y.D. Su, and W.T. Zheng *"Effects of nitrogen flow rate on the preferred orientation and phase for niobium nitride films grown by direct current reactive magnetron sputtering"* J. of Phys. D: Appl. Phys. 42 p.035304 (2009)

[Wep 1996] E. Weppelmann, M. Wittling, M.V. Swain, D. Munz, in R.C. Bradt, et al. (Eds.) *"Fracture Mechanics of Ceramics."* Vol. 12 (1996)

[West 1981] R. West and M.J. Astl, *"CRC Handbook of Chemistry and Physics"* 62nd ed., The Chemical Rubber Co, USA, p.D55 (1981)

[Wil 2004] D.B. Williams and C. Barry Carter *"A Textbook for Materials Science"* (4-Vol Set) Springer 1-st edition 2004 (2004)

[Will 2008] H. Willmann, M. Beckers, J. Birch, P.H. Mayrhofer, C. Mitterer, L. Hultman *"Epitaxial growth of Al–Cr–N thin films on MgO(111)"* Thin Solid Films 517(2) p.598 (2008)

[Win 1992] H. Windischmann *"Intrinsic stress in sputter-deposited thin films"* Crit. Rev. Solid State Mater. Sci. 17(6) p.547 (1992)

[Wrz 2003] H. Wrzesinska, J. Ratajczak, K. Studzinska, J. Kacki *"Transmission electron microscopy of hard ceramic superlattices applied in silicon micro-electro-mechanical systems"* Mater. Chem. Phys. 81 p.265 (2003)

[Yang 2002] Q. Yang, C. He, L.R. Zhao, J.-P. Immarigeon *"Preferred orientation and hardness enhancement of TiN/CrN superlattice coatings deposited by reactive magnetron sputtering"* Scripta Mater. 46, p.293 (2002)

[Yas 1999] P.C. Yashar, W.D. Sproul *"Nanometer scale multilayered hard coatings"* Vacuum 55 p.179 (1999)

[Xie 2006] Z.H. Xie, M. Hoffman, R.J. Moon, P.R. Munroe *"Deformation of a hard coating on ductile substrate system during nanoindentation: Role of the coating microstructure"* J. Mater. Res. 21(2) p.437 (2006)

[Zha 2007] RF. Zhang, H.L. Wang, S.E. Ong, D.Sun and X.L. Bui *"Hard yet tough nanocomposite coatings – present status and future trends"* Plasma Process and Polymers 4(3) p.219 (2007)

[Zha 2008] R.F. Zhang, S.H. Sheng, S. Veprek *"Stability of Ti–B–N solid solutions and the formation of nc-TiN/a-BN nanocomposites studied by combined ab initio and thermodynamic calculations"* Acta Mater. 56(16) p.4440 (2008)

[Zhao 1997] J.P. Zhao, X. Wang, Z.Y. Chen, S.Q. Yang, T.S. Shi, X.H. Liu *"Overall energy model for preferred growth of TiN films during filtered arc deposition"* J. Phys. D: Appl. Phys. 30(1) p.5 (1997)

[Zhao 1984] B. R. Zhao, L. Chen, and H. L. Luo M. D. Jack D. P. Mullin, *"Superconducting and normal-state properties of vanadium nitride"* Phys. Rev. B 29, p.6198 (1984)

Streszczenie

Głównym celem niniejszej rozprawy habilitacyjnej była identyfikacja i klasyfikacja różnych rodzajów powierzchni granicznych występujących w cienkich powłokach azotków metali przejściowych poprzez bezpośrednią obserwację transmisyjnym mikroskopem elektronowym (TEM). Poddany został również analizie wpływ obecności wyżej opisanych powierzchni granicznych na mechanizmy utwardzania występujące w powłokach o różnych strukturach. Badane powłoki zostały podzielone według ich struktury na trzy grupy: powłoki kolumnowe, wielowarstwowe i nanokompozyty. Aby lepiej uwidocznić mechanizmy rządzące zachowaniem powłok podczas odkształceń plastycznych, mikrostruktura wszystkich trzech grup powłok została dokładnie przebadana techniką TEM bezpośrednio po wytworzeniu, po wygrzewaniu oraz po nanowgłębianiu. Przeanalizowano również wpływ zmian składu chemicznego na mikrostrukturę powłok.

Badania TEM w skali atomowej powłok nanokompozytowych TiAlSiN o zmieniającym się gradientowo składzie pozwoliły zaproponować mechanizm powstawania struktur nanokompozytu. Obrazy TEM przekroju powłoki wykonane w części bogatej w Ti pokazały krystaliczną strukturę kolumnową z granicami ziaren nie zawierającymi wydzieleń ani fazy amorficznej. Wraz ze wzrostem zawartości Al i Si, pojawiała się faza międzygraniczna o strukturze krystalicznej przechodząca w fazę amorficzną. Obserwowana struktura przy powierzchni powłoki nanokompozytu, składała się z krystalicznych ziaren otoczonych osnową amorficzna. Ponadto wykazano, że struktura nanokompozytu cechującego się wysoką twardością, może zostać utworzona z dwóch faz takich jak TiN i SiN, stykających się wyraźnie zaznaczonymi powierzchniami granicznymi. Nie udało się natomiast wytworzyć nanokompozytu o podwyższonej twardości zbudowanego z faz Al i Si. Jest to związane z lokalną epitaksją na powierzchniach AlN/SiN, badanych w modelowym układzie wielowarstw AlN/SiN. Udowodniono, że warstwa SiN o grubości 0,7 nm, co odpowiada grubości trzech monowarstw, rośnie w formie krystalicznej na AlN, faworyzując epitaksję.

Utworzenie powłoki o strukturze nanokompozytu nie jest jedyną z możliwości uzyskana wzrostu twardości w opisywanych powłokach azotków metali przejściowych. Również powłoki o strukturze kolumnowej mogą wykazywać wysoką twardość. Rozwiązaniem jest wprowadzenie wystarczającej gęstości barier dla dyslokacji, w innej postaci niż granice międzykolumnowe. Pierwsze polega na wprowadzeniu wielowarstw o zmieniającym się gradientowo składzie chemicznym, które powodują zniekształcenia sieci, ale nie blokują

wzrostu kolumnowego. Drugie rozwiązanie opiera się na koncepcji struktury modulowanej fazowo, tzn. wewnątrz kolumn utworzone zostają strefy o różnych fazach. Tak się dzieje w przypadku fazy prymitywnej i heksagonalnej NbN przy zachowaniu struktury kolumnowej.

W wielowarstwach, obserwowane były trzy typy powierzchni granicznych wpływających na ich własności: powierzchnie pół-koherentne z całkowitą epitaksją, takie jak w przypadku warstw $AlN_{10\ nm}$/ $SiN_{<0,7\ nm}$ lub w układzie NbN/CrN na powierzchniach granicznych między CrN i NbN w kierunku wzrostu; pół-kohetrentne z lokalną epitaksją jak w systemie TiN/NbN; oraz całkowicie niekoherentne - jak w powłokach TiN/SiN. Wymienione typy powierzchni granicznych były barierami dla ruchu dyslokacji, co prowadziło do wyższych wartości twardości w tych powłokach w stosunku do powłok referencyjnych o strukturze kolumnowej.

W celu lepszego uwidocznienia i zidentyfikowania mechanizmów utwardzania, opartych na blokowaniu dyslokacji w powłokach azotków metali, wykonano celowo odkształcenie plastyczne powłoki poprzez nanowgłębianie. Przekroje przez odciski, powstałe w wyniku penetracji wgłębnika w powłokach o strukturze kolumnowej i wielowarstwowej, zostały poddane obserwacjom w transmisyjnym mikroskopie elektronowym. Stwierdzono, że powłoki zawierające TiN, niezależnie od ich struktury czy grubości poszczególnych warstw, odkształcają się poprzez poślizg po granicach ziaren. Mechanizm ten był obserwowany w dwóch różnych skalach. W szerszej skali cale fragmenty wielowarstw byly przeuwane o ok. pół grubości jednej warstwy TiN. Natomiast lokalnie, tylko pojedyncze ziarna były pionowo przesuwane na dystansie kilku nanometrów. Mechanizm ten najlepiej widoczny był dla kombinacji NbN/TiN oraz dla TiN/amorficzne SiN.

Na podstawie obserwacji mikrostrukturalnych TEM udowodniono, że podłoże również steruje mechanizmami odkształcenia w powłokach kolumnowych TiN. W przypadku TiN, nałożonego na miękkie podłoże krzemowe, podczas wgłębiania ziarna kolumnowe ulegają ścinaniu poślizgowemu po granicach ziaren i są wpychane w podłoże tworząc stopnie na powierzchni granicznej pomiędzy powłoką a podłożem. W przypadku TiN o strukturze kolumnowej na twardym podłożu polikrystalicznym WC-Co pojawjają się pęknięcia na granicach. Kolumny, które rosną na miekkiej osnowie Co są w nią wciskane. Natomiast te kolumny, które rosną na twardych ziarnach WC są ściskane, wyginane oraz pojawiają się pęknięcia wewnątrz kolumn.

Rozważając odporność powłok na utlenianie ustalono, że zasadniczą role odgrywają w niej zarówno skład chemiczny, ich struktura oraz granice ziaren. Poprzez obserwacje mikrostrukturalne dowiedziono, że powłoki o strukturze kolumnowej, takie jak bogata w Ti TiAlSiN lub ZrAlN, nie są odporne na utlenianie niezależnie od ich składu chemicznego. Stwierdzono, że odporność na utlenianie zależy głównie od mikrostruktury i że granice międzykolumnowe służą jako kanały dyfuzyjne dla tlenu. Natomiast dla powłok nanokompozytowych, takich jak bogate w Al i Si TiAlSiN nie zaobserwowano penetracji tlenu do wewnątrz struktury powłoki. Zaobserwowano natomiast ostrą powierzchnię graniczną z tlenkiem rosnącym tylko na powierzchni powłoki.

SŁOWA KLUCZOWE:

Twarde powłoki azotków metali; mechanizmy utwardzania; powierzchnie graniczne, transmisyjna mikroskopia elektronowa (TEM); mechanizmy odkształcania; pękanie; poślizg po granicach ziaren; podwyższanie twardości; nanokompozyty; multiwarstwy; odporność na utlenianie.

Acknowledgements

First of all, my gratefulness goes to Dr Jörg Patscheider from Empa, who inspired and launched my interest in hard coatings and for his trust and freedom he offered me when I was working in his team. Thank you also for giving me the opportunity to present my work on numerous international conferences, which were sources of new ideas.

I would also like to thank Prof. Hans-Josef Hug, the head of the Nanoscale Materials Science Department at Empa for giving me the chance to work in his Laboratory and the ongoing collaboration.

Special thanks to Dr. Aude Pélisson-Schecker for the deposition and investigation of the AlSiN system during her PhD, all the fruitful discussions we had, out common idea of the epitaxial AlN/SiN multilayer system grown on Al_2O_3 and the time we shared in the office for four years.

Thanks also to Dominik Jaeger for growing epitaxial TiN film on differently oriented MgO substrates and all other weird TiN samples which I ordered to investigate fracture damage.

Thanks to Dr. Kilian Wasmer from Empa for performing all the indentations necessary to study the fracture damage of the coatings.

I would also like to express my gratitude to Michael Stiefel for his skills in preparing numerous and challenging FIB cross-sections through the indent imprints. He accomplished wonders with the FIB to get really thin lamellas.

I would like to acknowledge Mr. J.C. Cancio for depositing the TiN/SiN multilayers and Dr. K. Rzepiejewska-Małyska for making available for TEM studies the TiN, NbN and CrN monolythic coatings and their multilayered combinations.

My gratefulness goes also to Dr Ireneusz Piwoński for his corrections of the polish version of the abstract, valuable comments, fruitful discussions and cheerfulness.

Thanks to Karolina K. Sosnowska for her bright ideas and suggestions for an accurate title of the present work.

Special thoughts go to my office colleagues Dr Rolf Erni and Daniel Schreier as well as my polish friends at Empa: Karolina Sosnowska, dr Magdalena Pawełkiewicz Koebel, Agnieszka Hamburger and dr Katarzyna Michałów-Mauke for a great scientific and working atmosphere.

I would also like to thank all the co-authors of my publications.

Finally I would like to thank my family: my husband Leszek, and in particular my Parents for continuous support and taking care numerous times and during all holidays of my two daughters Łucja and Laura.